UNIVERSITY OF HELSINKI

Determination of water content in pharmaceuticals by near-infrared spectroscopy

Master’s Programme in Chemistry and Molecular Sciences

Master's thesis

Author:
Sanna Hiukka

Supervisors:
Prof. Susanne Wiedmer
Ph.D. Tiina Lipiäinen
Ph.D. Laura Matilainen

19.5.2025

Helsinki

Faculty: Faculty of Science

Degree programme: Master's Programme in Chemistry and Molecular Science

Study track: Analysis and Separation Methods

Author: Sanna Hiukka

Title: Determination of water content in pharmaceuticals by near-infrared spectroscopy

Level: Master's thesis

Month and year: May 2025

Number of pages: 82

Key words: hydroxypropyl cellulose, hydroxypropyl methylcellulose, near-infrared spectroscopy, process analytical technology, Raman spectroscopy, theophylline, water content

Supervisors: Prof. Susanne Wiedmer, Ph.D. Tiina Lipiäinen, Ph.D. Laura Matilainen

Where deposited: Digital Repository of the University of Helsinki (HELDA)

Additional information: -

Abstract:

Water content is a pivotal factor in pharmaceutical formulations as it may have an impact on stability, efficacy and manufacturing processes. The literature review explores the use of near-infrared spectroscopy as a rapid and non-destructive method for moisture content determination of samples in pharmaceutical industry. NIR offers an alternative technique for moisture analysis compared to traditional methods, such as Karl Fischer titration. An overview of the theoretical principles of NIR, instrumentation, and its advantages and limitations are provided. Chemometric models are discussed together with multivariate data analysis and calibration models for accurate moisture quantification.

The applications of NIR in raw material analysis, process analytical technology, and in quality control as well as moisture content determination in lyophilized products are reviewed with the practical implementation of it. This thesis highlights the potential and effectiveness of NIR as a sustainable and valuable analytical technique in pharmaceutical research and production, providing reliable and reproductible results for the determination of moisture content of pharmaceutical samples.

The experimental part focused on how different polymers affect the hydrate conversion of theophylline. Theophylline can exist in multiple solid-state forms, including anhydrate and monohydrate. The stability and transformation between these forms can influence the stability and bioavailability of pharmaceutical products, as they play a critical role in pharmaceutical formulations.

Various grades of hydroxypropyl methylcellulose and hydroxypropyl cellulose were tested and their effect the hydrate conversion kinetics of theophylline in binary mixtures. A variety of analytical techniques, such as NIR and Raman spectroscopy, were employed to assess the hydrate conversion behavior. Results indicate that the individual polymer properties influence the hydrate conversion kinetics of theophylline, providing insights for optimizing the formulation and manufacturing of pharmaceuticals.

TABLE OF CONTECTS

Abbreviations

(A)NN	(artificial) neutral network
API	active pharmaceutical ingredient
A_w	water activity
GMP	good manufacturing practices
HDP	hydroxypropyl
HPC	hydroxypropyl cellulose
HPLC	high performance liquid chromatography
HPMC	hydroxypropyl methylcellulose / hypromellose
KF	Karl Fisher -titration
LOD	loss on drying
MDA	multivariate data analysis
MEMS	micro-electro-mechanical systems
MLR	multivariate linear regression
MSC	multiplicative scatter correction
MT	methoxy
MW	molecular weight
NIR	near-infrared spectroscopy
PAT	process analytical technology
PC	principal components
PCA	principal component analysis
PCR	principal component regression
PLS(R)	partial least squares (regression)
RH	relative humidity
RMSEC	root mean square error of calibration
RMSECV	root mean square error of cross-validation
RMSEP	root mean square error of prediction
SEM	scanning electron microscopy
SNV	standard normal variate
THA	theophylline anhydrate
THM	theophylline monohydrate
TH	theophylline

1. Introduction

Of all the compounds in the world, water has certainly received the most attention considering its chemical and physical properties in analytical chemistry. Water and the moisture content of substances have been determined using various techniques from conventional methods to modern and newer approaches already since the 1960's.[1] Despite the fact that there are several methods for determining the water content of chemical compounds, only a few techniques have achieved widespread acceptance. However, many of the general and classical methods, such as Karl Fischer titration and thermogravimetry are time-consuming and sample destructive analytical techniques.[2,3] Instead, near-infrared spectroscopy provides plenty of advantages for a broad range of applications.

NIR is a simple, rapid and non-destructive analytical method that offers analyses of solid and liquid chemical compounds in any matrix.[4,5] A spectrum of the analyzed sample is recorded in a few seconds and the speed of performing the analysis is a huge advantage in any industrial application.[6] It is a low-cost and sustainable technique as there is no need for solvents or reagents and sample preparation is only minimal or not required at all, which on the other hand avoids errors.[3,4,7] Nonetheless, the interpretation of the NIR spectrum is demanding due to severe overlapping of the bands.[1] Thus, chemometric tools and multivariate data analysis methods are typically required.[8–10]

NIR combined with chemometrics is an effective method for both qualitative and quantitative analyses in many different fields including pharmaceutical industry.[1] NIR spectra contain broad information about the chemical compound, such as physical properties or water content, which can be implemented in the manufacturing process in pharmaceutical products.[6] Active pharmaceutical ingredients and pharmaceutical products are often sensitive to water induced degradation and NIR is well suited to the determination of water due to its strong absorption band of water.[1,8,11] The moisture determination with NIR can be applied to a wide range of pharmaceutical formulations, such as powders, tablets and solutions.[3–5] Therefore, the interest towards NIR has grown over the decades in the pharmaceutical field.[10] In addition, the improvement of instruments, on-line analysis and in-line in situ as well as the diversity of the probes have taken a leap forward.[4,12]

2. Literature review

2.1. Theory and principle of near-infrared spectroscopy

NIR is an analytical spectroscopic technique which utilizes light in near-infrared regions of the electromagnetic spectrum. It gathers information about a sample due to the absorption of a defined chemical compound or solution. According to the Lambert-Beer law (Equation 1), the absorption of electromagnetic radiation depends exponentially on the number of absorbing substances. In equation (1) the absorbance is defined as:

$$A = \varepsilon bc \tag{1}$$

where ε is the molar absorption coefficient of the substance at a certain wavelength ($M^{-1}cm^{-1}$), c is a molar concentration of a solution (M) and b is the optical path length (cm). The higher the concentration of solutions, the more radiation will be absorbed. A can also be defined as in the equation (2):

$$A = -\lg T = -\lg \frac{I}{I_0} = 10^{-\varepsilon cl} \tag{2}$$

where T is the transmittance which describes the intensity of radiation (I) that has passed through the sample divided by the original intensity of the radiation (I_0).

Light is electromagnetic radiation, and in spectroscopy it is utilized to analyze compounds by describing the transition of energy between light and physical matter. Compounds absorb electromagnetic radiation, which causes the compound to be excited from the ground state to an electronic excited state. Each compound has a characteristic level to which it can be excited. A compound can absorb energy equal to the difference between the ground state and the excited state, and when it is released, the compound emits a photon. A photon is a particle that mediates electromagnetic interaction, also known as a particle, which travels between excited states. The energy of this photon (E) is inversely proportional to the wavelength (λ) which is defined as:

$$E = h \cdot v = \frac{h \cdot c}{\lambda} = h \cdot c \cdot \tilde{v} \tag{3}$$

In equation (3) h is Planck's constant, v is a frequency of light and c is speed of light. The equation (3) shows the higher the photon's energy and frequency, the higher the

wavenumber (v) and the shorter the wavelength which is observable in an equation (4) below:

$$\tilde{v}\ (\mathrm{cm}^{-1}) = \frac{10^7}{\lambda\ (\mathrm{nm})} \quad (4)$$

The molecules of compound absorb the frequencies of infrared light that correspond to its molecular vibrational transitions. Thus, the vibrational frequencies provide information of the investigated compound. NIR is based on molecular vibrations such as overtones and combinations of fundamental vibrational frequencies of molecules.[10] An overtone is any resonance frequency which is above the fundamental vibrational frequency absorptions, and regarding their NIR spectrum the bands are multiples of the fundamental absorption frequency. In turn, the bands of combinations occur if two or more simultaneous fundamental vibrations interact, and their frequency is the sum of the multiples of fundamental vibrational frequency.

The near-infrared region is defined as a range of 700-2500 nm (4000-14300 cm^{-1}) and the transitions of overtones emerge between 780 nm and 2000 nm, whilst the combination vibrations appear 1900 nm and 2500 nm.[4] The characteristics of NIR are suitable for the moisture content determination since water exhibits unique absorption bands in the NIR spectral region centered approximately 1400-1450 nm (6800-7100 cm^{-1}) and 1900-1940 nm (5000-5500 cm^{-1}).[8,11] The first overtone band is caused by the O-H stretching and the latter absorption region is the combination of the O-H stretching and the O-H bending band.[3,13] However, the position of these bands may shift at higher wavelength due to the environment of hydrogen bonding.[1] The chemical and physical state of water in a molecule affects the position of spectral bands and for that reason the wavelength may differ in diverse samples and temperatures.[5] Alternatively, the absorption band of other compounds near the spectral region of water may be covered by water as it absorbs very strongly. Simultaneously, this powerful absorption contributes to the quantitative determination of water in a sample by NIR, but it requires multivariate calibration methods. Below is an NIR absorption spectrum (Figure 1), in which different colors represent the moisture content of the samples. The spectrum visualizes the effect of moisture on the spectrum.

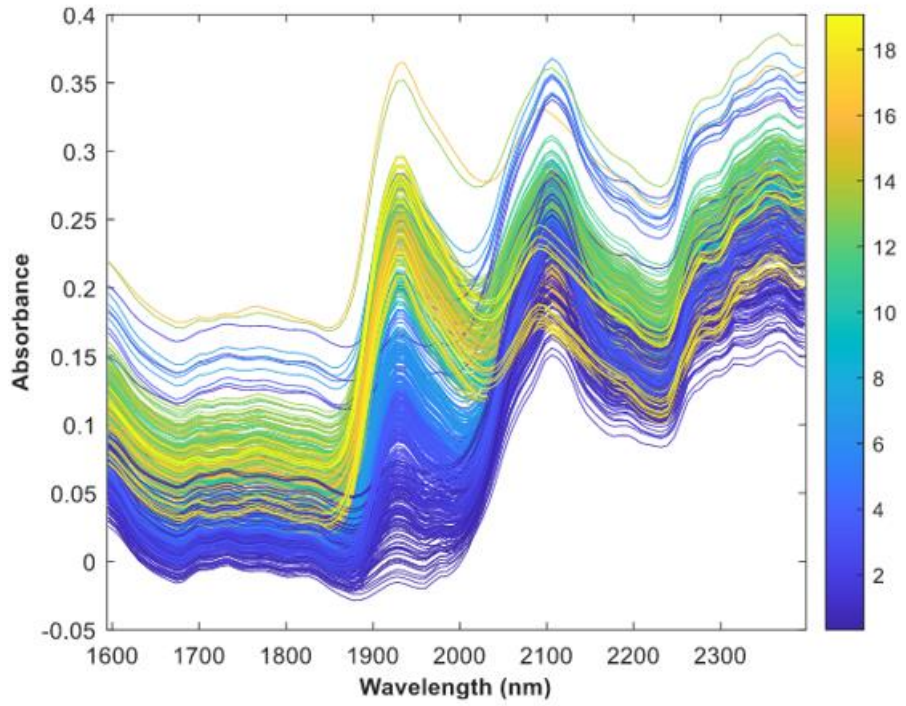

Figure 1. NIR spectra of samples with different moisture content level indicated by the color bar. Reprinted with permission from Elsevier.[3]

2.1.1. Benefits and limitations of near-infrared spectroscopy

NIR spectroscopy has several unique benefits over classical analytical techniques, which makes it a powerful, modern analytical tool in a broad range of applications in the pharmaceutical industry. Additionally, it is utilized in multiple other industries, such as in the food industry, agriculture and textile industry, but this thesis highlights only advantages of the pharmaceutical industry.[14,15] However, like any other analytical method it also has some limitations and drawbacks.

2.1.1.1. Advantages

One of the key benefit of NIR is the conservation of sample integrity by being a non-invasive method which requires minimal to no sample preparation and the NIR spectra of samples can be collected through the package.[16] Therefore, it allows the further use of a test sample and decreases the time of analysis as well as resources which make it an environmentally friendly and cost-effective technique.[1,17] The versatility of analyzing various pharmaceutical forms and their parameters such as blend uniformity and coating thickness, is making it an undeniable technique to be implemented as a process analytical technology.[11]

Moreover, in-line and at-line monitoring in analytical processes enhances quality control and process efficiency in pharmaceutical manufacturing.[18] NIR is well-suited for real-time process monitoring during manufacturing as the measurements are completed rapidly within seconds and the speed of data acquisition is a huge advantage.[12] With a single scan, NIR can perform simultaneous multi-component analysis to determine various properties of pharmaceuticals, such as the moisture content of active pharmaceutical ingredients. In addition to these advantages, NIR instruments enable an on-site drug analysis as recently many handheld and portable NIR devices are developed.[3]

2.1.1.2. Limitations

Despite all the advantages of NIR, it also has some limitations that must be considered. NIR has limited sensitivity of low concentration components, such as trace impurities and small amounts of API due to its measurement of combination and overtone bands and not fundamental vibrations. Only samples with functional groups with O-H, C-H, N-H and S-H are polar substances which absorb in the NIR region.[3] However, these functional groups have broad and overlapping absorption bands which make their data interpretation demanding and specific components are challenging to differentiate.[4,19]

Furthermore, the uniformity of the sample as well as properties of the compound such as particle size, density and moisture content can influence the spectra.[19] The NIR spectra can also be affected by the ambient humidity and other environmental factors such as temperature and light.[10,19] The complexity of calibration is one of the main drawback as the multivariate statistical methods shall be demonstrated and poor calibration models can provoke inaccurate results. Therefore, the expertise is required for calibration, model validation, data analysis and maintenance.[4] Additionally, the initial cost is high if real-time and in-line applications are applied.

2.2. Determination of water content

2.2.1. Measurement techniques

The transmission method and the diffuse reflectance method are the two most frequent NIR measurement techniques. In the transmission method light passes through the sample which is clear or semi-transparent, such as a liquid, aqueous solution or a transparent solid.[20,21] The amount of light transmitted through the sample is measured by a detector which gives an

accurate measurement of the absorption. In turn, the diffuse reflectance method is well suited for heterogenous samples such as solids, powders, and opaque samples. The NIR light is scattered and absorbed within a sample and the reflected light is measured which may cause lower spectral quality due to the scattering effect. Consequently, the spectra are influenced by additive and multiplicative shifts which leads to more complex data interpretation.[22] However, the diffuse reflectance method requires minimal sample preparation compared to the transmission method, in which a specific thickness of the sample is essential.[20] In the pharmaceutical field, the transmission method is used for moisture content analysis and the determination of active ingredients or excipients is performed with the diffuse reflectance method.[4]

2.2.2. Instrumentation

The requirements for NIR spectrometers depend on the applications it is utilized for. The main components are a light source which emits the specific range of near-infrared light and optics, such as lenses and mirrors to focus the light, as well as a detector to convert the near-infrared radiation to electrical signals to obtain spectra. The system for data acquisitions and processing for collected data is essential since software is used for spectral interpretation, calibration, and validation as well as chemometrics models to acquire qualitative and quantitative results. Moreover, there must be a reference standard to verify the wavelength accuracy. If the spectrometer is used for in-line measurements for evaluating the moisture content of a drying process, it should be placed in a low-pressure position with a steady stream flow of product to avoid the uncertainty of NIR scattering due to the dynamic mixing of the product in the drying tube.[18] Table 1 presents a selection of NIR spectrometers utilized in pharmaceutical applications. There are many NIR spectrometers from different manufacturers with multiple features. The spectral range of spectrometers varies between devices and different devices has individual advantages. The choice of NIR spectrometer is mainly influenced by the application of use.

Table 1. Selected commercially available NIR spectrometers utilized in pharmaceutical applications.

Manufacturer & Device	Spectral range	Applications	Benefits
Benchtop devices			
ABB, MB3600	900-2500 nm	Process monitoring method development, at line process monitoring, final product QA, for liquids, powders, pellets and gels	No consumables, open sample compartment
ABB, MB3600-CH40	650-2700 nm	Determination of raw materials, in-process or finished products in solid form such as powders and pellets	Maintenance-free, various interchangeable accessories
ABB, MB3600-PH	900-2500 nm	R&D and at-line PAT applications, QA/QC analysis, raw material identification and qualification	Can be used as a benchtop or portable with movable cart, maintenance-free and user-friendly
Bruker OPTIK GmbH, BEAM	N/A	Monitoring mixing processes or the end point determination of API drying, for solid and semi-solid material, only single-point measurement	Can be applied at any part of the production line
Bruker OPTIK GmbH, MATRIX-F II	N/A	Online measurements for process controlling & direct measurements in process reactors and pipelines	Measurements in contact or contactless, easy maintenance, rugged design
Bruker OPTIK GmbH, MPA III	N/A	Daily QA/QC routine work	Easy operation, developing sophisticated calibration methods & try out methods, modular design
Bruker OPTIK GmbH, TANGO	N/A	Raw material and final product inspection, process related analytics	Easy-to-use touch screen, small
Metrohm, 2060	N/A	Optimized for PAT applications, for liquids and solids directly in the process line or in a reaction vessel	High sensitivity and S/N ratio, remote configuration, flexible using fiber optics or contact probes, connect to five probes
Metrohm, DS2500	N/A	Quality control and routine screening for liquid or solid samples	Customizable sample feed, pre-calibrated models available, compact
Metrohm, OMNIS	N/A	For liquid, viscous, and solid samples	Minimal training required, built-in sample recognition, ability to determine multiple measurable parameters
Sentronic, SentroPAT BU II	1350-1800 nm	Monitoring blend uniformity during bin blending for PAT	Battery operation, long term stability, variety of software features with third party software packages
Sentronic, SentroPAT Compact	1100-1900 nm	Online monitoring for powders and granules, on field analysis	Easy-to-use, high stability, flexible, rugged, reliable process information during process development, only one cable connection, compact

(continues on the next page)

Table 1. (continues)

Manufacturer & Device	Spectral range	Applications	Benefits
Benchtop devices			
Sentronic, SentroPAT DA	1100 – 1900 nm	Online monitoring of pharmaceutical powder uniformity bin blending and quantitative analysis of APIs using chemometric models	Long-term stability, seamLess integration into PAT management systems user-friendly design, GMP-compliant surfaces, compact and lightweight
Sentronic, SentroPAT FO	1100-2100 nm	Simultaneous measurements of full NIR spectrum, for oral solid dosage pharmaceuticals	Flexibility with SentroProbe diffuse reflectance probes & single-channel or up to 4-channel configurations, integration to PAT management software, long-term stability
Thermo Fisher Scientific, Antaris II FT-NIR	800–2500 nm, can be optimized	Any sample type: solids, powders, grains, tablets, paste, gel, syrup, films, and liquids, can be migrated to at-line, online, and in-line analysis	Robust and reliable calibrations
Thermo Fisher Scientific, Antaris MX FT-NIR	N/A	Online process monitoring & in-line continuous analysis, for solid and liquid analyses	Flexible fiber optic channels
Handheld and portable devices			
Ibsen Photonics, PEBBLE XNIR	950 -1700 nm	Raw material identification	Cost-efficient, ultra-compact
InnoSpectra, NIR-S-G1	900-1700 nm	Suitable for on-site analysis	Bluetooth connectivity & user-friendly mobile app integration
Malvern Panalytical, ASD LabSpec 4 Hi-Res	350-2500 nm	Incoming, in-process, or finished materials analysis, detection and identification of solid raw materials	Different probes for flexibility
Malvern PanalyticaL, ASD LabSpec 4 Standard-Res	350-2500 nm	Real-time analyses of liquids and solids	Different probes for flexibility
Sentronic, SentroID	900 – 1700 nm	Integrated camera, only minimal amount of materials needed	raw material identification, Internal standard & Immediate results,
Si-Ware Systems, Si-NIR Matrix	1350–2550 nm	Cost-effective, Compact and integrable, Flexible Integration System to other devives	MEMS-based technology,
Si-Ware Systems, Si-NIR Mini	1350–2550 nm	Real-time material analysis	Miniature sensor, MEMS-based technology, can be embedded into compact products
VIAVI Solutions, MicroNIR 1700EC	950–1650 nm	On-site blend uniformity and tablet analysis, in-line monitoring	Lightweight, calibration model development tool
VIAVI Solutions, MicroNIR OnSite-W	950–1650 nm	Raw material analysis, real-time predictions on-site	Wireless connection to PC, ultra-compact, ruggedized and ergonomic designed

Further, miniaturized and portable NIR devices have been developed for in-situ field measurements and on-site analysis.[3,19] Recently, there has been progress in microfabrication techniques and optics of micro-electro-mechanical systems which has increased the popularity of handheld NIR spectrometers as analytical performance is preserved also on real-time field analyses.[3] The capability of NIR spectrometers to perform rapid and low-cost measurements with ease of use has led it to be utilized in pharmaceutical applications from raw material identification to process analysis. Despite the wide use of qualitative analysis, their use for quantitative analysis is still limited, which may be due to the lack of application platforms for pharmaceutical products at this time to collect the real-time data.[19] Those applications use spectral correlation algorithms to calculate the similarity between analyzed spectra and a reference library to identify the unknow components.[23] Although they are promising devices, work remains to be done to make them more widely available for routine analysis.[24]

2.2.3. Chemometrics

Chemometrics is an approach using mathematical and statistical algorithms as well as conventional logics to design optimal experimental procedures for broad and complex chemical data obtained from spectroscopic analyses. Chemometric methods can be divided into unsupervised and supervised classification methods. The unsupervised classification methods, also known as clustering, are for samples which are classified based on their similarities of their spectra without previous information. In turn, the supervised classification is a method that requires prior knowledge of sample categories which are compared to the actual categories of validation samples to assess the predicted membership of categories.

In the pharmaceutical field chemometric tools are used in research, identification and qualification of raw materials and final products as well as in quality control of pharmaceutics and pharmaceutical processes when NIR is employed in these applications. Especially, active pharmaceutical ingredients can occur in different polymorphic forms during production which can influence the performance of the product. Consequently, qualitative and quantitative analysis of polymorph mixtures by NIR is widely used in the pharmaceutical industry.[7] Generally, NIR spectra are unclear and challenging to interpret due to overlapping caused by molecular overtones and combination vibrations.[25] In addition, unavailing information, such as background noise, scattering and other interpreting signals have an impact on sample

spectra and requires specific chemometric techniques for quantification.[10,23] Chemometrics has various preprocessing methods to clean up the data as typically the sample is analyzed as it is.[3]

Mathematical pre-treatments and regression methods are the most common chemometric tools to reduce irrelevant information of NIR spectrum and to extract significant ones.[12] Pre-processing with mathematical techniques reduces the impact of systematic variations that do not directly represent the chemical composition of the sample or are not related to measured parameters.[10,12] However, mathematical pre-treatments minimize spectral variations caused by physical factors, such as light scattering due to particle size differences and the interaction of light, which can be corrected using multiplicative scatter correction (Figure 2).[8,26]

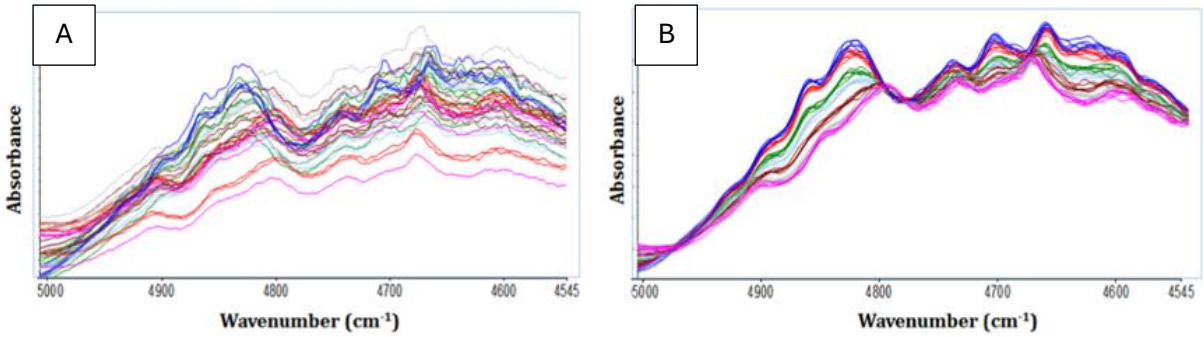

Figure 2. Raw (A) and MSC (B) treated NIR spectra from binary mixtures (API and excipient). Reprinted with permission from Elsevier.[10]

Other examples of these are first and second derivate calculations, such as Savitzky–Golay which is a smoothing filter to emphasize peak shapes, and standard normal variate.[26] The latter normalizes spectral data and corrects baseline shifts which are affected by sample heterogenicity. On the other, these mathematical pre-processing methods can be used as combinations as well.[10] Figure 3 shows how pretreatment affects the NIR spectrum of samples with different moisture contents.

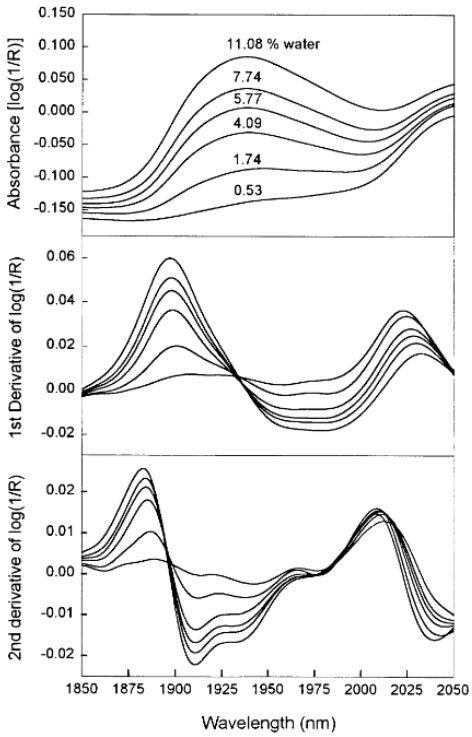

Figure 3. Raw, first and second derivative spectra of the samples at different humidity levels in the spectral range 1850–2050 nm. Reprinted with permission from Elsevier.[27]

The regression methods create a mathematical model to connect a spectrum of samples to a given concentration.[12] Examples of these include linear models, such as partial least squares regression, principal component regression as well as multiple-linear regression, and non-linear model; artificial neuronal network.

2.2.3.1. Multivariate data analysis methods, multivariate calibration methods and calibration models

Multivariate data analysis methods, multivariate calibration methods and calibration models are all closely related to each other, and they are part of chemometrics analysis. As a matter of fact, to determinate and achieve quantitative results of water analysis by NIR spectroscopy all of those above are applied.[11] They help to extract relevant chemical information from complex spectral data and eventually to predict unknown analytes and their concentrations from their NIR spectra.

MDA methods are a broad category of tools and techniques to analyze and interpret large datasets with multiple variables. It is focused on exploring trends as well as finding patterns and relationships from datasets. Multivariate calibration methods are specific regression techniques which are a subgroup of MDA methods. They are used to create models that

predict the concentration of an analyte from spectral data which correlates with a reference value.[4] Generally, when measuring the moisture content of a sample with NIR, KF or loss on drying is used as a reference analytical technique.[4]

A calibration model is a final mathematical equation when multivariate calibration methods are applied to convert NIR spectra into a quantitative predictive model for chemical properties. Spectral absorbance and reflectance values are used to establish a relationship with the target analyte, such as moisture content. The model must be validated to ensure accuracy and robustness. Since multivariate calibration models are designed for long-term use, robustness is essential when used for industrial applications, such as in quality control, process analysis, and in-situ measurements.[3] Consequently, a calibration model is a result when MDA and multivariate calibration methods are employed to spectral data. Moreover, calibration-free methods, which are based on the average relative standard deviation have risen popularity recently.[28,29]

Basically, there are linear and nonlinear calibration models that differ in their accuracy of prediction and how they can be validated.[8] All the mentioned calibration models have been used to determine the moisture content with NIR in the pharmaceutical field.[2,9,17,30] Nevertheless, the choice of calibration model depends on the type of chemical system being analyzed. Linear models, such as MLR and PLS, are bilinear and are based on a simple linear relationship between the spectral data and the measured property. Hence, they are fast, easy, and simple to interpret. However, they are not suitable for more complex chemical systems because they cannot predict nonlinear relationships, which reduces the predictability of the model.[8] The accuracy and predictability of nonlinear models depend on careful selection of variables and data preprocessing, as it uses large spectral data. However, complex and nonlinear relationships in chemical systems can possess too many irrelevant variables that overfit the calibration model, making it unreliable.[9] Therefore, linear calibration models cannot be applied for non-linear chemical systems and the other way.[8]

2.2.3.1.1. Linear calibration models

The most common linear calibration model is presumably partial least square regression when spectral data of NIR is extracted for quantification.[31,32] PLS is able to directly model the relationship between the NIR spectral dataset X and one or more of its features Y, such as moisture content of analyte, using a linear combination of variables.[9] PLS factors are latent

variables also known as principal components which are required to build the model and to handle collinearity to improve prediction accuracy. [2,33]

Principally, selecting too many factors can lead to overfitting, making the model more sensitive to small spectral differences.[1,12,26] However, not enough factors may result in underfitting which reduces the model's predictive accuracy. It is important to find the exact right number of PLS factors to meet the requirements of robust calibration model.[26] Using PLS on a small range of spectra is beneficial when it is compared to a simpler single-variable regression or a broader wavelength range with more spectral data.[2] Hence, to avoid a lacking predictive power with a simpler approach and more complex method approach, it is suggested to focus on a specific part of the spectra to achieve efficient and accurate predictions. Moreover, PLS can also be used if the spectral data has slight nonlinearity, and to remove features which are not consistent with the component concentrations.[8,10]

Principal component analysis is a linear technique used to recognize spectral patterns and reduce dimensionality by finding principal components to extract the main spectral variations.[2,9] However, PCA alone does not establish relationships between independent variables, such as the signal of wavelength, and dependent variables, such as analyte concentration. Therefore, principal component regression addresses this by first applying PCA to reduce dimensionality and then performing linear regression on the selected principal components.[9] Overall, PCA helps identify patterns that reflect spectral variations, which may be related to water content in a compound. However, regression models like PCR are required to quantify water content based on these spectral changes. In addition, to procure more robust calibration models with small prediction errors, PCA scores plot is a practical tool for determining an appropriate choice of the multiplying factor.[30]

Multivariate linear regression is a less frequently used calibration model to relate selected NIR wavelengths to water content when compared to PLS and PCA, as the first one/former is more accurate to handle highly correlated spectral data.[33] MLR calibration is not suitable for collinear data since it is able to use only specific wavelengths to perform data pretreatment and transformation which limits its use in complex spectral data.[22] This is not a problem in PLS, which offers the convenient advantage of using all wavelengths. In addition, PLS is more robust by being able to detect outliers which is a useful benefit in calibration model.

2.2.3.1.2. Nonlinear calibration models

Artificial neural networks are computational models employed for data analysis and predictions in NIR spectroscopy.[9] In the last few decades, machine learning has grown in popularity in many different applications and the development of several ANNs has taken a leap forward. The main advantage of ANN is its capability of handling nonlinear problems by using previous and fragmental data. Compared to PLS, it has a better ability of recognizing nonlinearities of dissolution curve of excipients.

2.2.3.2. Validation

The calibration model must be validated to ensure accuracy and robustness. The validity of a model can be impaired by certain changes, such as changes in conditions or analytes. Those can include different NIR instruments or instrument settings. In addition, chemical or physical changes in the sample compositions may also affect the validity of the calibration model, which is why NIR methods of measuring water content should employ only one calibration model for one sample composition such as API or matrix.[11] A separate calibration model should be used for each product or process with a different composition to ensure that the result remains accurate and free from bias. Robustness is essential when model is used for industrial applications, such as in quality control, process analysis, and in-situ measurements.[3]

2.3. Applications in the pharmaceutical industry

2.3.1. Analysis of raw materials

In the early days, NIR was only utilized in raw materials analysis for identifying and verifying as it provides relevant information about both chemical compositions, such as APIs or excipients, and physicochemical characteristics of substances, i.e. crystallinity and moisture.[4,34] Notwithstanding, it must be coupled with appropriate chemometric modelling technique for classification.[35] Prior to NIR, laboratory-based analytical techniques, such as chromatographic or KF, were used for pharmaceutical raw material identification. Additionally, large-scale classification was demanding with previously employed technologies due to time-consuming techniques and a large number of samples.[36] Recently, NIR has gained wide acceptance for raw material identification as processing capability has improved making it more efficient and accessible to users.[35] Currently, the classification or determination of

moisture content of many pharmaceutical products by NIR is regarded as a standard method as well.[4]

Together with his research colleagues, Mainali developed a single comprehensive calibration model for the rapid determination of the moisture content of pharmaceutical tablets by NIR.[11] The developed calibration model was applicable to a wide range of pharmaceutical tablets. Three different tablets containing active pharmaceutical ingredients with water contents ranging from 2% to 13% (w/w) were used to build the model.

The water content was determined by utilizing the ability of NIR to detect the strong absorption of water, which is visible in the NIR spectrum at wavelengths of 6800–7100 cm^{-1} and 5100–5300 cm^{-1}. First, the selection of an appropriate measuring mode between transmission and diffuse reflectance mode must be done. The measurements were performed using a Fourier-Transform Near Infrared analyzer equipped with a detector in diffuse reflectance mode. Then, samples were measured for their moisture content with NIR. Below (Figure 4) is a comparison of the NIR spectra of the different tablets used in the study, where the different water contents are clearly visible at 5100 cm^{-1}.

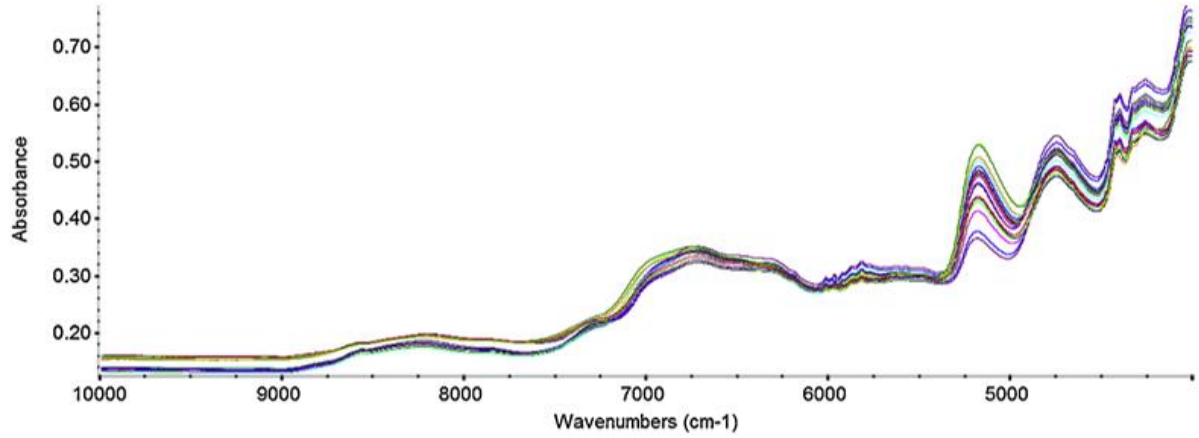

Figure 4. NIR spectra of tablet samples. Reprinted with permission from Elsevier.[11]

Spectral pretreatments, such as SNV and second derivatives are commonly used to correct, such as scattering effect in NIR spectra and remove physical differences between tablets and reducing spectral noise. In this study, the first derivative pretreatment was done, which highlights the effect of water content on the absorption bands and is observable in Figure 5.

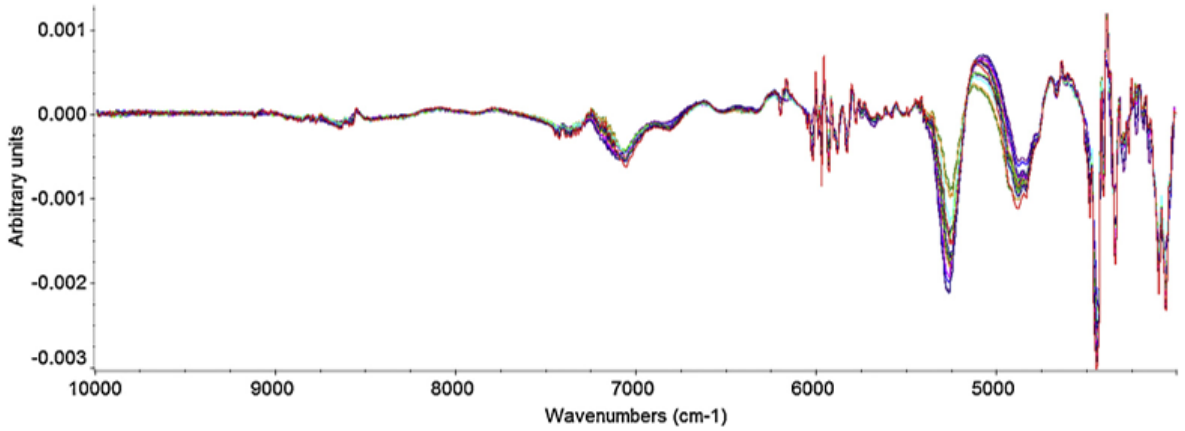

Figure 5. First derivate pretreated NIR spectra of tablet samples. Reprinted with permission from Elsevier.[11]

Several models can be developed and evaluated. The selection is usually based on conventional criteria, which are coefficient factor of determination (R^2), RMSEC and RMSEP.[10] Mainali et al. initially built individual calibration models for different tablet types.[11] However, finally only one comprehensive model was developed which was able to predict the water content for all different formulations and tablets containing API. KF was used as a reference method for water content determination. The accuracy of the model was improved by preprocessing the spectra, such as Savitzky-Golay simulation and the use of the first derivative. The developed comprehensive calibration model proved to be reliable and accurate. It enabled rapid and non-destructive prediction of water content for different pharmaceutical tablet types.

Additionally, according to Gabel et al. the mass percentage of API is a crucial factor, though not the only one which affects NIR spectra of commercial products and thus their identification.[36] Mass percentages of APIs in the total tablet weight may be significantly inconsistent when comparing different commercial brands. Occasionally, the same manufacturer with two different batches of products may differ from mass percentages due to the various manufacturing protocols. In addition to API mass percentage, excipient composition and physicochemical properties vary in different manufactures resulting in differences in the NIR spectra. However, the principal spectral features are specific on the respective API, despite the chemical similarities which can be observed from Figure 6 below when comparing two beta-lactam antibiotics (penicillin V and amoxicillin).[36] Consequently, it is possible to distinguish between closely related chemical compounds.

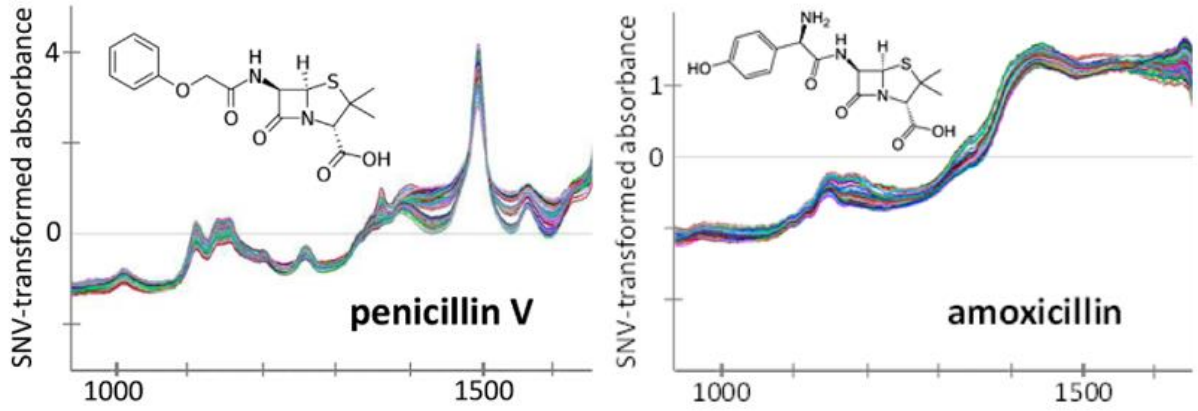

Figure 6. NIR spectra of similar molecular structure compounds. Reprinted with permission from Elsevier (open access).[36]

Raw material identification by NIR is not only related to API, but also the discrimination of excipients is involved.[35] Different excipients show different NIR spectra between 5400-6100 cm^{-1}, which can be observed in Figure 7.[37] In each spectrum, water is approximately at the same point below 5400 cm^{-1}, however the exact location depends on the chemical and physical environment. A reference peak is also visible between 5700-57800 cm^{-1}. These spectra clearly reflect varying water concentrations, which are characteristic of water absorption features.

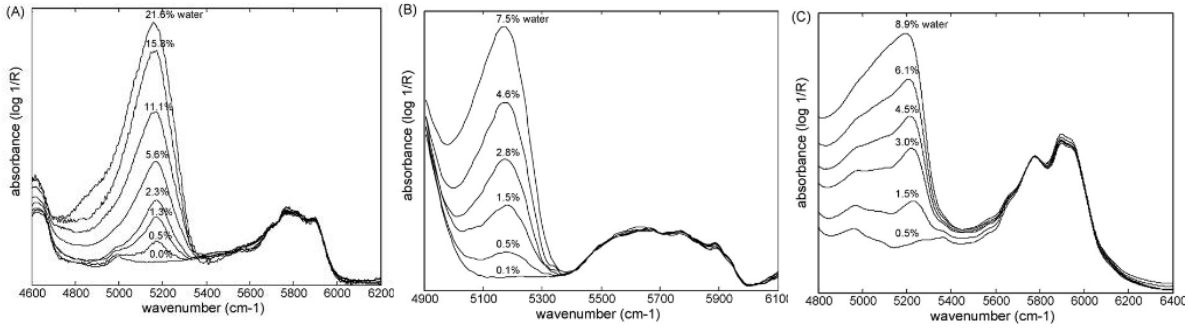

Figure 7. SNV pretreated NIR spectra of PVP (A), hydroxypropyl-β-cyclodextrin (B) and the lyophilized formulation (C) with different moisture levels. Reprinted with permission from Elsevier.[37]

2.3.2. Process analytical technology

Recently, major interest has gained towards process analytical technology tools as they play a crucial role in the pharmaceutical manufacturing industry.[38] However, only a limited number of continuously manufactured pharmaceutical products are available in the global market today.[39] To maintain the high-quality of pharmaceuticals, the pharmaceutical production

process is based on good manufacturing practices which are highly regulated as the final products must meet strict quality standards.[38]

Today, large-scale manufacturing processes are frequently used and monitored by conventional off-line analyses in analytical laboratories.[38] However, large-scale manufacturing requires scaling up which may have issues since traditional batch control cannot be applied in continuous manufacturing of high-quality pharmaceuticals without losing its benefits.[40] Despite the concerns about the scaling up, continuous pharmaceutical manufacturing processes hold the great potential, and several studies have addressed the challenge of transferring laboratory-scale development methods to large-scale manufacturing.[39] Continuous pharmaceutical manufacturing processes have increased the popularity over traditional batch processing as the former is fast with better process capacity and batch size flexibility, has lower equipment, operating and manufacturing costs, as well as being an efficient technique with no need for intermediate product storage.[6,39] Nevertheless, it has drawbacks including significant high start-up investment, hiring skilled personnel and the tightly regulated manufacturing process in line with GMP which can increase production time.[38]

The key tool for process analytical technology is NIR for both qualitative and quantitative real-time analyses.[41] It is suitable for a variety of PAT applications, particularly monitoring of partial processes, such as intermediate and end-products.[38] Monitoring each step of the manufacturing process enhances the quality and safety of pharmaceutical products, with NIR being one of the most suitable techniques for routine use.[4,6] Providing chemical and physical characteristics information of material makes it a valuable tool for monitoring the critical pharmaceutical attributes.[42] In order to the routine use, chemometric methods must be developed and validated to extract spectroscopic data on multicomponent samples.[6,43] Moreover, widespread implementation of NIR requires the reduction of costs and the improvement of measurement robustness.[41] Nonetheless, the versatility of optical probes allows at-line, on-line, or in-line applications, providing high-resolution moisture signals that support efficient process control.[11,12,41]

The implementation of PAT tools to continuous drug product manufacturing is an innovative approach in the pharmaceutical industry for process monitoring and controlling in real-time analyses.[38] The quality of pharmaceutical products can be enhanced by scientific

understanding of manufacturing processes through at-line, on-line and in-line measurements.[44,45] The scope of the PAT tools is enormous. It is utilized in (powder) blending, (wet) granulation and drying for monitoring of moisture content, and controlling the solid form production process, such as tablet pressing and coating.[43,46–49] When performing real-time moisture determinations by NIR, online NIR spectra are compared to offline measurements.[41] The determination of moisture content must be done as soon as feasible in the development phase of pharmaceutical manufacturing to applying it at-line in the process.[50] Moisture content determination during blending, granulation, and drying is performed using NIR, which provides an invaluable PAT tool for process control and product development support.[9,11]

2.3.2.1. Blending

In the pharmaceutical manufacturing process, blending is a crucial step in the solid-state dosage forms.[51] Powder homogeneity and blend uniformity are pivotal, especially as pharmaceuticals become increasingly potent, with API concentrations of less than 1% of the total tablet weight. In order to achieve high quality components for use in the final product, the application of NIR in blend uniformity determination is applied.[52] However, ensuring the homogenization of ingredients using NIR is challenging, although it can avoid some of the disadvantages of conventional methods.[29] To obtain real-time process mixture uniformity analysis is performed using in-line measurement instead of off-line measurement.[51]

Water is highly used as a lubricant in drug substances, and it can interfere with the NIR spectra of API and excipients due to water's significantly high absorbance values compared to components in blending mixture.[51] The interferences of water in NIR spectra are likely minimized if the concentration of the API is relatively high compared to the lubricant or the lubricant is added after the primary blending step. The concentration of API must be at least 2.98 % (w/w) to monitor blend uniformity.[51] Even a small amount of water can cause polymorphism in a solid composition, which can be seen by NIR spectroscopy, as it is sensitive to polymorphic transitions.[4]

In-line concentration measurements of the powder blend and the obtained NIR spectra of them are mainly affected by the location of NIR probe.[14] Other affecting factors were found to be the loading order of components in the bin and the speed of the paddle wheel in the

bin blender which had an influence on the powder flow behavior and the sample size variation.[14,29] Instead, the shape of the paddles did not seem to have an effect.[14] There are different perspectives where the NIR probe should monitor the blending process from the bin blender.[29,53] To achieve optimal alignment between in-line and off-line measurements, two NIR sensors should be placed—one on the top and the other on the side of the blender.[53] The combination of two sensors provides the information on the powder flow, mixing kinetics and the behavior of each active ingredients which highlights the value of continuous monitoring during the blending process.[29,40]

2.3.2.2. Granulation and drying

Wet granulation includes high-shear and fluid bed granulation. Monitoring the residual moisture content of lyophilized, also known as freeze-dried products is described later. Controlling the moisture content during the wet granulation process is critical since APIs can experience the process-induced transformation due to the stress and nature of the process.[18,54] In addition, inappropriate excipients can induce undesired changes in crystal form of APIs.[7] In the wet granulation process, NIR is utilized to monitor moisture content, ensure the granulate quality, and detect the drying endpoint.[18,41] NIR can be applied in-line quantitative water determination as it is able to determinate the state of water in the sample.

In the fluid bed granulation, granules are dried by ambient air with uncontrolled humidity which leads to the variation of physical composition, such as particle size.[18] At the moment, there are no NIR sensors which is able to measure the moisture content of samples directly in a processing line. When measuring NIR spectrum of drying granulates in a fluidized bed in situ, granulates flow past the tip of NIR probe with a broad range of distances and random positions of particles.[41] This leads to substantial changes in the spectrum caused by inhomogeneity of material and requires spectral preprocessing to remove spectral artefacts. Alternatively, few studies have proposed that the calibration model developed from at-line spectrum could be used to generate the moisture content prediction of samples scanned by an in-line spectrometer.[18,55] The positioning of NIR sensors should be carefully selected, in order to avoid the unstable stream flow, even though they are robust towards vibrations and ambient temperature change when predicting the moisture content according to Avila et al.[18,41] Figure 8 below is show changes in the water content during the drying process and how it affects the NIR spectrum.

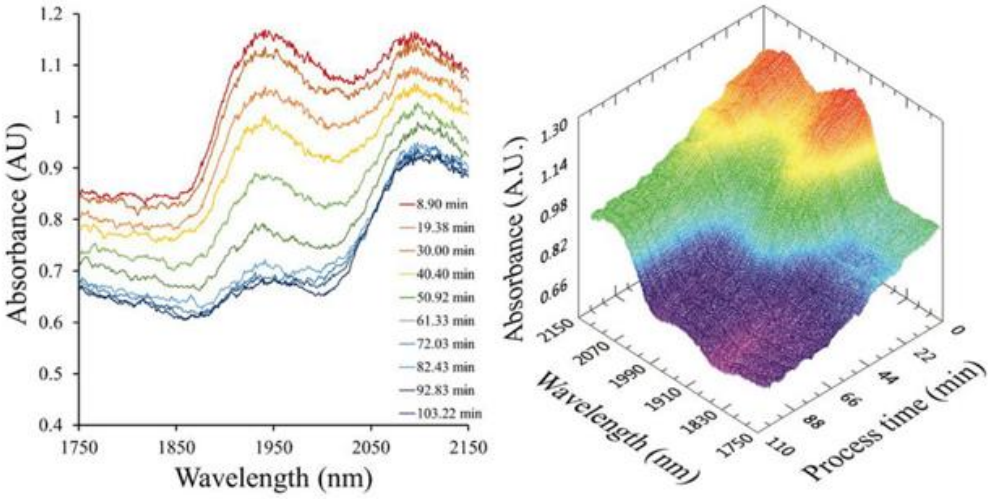

Figure 8. Preprocessed NIR spectra of drying evolution in situ resulted good prediction when compared to offline LOD analytical moisture content with PLS model. Reprinted with permission from Springer Nature (open access).[41]

2.3.2.3. Coating

NIR is also used as a PAT tool for determination of coating thickness of tablets as monitoring coating improves the predictability of the reaction of tablets.[52] The use of NIR provides an alternative way to determine the coating of tablets by image analysis and scanning electron microscopy or weighing, where the increase of average weight gain is measured.[51] The NIR spectrum shows an increase in the absorbance of the components of the tablet coating, while the components of the tablet core decrease, since the NIR radiation cannot reach the core as well when the coating increases.[56]

This can be observed in Figure 9 (A), in which the absorbance value of the spectrum of the uncoated tablet is higher between 7000 and 6000 cm^{-1}.[51] The thicker the coating, the lower the absorbance value of components of tablets. In addition, the spectra differ at 7200 cm^{-1}, where the coating gives a distinguishing sharp but small peak, while the uncoated tablet does not have this peak. It can also be observed in Figure 9 (B), which shows the spectra of the uncoated and coated tablets, as well as the spectrum of the pure coating powder alone.

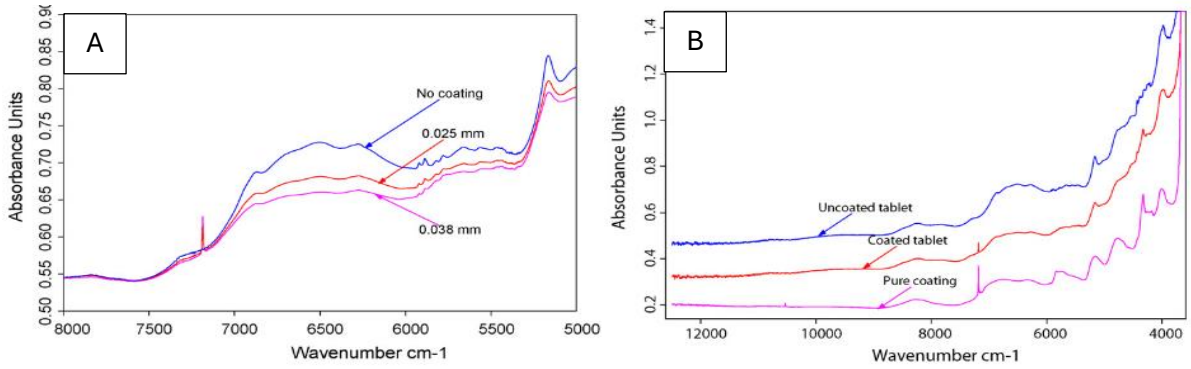

Figure 9. NIR spectra (A) of three coating thicknesses. NIR spectra (B) of coated tablet and pure coating with a distinguished peak, and an uncoated tablet with no peak. Reprinted with permission from Elsevier.[51]

Additionally, the shape of the tablet has not appeared to influence the thickness value measured by NIR.[51] The tablet coating has been determined by reflectance and transmittance spectroscopy, but it was observed that the reflection spectra was more responsive to variation of coating thickness. In addition, NIR has been applied to moisture content determination in the pellet coating process in-line as NIR probe can be used as a single tool.[57]

2.3.3. Quality control of finished pharmaceutical products

NIR is a tremendously valued tool in quality control in the pharmaceutical industry due to its possibility to discriminate falsified products from authentic products despite their similar composition.[36] Although pharmaceutical products from different manufacturers may exhibit slight variations, significant emphasis is placed on their quality control to ensure that the formulations meet the required standards for film-coated tablets, and the API concentration is correct.[14,58] Quantitative analysis of API content in tablets is a critical component of both routine drug manufacturing and early-stage drug development, for which NIR serves as an effective analytical technique.[14] Counterfeit products are frequently identified by reduced API levels or the complete absence of the API, which is observable in Figure 10. To assess API content, quantitative models, such as partial least squares, are developed to be applicable across various morphological forms.[14] Nonetheless, the most accurate predictions are typically obtained from uncoated powder samples. While distinguishing these from raw material spectra alone can be challenging, appropriate spectral preprocessing and the selection of informative wavenumbers enable successful differentiation.

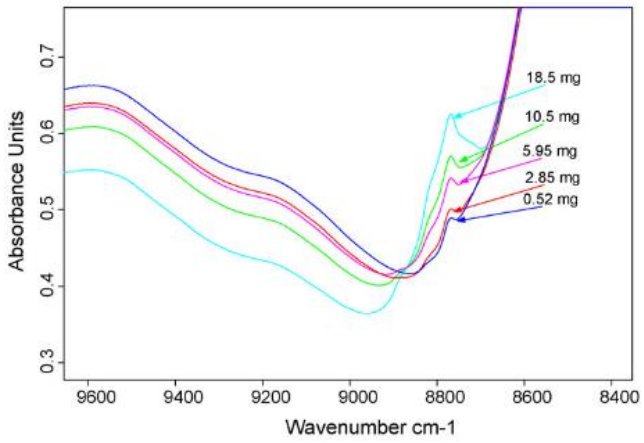

Figure 10. NIR spectra of tablets containing varying amounts of API show an increased absorbance at 8800 cm^{-1} as the API concentration rises while decreased absorbance value at 9600 cm^{-1}. Reprinted with permission from Elsevier.[51]

Lately, coupling NIR with chemical imaging (CI), such as hyperspectral imaging HSI, is also used as it has been demonstrated to be an accurate and robust tool to enhance quality control in both pharmaceutical development and manufacturing process.[52] It has not traditionally been considered a suitable method for quality control according to Corredor et al.[50] Namely, it requires careful calibration and, when measuring moisture, reference calibration standards with known moisture contents.[37] It is therefore advisable to use as few standards as possible for calibration. NIR is already used for in-line process monitoring of moisture content and would be useful for testing large batches. The measurement situation is not as optimal for in-line process monitoring as offline, which is caused by noise and causes greater variability. Despite being a very encouraging alternative to conventional QC tools, it still requires further testing and validation.[59]

2.3.4. Determination of moisture content in lyophilized products

In the lyophilization NIR is used to monitor the drying process of the pharmaceuticals in real-time.[60] The lyophilization, also known as freeze-drying, is implemented to stabilize, particularly the active pharmaceutical ingredients, during the preservation and storage.[8,60] The process of lyophilization has three stages, which are freezing, primary drying and secondary drying. [60] The NIR spectra of these stages are in Figure 11, in which the water signal is highlighted.[60] First, the solvent is transferred into ice by freezing. In primary drying, ice is sublimated into a porous solid with the low temperature and pressure. Finally, the bound

water is removed by raising the temperature to ensure the stability of the product. Not only to monitor the process, NIR combined with linear quantification methods is also applied to estimate and determinate the residual moisture content of freeze-dried samples for stability testing.[1,8] KF has traditionally been regarded as the standard method for this type of determination.[8] Besides, ambient humidity can cause errors in KF titration, especially when determining the extremely low residual moisture content of freeze-dried products.[61]

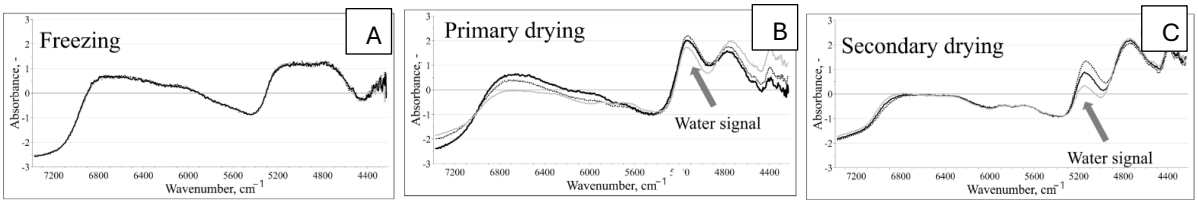

Figure 11. NIR spectra of phases of lyophilization: (A) freezing, (B) primary drying and (C) secondary drying. Reprinted with permission from Multidisciplinary Digital Publishing Institute (open access).[60]

Determination of residual moisture is important in the pharmaceutical manufacturing process, as water content is the most crucial factor affecting stability and thus the quality of the pharmaceutical products.[62] Freeze-dried products can have a high variability of moisture content within sample set, which can lead to batch inconsistencies.[1,60] Consequently, this may result in batch rejections, which can be reduced through early fault detection enabled by real-time monitoring with NIR spectroscopy.[60] By ensuring product consistency, batches can be released faster with improving efficiency of the pharmaceutical manufacturing. The determination of moisture content of freeze-dried products by NIR is based on band shifts, which is the reason a multivariate method is recommended rather than single or dual wavelength calibration methods.[1] The higher the moisture content of the sample, the greater the amount of free water present, which vibrates more readily than bound water and causes the absorption band to shift to a higher wavelength. In conclusion, NIR provides a non-destructive and efficient alternative technique to the conventional moisture measurement methods for the lyophilized samples.

3. The experimental part: The effect of polymer properties on hydrate conversion kinetics of theophylline

3.1. Background of the research

The goal of the experimental study was to compare the properties of certain polymers and their effect on the crystal structure of theophylline. Theophylline is a medicine used for asthma treatment, but this research was not focused on the effects of the medicine rather than theophylline was appointed as the model compound due to its ability to form hydrate at process and storage relevant conditions. Moreover, the solid-state forms of theophylline are relatively stable under normal conditions in order to study them and their stability in the presence of selected excipients.[5,63]

A hydrate conversion is a pseudo-polymorphic transformation of the solid-state structure where theophylline anhydrate (Figure 12 A), which has no water in a crystal structure, uptakes water and converts to theophylline monohydrate (Figure 12 B) with water in a crystal structure, and the other way.[64] Hydrates may have a variable number of water molecules and generally they are named by the number of H_2O molecules in the structure. For example, dihydrate indicates two water molecules having an H-bond with the API molecule. Regarding theophylline, it forms monohydrate which has only one H_2O per theophylline molecule in a crystal structure and anhydrate form, which are under the investigation of this study.

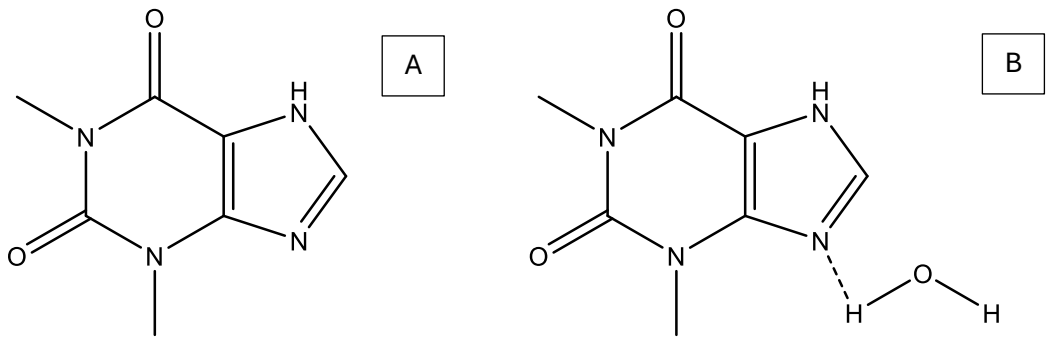

Figure 12. Chemical structure of theophylline anhydrate form (A) and monohydrate form (B).

Some active pharmaceutical ingredients are prone to hydrates, such as carbamazepine and nitrofurantoin, and even small variations in the product may affect the performance of pharmaceutical solid form.[65–67] In the pharmaceutical industry, it's crucial to have APIs remain in the form they are intended to as different pseudo-polymorphic forms may differ in

chemical and physical properties, such as solubility etc. which may affect their stability and bioavailability.[7,68] In the case of theophylline, the monohydrate form is less soluble in water compared to its anhydrate form, which can have an influence on bioavailability of the drug since only dissolved drug is able to absorb in the body.[5,43,63]

The binary mixtures consisted of a model compound and one of the two polymers under investigation which was either hydroxypropyl cellulose or hydroxypropyl methylcellulose, also known as hypromellose. Theophylline and excipients were mixed as 1:1 (w/w). Based on a previous study conducted at Orion, HPC and HPMC were selected to be investigated. The selection of these specific polymers was driven by the desire to study the potential effects of their individual properties on the hydrate conversion kinetics of theophylline under two different conditions. Various chemical and physical properties of the polymers were analyzed, including the ratio of substituents, particle size, and molecular weight. In addition, the consequences of storage conditions and the different initial moisture of polymer were examined. It has been demonstrated in several previous studies that excipients can have an impact on crystal polymorphism of theophylline.[5,43,69]

Near-infrared spectroscopy was used to monitor the changes in the state of water in binary mixtures. Additionally, Raman spectroscopy was utilized to observe the hydrate conversion of theophylline, while water activity and loss on drying were used to determine the water content of polymers. The purpose of this research was not to develop and validate a method for determining the rate of hydrate conversion of theophylline since the method and parameters used are dependent on the substances involved.[3,11,22] Instead, the purpose of the method development for NIR in the study was to examine the effect of different polymer properties on free and crystalline water movement kinetics in the binary mixtures. Furthermore, NIR was explored as a screening tool for the measurement and evaluation of different types of water forms. Overall, this study aims to investigate how the individual properties of polymers influence hydrate conversion kinetics of theophylline and changes in the water content within binary mixtures.

3.2. Materials and methods

3.2.1. Materials

Hydroxypropyl methylcelluloses Pharmacoats were acquired from Shin-Etsu Chemicals Co., Ltd. (Tokyo, Japan), Anycoat-Cs from Lotte Fine Chemicals (Incheon, South Korea) and Benecel™ polymers from Ashland (Texas City, USA). Hydroxypropyl celluloses L-HPC were procured from Shin-Etsu Chemicals Co., Ltd. (Tokyo, Japan) and Klucel™ polymers from Ashland (Texas City, USA). The properties of investigated polymers are assembled in Table 2. Theophylline anhydrate was obtained from Orion Corporation. TPO and TPP as well as methanol used in HPLC were purchased from Merck (Darmstadt, Germany). All chemicals were used without further purification. Chemical structures of HPMC and HPC are in Figure 13.

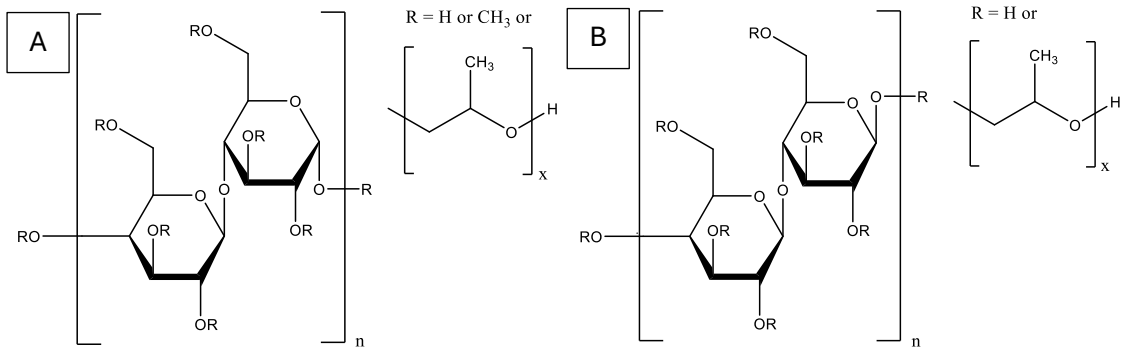

Figure 13. Chemical structure of HPMC (A) and HPC (B).

Figures 14-16 display the 30-folded magnification of HPMC and HPC polymers at ambient conditions (~21.5 ^{o}C & RH ~45%), excluding Figure 14 B which is preconditioned in RH 75% (21.5 ^{o}C) for 12 days. The HPC polymer ELF (Figure 14 A) at ambient is acicular and a few of the particles exhibit flaky and some of the smaller fragments resemble granular shape, while compared to preconditioned is more fibrous-like. The rest of the polymers show irregular, some kind of fibrous, and needle-like crystal structure. The examples of those polymers are in Figures 15 and 16.

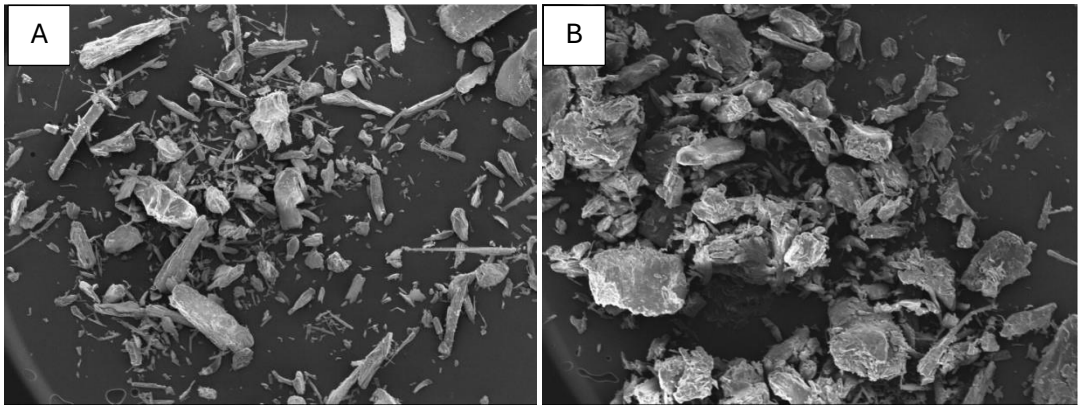

Figure 14. HPC polymers of Klucel™ ELF at ambient (A) and preconditioned in RH 75% (B).

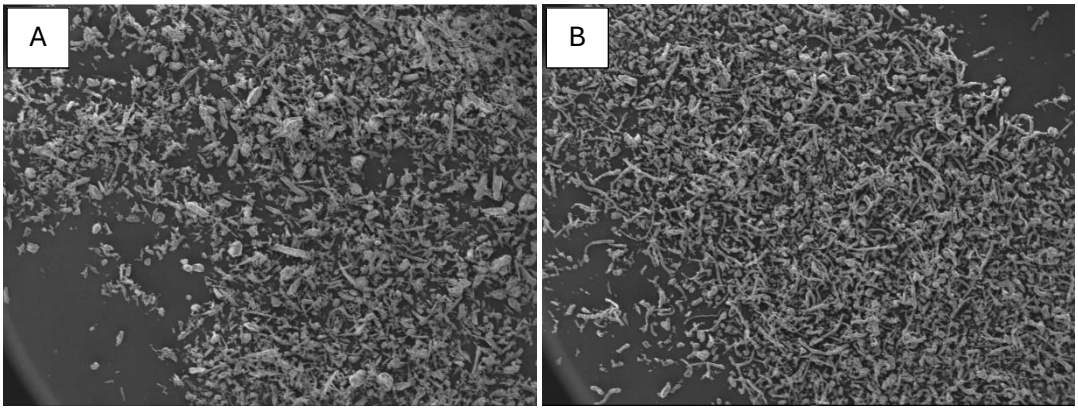

Figure 15. HPC polymers of Klucel™ EXF (A) and LH-21 (B) at ambient conditions.

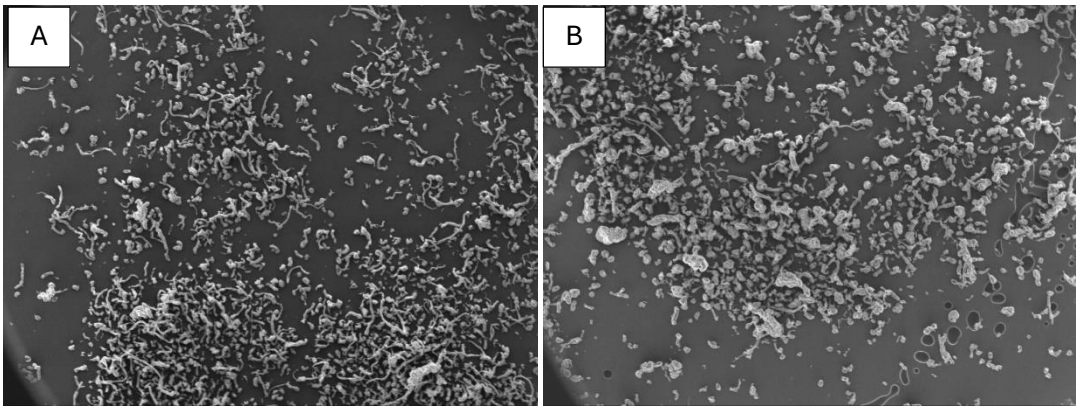

Figure 16. HPMC polymers of Benecel™ K200M (A) and Benecel™ E4M (B) at ambient conditions.

Table 2. Properties of investigated polymers.

Code name	Brand name of polymers	Substituent ratio		Particle size (µm) D_{50}	Molecular weight (g/mol)	Supplier
		Hydroxy propyl content (%)	Methoxy content (%)			
Hydroxypropylmethoxy celluloses (HPMC)						
615	Pharmacoat 615	8.8	28.6	87.4	56400	Shin-Etsu
606	Pharmacoat 606	8.7	28.5	88.8	32800	Shin-Etsu
AN6	Anycoat-C	8.6	29	75.5	10 000 - 1 000 000	Lotte Fine Chemical
AN6 exprired	Anycoat-C	8.5	28.2	-	10 000 - 1 000 000	Lotte Fine Chemical
K4M	Anycoat-C	9.2	23	75.4	N/A	Lotte Fine Chemical
E4M	Benecel ™ E4M PHARM	8.8	29	89.7	400 000	Ashland
XR	Benecel ™ K4M PHARM XR	8.4	23.9	94.3	400 000	Ashland
DC	Benecel ™ K4M PH DC	8.6	22.4	66.9	400 000	Ashland
K100LV	Benecel ™ K100LV PHARM	9.8	22.9	61.0	164 000	Ashland
K200M	Benecel ™ K200M PHARM	8.6	22.8	149.4	1 200 000	Ashland
Hydroxypropyl celluloses (HPC)						
LH-11	L-HPC LH-11	11	-	58.6	N/A	Shin-Etsu
LH-21	L-HPC LH-21	11	-	52.9	N/A	Shin-Etsu
LH-22	L-HPC LH-22	8.2	-	46.6	N/A	Shin-Etsu
LH-31	L-HPC LH-31	10.8	-	17.5	N/A	Shin-Etsu
NBD	L-HPC NBD	13.6	-	40.5	N/A	Shin-Etsu
EXF	Klucel ™ EXF Pharm	53.4–80.5	-	53.5	80 000	Ashland
ELF	Klucel ™ ELF Pharm	73.9	-	339.3	40 000	Ashland
EF	Klucel ™ EF Pharm	74.4	-	421.4	80 000	Ashland
EF exp.	Klucel ™ EF Pharm	72.8	-	456.1	80 000	Ashland
GF	Klucel ™ GF Pharm	73.7	-	461.3	370 000	Ashland
HF	Klucel ™ HF Pharm	53.4–80.5	-	508.2	1 150 000	Ashland

3.2.1.1. Preconditioning polymers for binary mixtures

All polymers were preconditioned in three different conditions before mixing them with theophylline. The preconditioned relative humidities were ambient conditions (~21.5 °C & RH ~45%), RH 5%, and RH 75%. The desired RH conditions were prepared with saturated salt solutions of sodium chloride (RH 75%), and dry storage (RH 5%) was realized by closed desiccators with silica. Polymers were set in conditions of RH 5% and RH 75% for 12 days before use as results of pre-tests shown they would be stabilized within this time which is explained in section 3 Results and discussion (3.1. Pre-tests).

3.2.1.2. Preparation of theophylline monohydrate

THM was prepared by conditioning THA powder in a desiccator of RH 95% (21.5 °C) and after a week transferred into a desiccator of RH 75% (21.5 °C) for storing until further use. The transformation of monohydrate was confirmed by Raman spectrometer. Previous studies indicated that no change in particle morphology should occur during the manufacturing since the change happens through a solid-state transformation, and unexpected conversion to anhydrate would not take a place as the critical water activity is above 0.25.[26,70]

3.2.1.3. Preparation of binary mixtures

Binary mixtures composed of HPMC/THM or HPC/THM were prepared by weighing 5 g of polymer and 5 g of theophylline monohydrate into a 25 mL bottle as the total mass of 10 g mixture. One polymer from three different preconditions (ambient conditions and RH 5% and RH 75%) was mixed with theophylline to obtain three binary mixtures of each polymer. All binary mixtures were mixed by Turbula® (Turbula T2C, Willy A. Bachofen, Basel, Switzerland) with the speed of 21 rpm for three minutes.

3.2.2. Methods

All analytical methods were not only performed on the binary mixtures but also every polymer undergone preliminary tests before preparing the binary mixtures from them. All samples were stored in defined RH conditions (21.5 °C) and were characterized after a certain period.

3.2.2.1. Near-Infrared Spectroscopy

The NIR spectra was measured using diode array Near-infrared Process Spectrometer (SentroPAT FO, Sentronic GmbH, Dresden, Germany) with SentroProbe DR LS NIR reflectance probe and data was acquired using SentroSuite software (Sentronic GmbH, Dresden,

Germany). Each spectrum was an average of 60 scans in 1100-2100 nm spectral region with resolution of 8-12 cm^{-1}. As the pre-tests, the NIR spectra of all polymers was measured at ambient temperature as well as from conditions of RH 75% and RH 5% for 9 days in a row, excluding a weekend. All the samples were scanned through the bottom of the Aqualab cup with the NIR beam pointing at the bottom of the sample cake. On the mixing day, binary mixtures were measured with NIR before Raman.

3.2.2.2. Raman

Raman spectra were measured using Ramina Process Raman Instrument (ThermoScientific, Tewksbury, USA) with the fiber optic non-contact probe (Proximal BallProbe®, MarqMetrix, Seattle, USA) and the thermally stabilized CCD detector. The spectra were acquired from six different spots of the sample to avoid bias as all samples were possibly not homogeneous, and they were composed of one scan with the varying integration time between 200-800 ms. The range of spectral measurements was 100-3250 cm^{-1} with a diode laser varying between 200-400 mV at 785 nm. The spectra of theophylline anhydrate and monohydrate were measured before use to differ their Raman spectra from each other.

3.2.2.3. Water activity

The pre-tests of the initial water activity of all polymers were measured by Aqualab 4TE (Water activity meter, Meter Group Inc., Washington, USA) as well as polymers from conditions of RH 75% and 5% after selected days. After 3 days and 7 days as well as 9 days the water activity was measured again for polymers kept in condition of RH 75%. Polymers kept in conditions of RH 5% was measured after a day, 4 days and 8 days. Before measurements, the standards were measured with 17.18 mol/kg LiCl solution for the value of 0.150 ± 0.005 and with 6.00 mol/kg NaCl solution for the value of 0.7600 ± 0.003. Binary mixtures were measured on the preparation day as well as on day 1, 2, 3 and 6.

3.2.2.4. Loss on drying

LOD of polymers was measured as a pre-test with Halogen Moisture Analyzer HX204 (Mettler Toledo, Ohio, USA) at conditions of 115 degrees and the measuring time was circa 2 min per 2 g of sample. In addition, LOD measurement was used for the calibration model, which is later presented in more detail.

3.2.2.5. Particle size distribution

Particle size distribution of each polymer was carried out with LS 13 320 Laser Diffraction Particle Size Analyzer (Beckman Coulter Inc., Danaher Corporation, California, USA). The pre-test measurements were performed for polymers kept at ambient conditions and after 9 days particle distribution was measured again when polymers were kept in condition of RH 75%. The polymers were cautiously stirred with a spatula once on day 7 to attain uniform moisture throughout the polymers sample.

3.2.2.6. High performance liquid chromatography

The investigation of the peroxides of HPMC and HPC were analyzed using an Agilent Infinity 1260 II HPLC system (Agilent Technologies, California, USA) with UV detection at wavelength 222 nm to determine peroxides. Chromatographic separation for investigation of the peroxides of HPMC and HPC was carried out at 45 ^{o}C using a Phenomex Synergi Polar-RP column (50x4.6 mm I.D 2.5 um) with methanol/water 75:25 (v/v) as the mobile phase in isocratic conditions. The flowrate for mobile phase was 0.1 mL/min and injection volume was 10 uL, except 4.0 uL for TPP stock solution analysis.

TPO stock solution was prepared by weighing approx. 25 mg of TPO and transferred into a 100 mL volumetric flask, then diluted to volume with MeOH. The TPO standard solution was prepared by diluting 2 mL of TPO stock solution into a 100 mL volumetric flask with MeOH as well as LOQ solution, except 5 mL of TPO standard solution was diluted. Preparation of TPP stock solution was performed by weighing approx. 20 mg of TPP and transferred in a 100 mL, then filled the flask up to neck, sonicated solution for 5 min, and finally filled up to volume. The absence of TPO in the TPP stock solution was verified by performing a preliminary HPLC analysis with UV detection at 203 nm, and TPO/TPP ratio of maximum 3/97 was checked before continuing sample preparation.

Preparation of sample solution with 50 mg/mL final concentration was performed by weighing approx. 500mg of sample (each polymer) and dissolved into 5 mL of MeOH using a 10 mL volumetric flask. 4 mL of TPP stock solution was added and stirred for 30 min with magnetic stirrer at RT, then diluted to volume with MeOH. An aliquot was transferred into a 10 mL centrifuge tube and centrifuged at 14 500 rpm for 5 min before supernatant was collected for HPLC vial. TPO control sample was prepared the same as sample solutions,

except no sample was weighed before pipetting 4 mL of TPP stock solution and adding 5 mL of MeOH.

HPMC Pharmacoat-C AN6 and HPC Klucel® EF as well as the same but expired samples of them and Klucel® EXF, LH-21 and LH-31 from ambient temperature were analyzed. Three parallel samples were made from EF and EF exp. In addition, all selected samples except AN6 and AN6 exp. were analyzed from RH 75 % and RH 5%. Samples in RH 75% were measured after two days when RH was 65% and after eight days. Samples from RH 5% were also measured after eight days. The results of the peroxides were analyzed by using Empower™ software (version 3.6., Waters Corporation, Massachusetts, USA) in samples were calculated by an equation (5).

$$\frac{(sample\ (area) - control\ (area))}{std\ (area)} \cdot \frac{std\ weight\ (mg)}{std\ volume\ (ml)} \cdot \frac{diluted\ volume\ (ml)}{dilution\ volume\ (ml)} \cdot \frac{100\%}{100\%} \cdot \frac{1}{278\frac{g}{mol}} \cdot 10^6 \frac{nmol}{mol} \cdot \frac{sample\ volume\ (ml)}{sample\ weight\ (g)} = \text{nmol/g} \quad (5)$$

3.2.2.7. X-ray powder diffractometry and scanning electron microscopy

X-ray powder diffractometer SmartLab (Rigaku Corporation, Tokyo, Japan) was used to execute for the polymers to obtain information about their crystallinity. SEM were performed with benchtop emission scanning electron microscope JSM-IT800 (JEOL Ltd., Tokyo, Japan) to view the shape of the polymers.

3.2.2.8. Measurements of binary mixtures

The binary mixtures were prepared as explained in section 3.2.1.3. Preparation of binary mixtures. After mixing the binary mixture was shared in four Aqualab sample cups. The water activity was measured from another cup and NIR was measured before Raman spectra from the other. The sample cups analyzed were transferred into the closed desiccators of RH 5% and RH 34%. The relative humidity of 34 % was prepared with saturated salt solutions of magnesium chloride hexahydrate (MgCl * 6 H_2O). The measurements were repeated for samples of both conditions on day 1 and on selected days, following their transformation until the hydrate conversion was completed from THM to THA.

3.2.2.9. Data preprocessing

PEAXACT 5 software for Quantitative Spectroscopy and Spectral Hard Modelling (version 5.4, S-PACT GmbH, Aachen, Germany) was used to analyze the collected Raman and NIR spectra by first converting the data with it and then utilizing Spotfire (TIBCO Software Inc., California,

USA) for graph plotting of quantitative results on hydrate conversion of theophylline. The factors affecting the variability of Raman signals, such as a particle size or a sample distance from a probe, are perceived to be reduced by mathematically preprocessing.[71] Hence, all spectra were standardized with SNV scaling to decrease variability in Raman and NIR signals and rubber band correction was used to correct the baseline drift and smooth the noise in the baseline.

3.2.2.10. Calibration models for quantitative results

Existing data was used to build a calibration model for quantifying theophylline anhydrate. Data consisted of Raman spectra measured from 9-14 spots within each sample. Samples were physical mixtures of THA and THM in geometric series in 10 % (w/w) intervals. For the calibration model of water content (%), LH-21 polymer was stored in petri dishes and Aqualab cups at six different relative humidity of desiccators which were 5 %, 11 %, 34 %, 43 %, 65 % and 75 %. Approximately 4 grams of each polymer were stored in a petri dish for LOD measurements and 1.5 g in Aqualab cup for NIR spectra measurement. LOD was measured twice and four NIR spectra were measured for each polymer which were used to quantify the water content.

PLS was utilized as a calibration model for the quantification of anhydrate and to model the relationship between water content (%) of binary mixtures and the NIR spectra. The calibration models were created by using PEAXACT. For evaluating the models RMSEC, RMSECV and RMSEP were used.

3.3. Results and discussion

3.3.1. Preliminary tests for polymers

The particle size distribution of polymers kept at ambient conditions (~21.5 ^{o}C & RH ~45%) are shown for HPMC (Figure 17 A) and HPC (Figure 17 B). The HPMC polymer of Benecel® K200M's particle size is larger, and the distribution range is smaller compared to other HPMC polymers which are approximately the same. Instead, HPC polymers form two populations where polymers from supplier of Shin-Etsu form one population on the left side of Figure 17 B and the other population on the right-hand side contains polymers from supplier of Ashland, except Klucel® EXF which has small particle size as well.

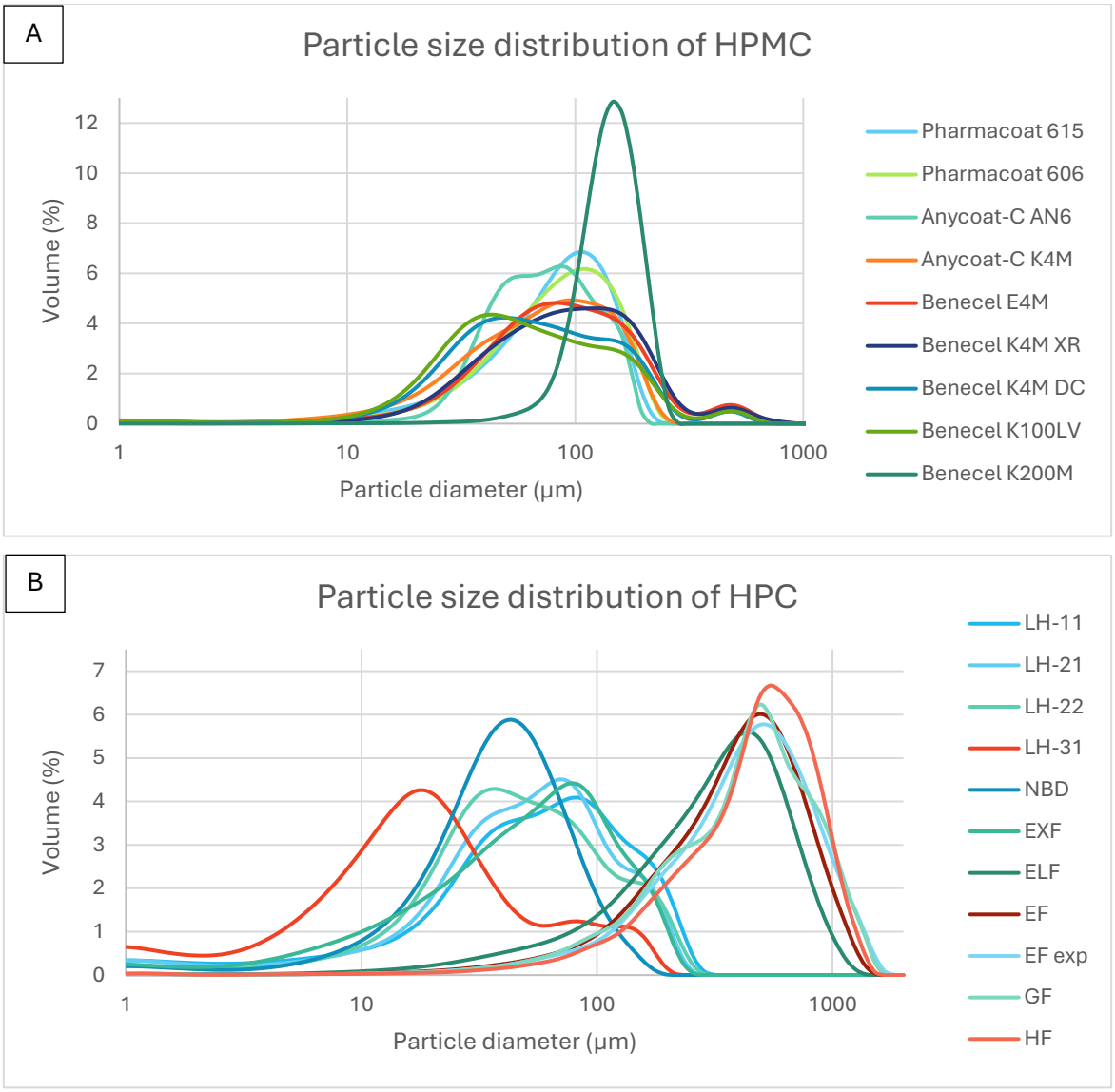

Figure 17. Particle size distribution of HPMC (A) and (B) HPC polymers kept at ambient conditions.

Figure 18 shows the particle size distribution of polymers which were kept in conditions of RH 75% and measured after 9 days. Excluding HPMC K200M, every polymers' particle size increased or decreased slightly but not notably so they were left out from Figure 5 to keep it clearer. Only K200M is shown since its particle size decreased significantly. This could perhaps be due to the sampling of particles that are randomly smaller or about the molecular weight, which is the heaviest of all HPMC sample polymers. As a comparison, HPC GF has triple the particle size compared to K200M and has a generally large particle size, but particle size change of GF was in line with the other polymers. HPC polymers ELF, EXF and EF couldn't be measured as they formed a clump in RH 75%.

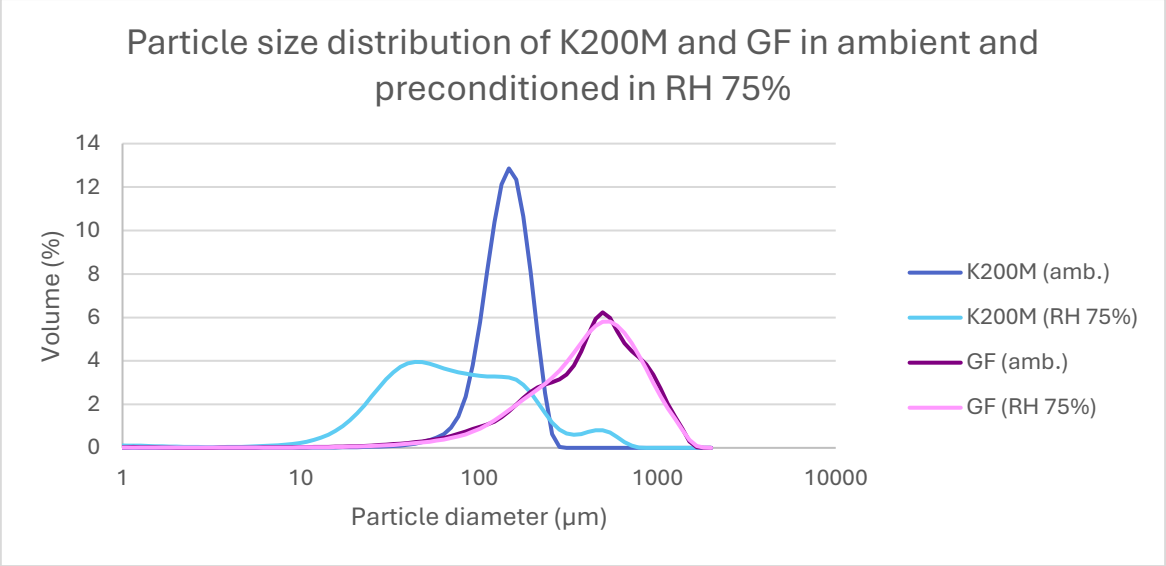

Figure 18. Particle size distribution of HPMC K200M (bright blue) and HPC GF (purple) at ambient conditions as well as K200M (light blue) and GF (lavender) kept 9 days in RH 75% (~21.5 °C).

The results of peroxides are shown in Table 3. Peroxide tests were performed only for six polymers due to the schedule and the results were calculated with an equation (5).

$$\frac{(sample\ (area) - control\ (area))}{std\ (area)} \cdot \frac{25\ mg}{100\ ml} \cdot \frac{2\ ml}{100\ ml} \cdot \frac{100\%}{100\%} \cdot \frac{1}{278 \frac{g}{mol}} \cdot 10^6 \frac{nmol}{mol} \cdot \frac{10\ ml}{0.500\ g} = \text{nmol/g}$$

Peroxide results of RH 5% and RH 75% (Table 3) were measured after eight days and RH ~65% were after two days of preconditioning. According to obtained data the formation of peroxides did not correlate the expiration date of sample, but the particle size may have as L-HPCs are smaller than Ashland Klucel® polymers which have noticeable higher number of peroxides. However, EXF has also a higher level of peroxides, but its expiration date was unknown, which may have an impact on the level. Previous study examined by Garbič et. al have illustrated that high humidity can decrease the formation of peroxide in pharmaceutical excipients.[72] The exact mechanisms are still unclear, but the potential actions could be due to water-peroxide exchange or quenching of reactive oxygen species. In this study, this pattern was also discovered when comparing in RH 5% preconditioned polymers to in RH 75% preconditioned, except for EF polymer. The result of EF may be incorrect because it differs significantly from other results, so it cannot be considered reliable. However, the formation of peroxides and features affecting it requires further investigation, as the influencing factors

may be the combined effects of several factors that are not revealed by this type of research setup.

Table 3. Peroxide results of polymers (~21.5 °C).

Code name	Peroxides (nmol/g)			
	Ambient (RH ~45%)	RH 5%	RH ~65%	RH 75%
606	160	-	-	-
AN6	167	-	-	-
LH-11	34	49	34	27
LH-22	58	74	49	43
EXF	311	310	325	298
EF	209 ± 2.4*	4	221	246
EF exp.	238 ± 11.6*	210	256	235

* The mean of three parallel samples and SD.

XRD was measured on all polymers to determine whether they are crystalline or amorphous. The data obtained from XRD is displayed in Figure 19. If there are peaks in the diffractograms, it would indicate the crystallinity of the material. The red, blue and green curves show small peaks on the right, but they are minimal and do not imply the crystal structure of polymer. None of polymers had significant peaks, which indicates that all the polymers are amorphous.

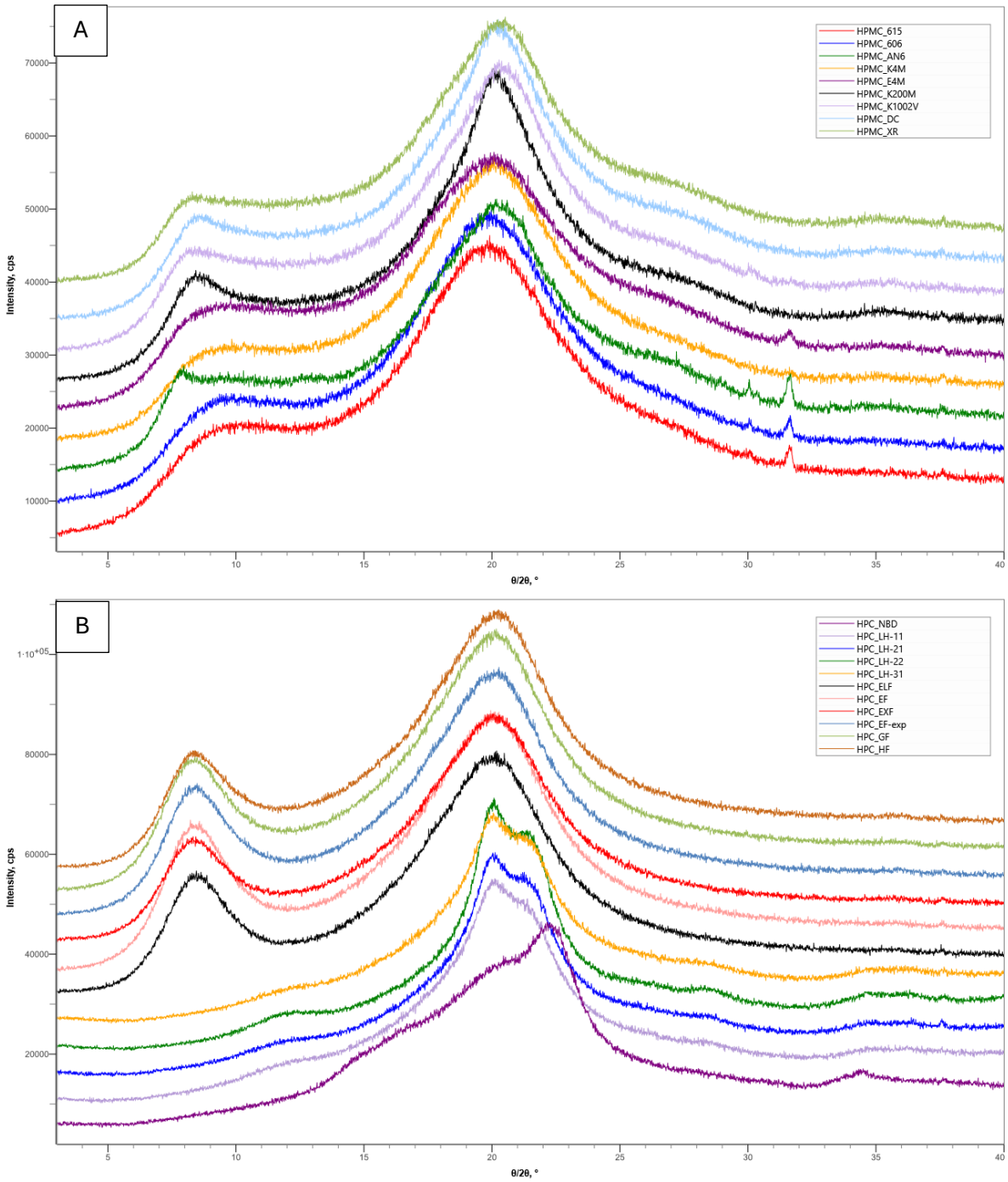

Figure 19. XRD curves of HPMC (a) and HPC (b) polymers.

Water activity during storage time in days for polymers retained in defined conditions are shown in Figures 20-22, which exhibit that polymers attain the precondition of RH 75 % (21.5 °C), most likely already before seven days and remain there. The starting points of HPMC polymers are approximately at the same level (Figures 20 and 22 A). There are two exceptions with HPMC polymers, whose initial points stand out while the other points are fairly consistent. The largest difference is between 615 and AN6 at the first measurement point (day 0), which does not seem to be explained by any property of the polymers.

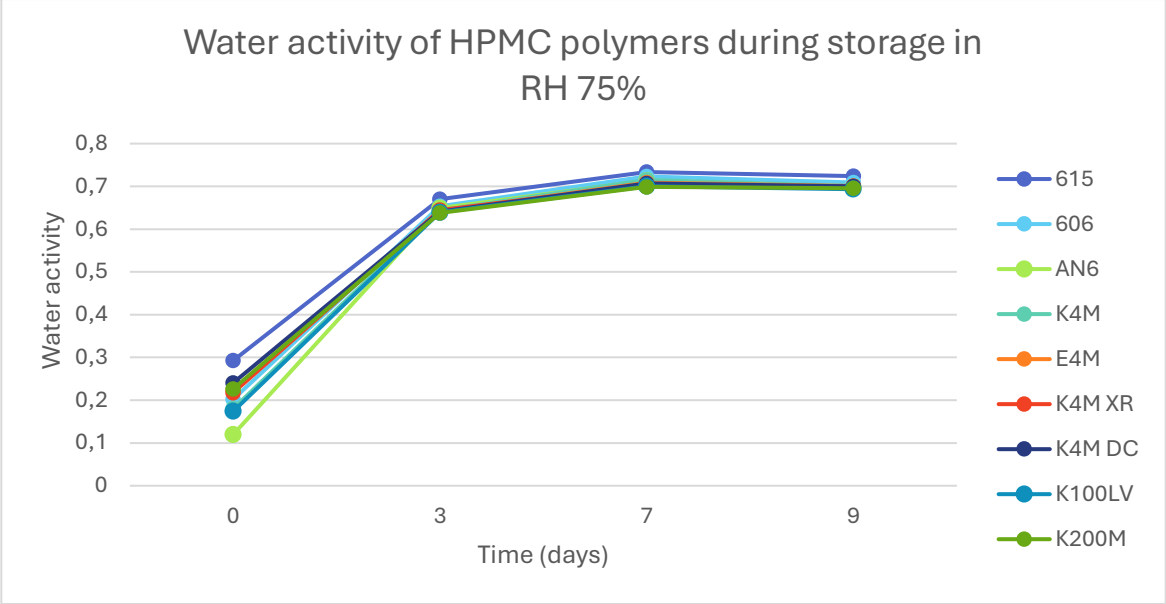

Figure 20. Water activity of HPMC polymers during storage in a desiccator of RH 75% (~21.5 ºC).

At the first measurement point HPC polymers appear to form two groups, with the Shin-Etsu supplier polymers having a lower water activity compared to the Ashland supplier polymers. EF (exp) has the highest water activity, which may be related to its expiration date, as it was the only polymer that was expired. Figures 20 and 21 are simpler and more straightforward to interpret when compared to Figure 22 A and B, which may be due to the fact that polymers distinctly absorb water more easily than they release it.[73]

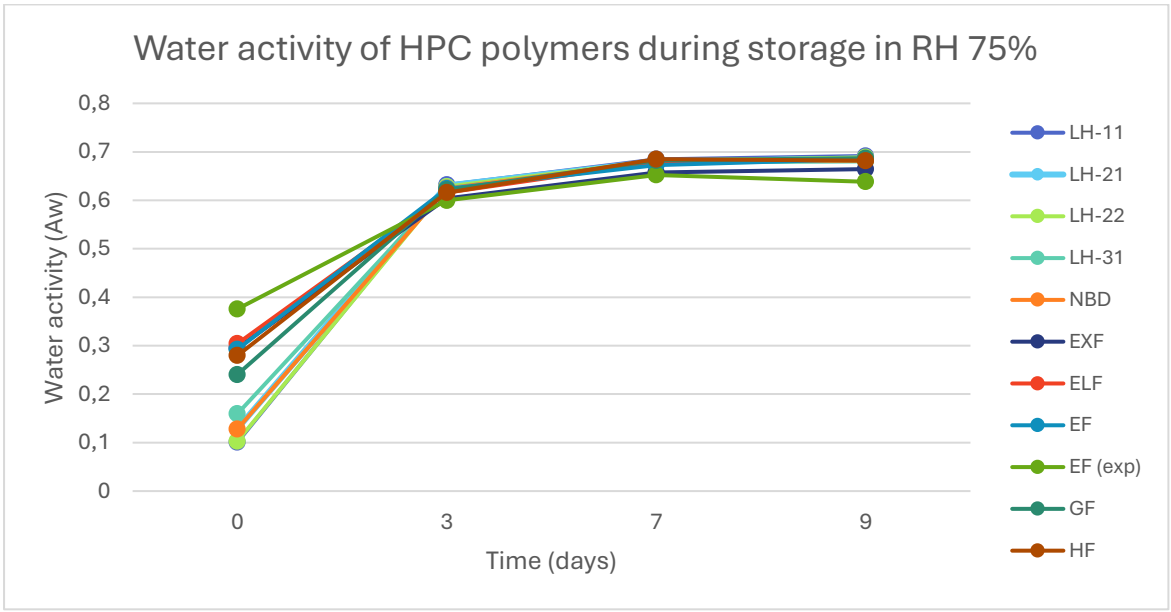

Figure 21. Water activity of HPC polymers during storage in a desiccator of RH 75% (~21.5 ºC).

HPMC polymers (Figures 20 and 22 A) have less variation between the initial points compared to HPC polymers (Figures 21 and 22 B) which have a larger dispersion of starting points. In RH 5% both polymers show a decreasing trend in water activity from day one and the dispersion of the first day measurement points is quite similar. Nevertheless, it is noticeable that the order of water activity measurements at the starting points remains the same as the points on day eight with a few exceptions, at least for HPC polymers (Figure 22 B).

With HPMC polymers (Figure 22 A), the trend is more variable which may be a result of measuring order. The HPMC polymers that were measured first (615, 606, AN6 and K4M) have the lowest water activity at every measurement point. Excluding the first measurement point, which was made for polymers at ambient conditions (~21.5 °C & RH ~45%). However, it is noteworthy that the polymers at ambient had the lowest water activity results have increased their water activity results at the first measurement point. During all the measurements, in RH 5% the humidity increased by up to RH 25%, and in RH 75% the humidity decreased to 55%. When evaluating the results, a possible change in humidity due to opening the desiccator must be considered.

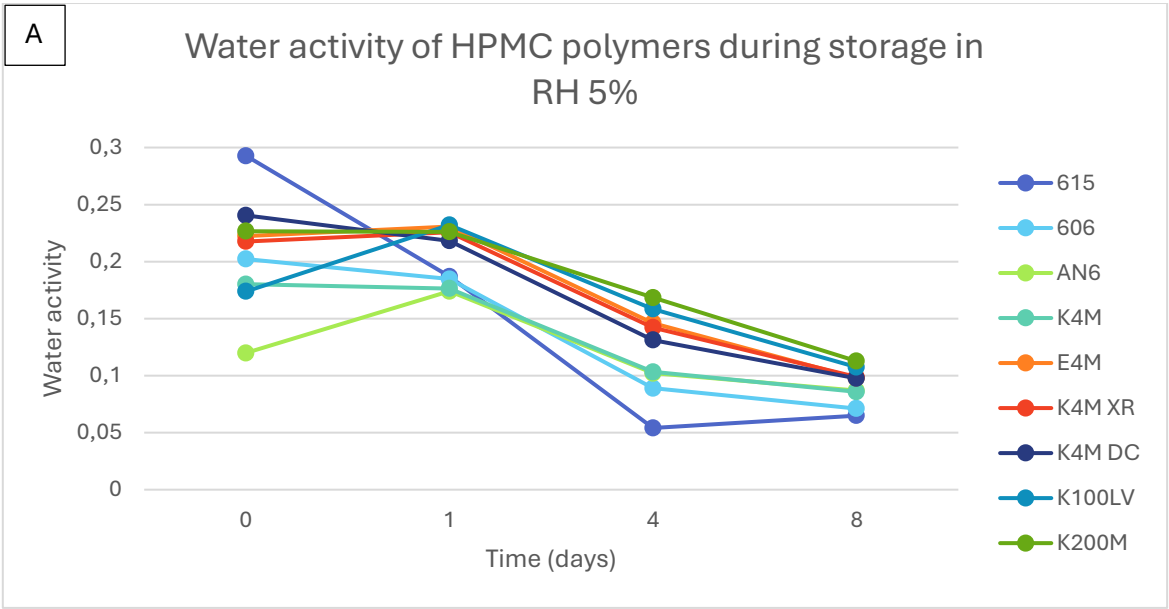

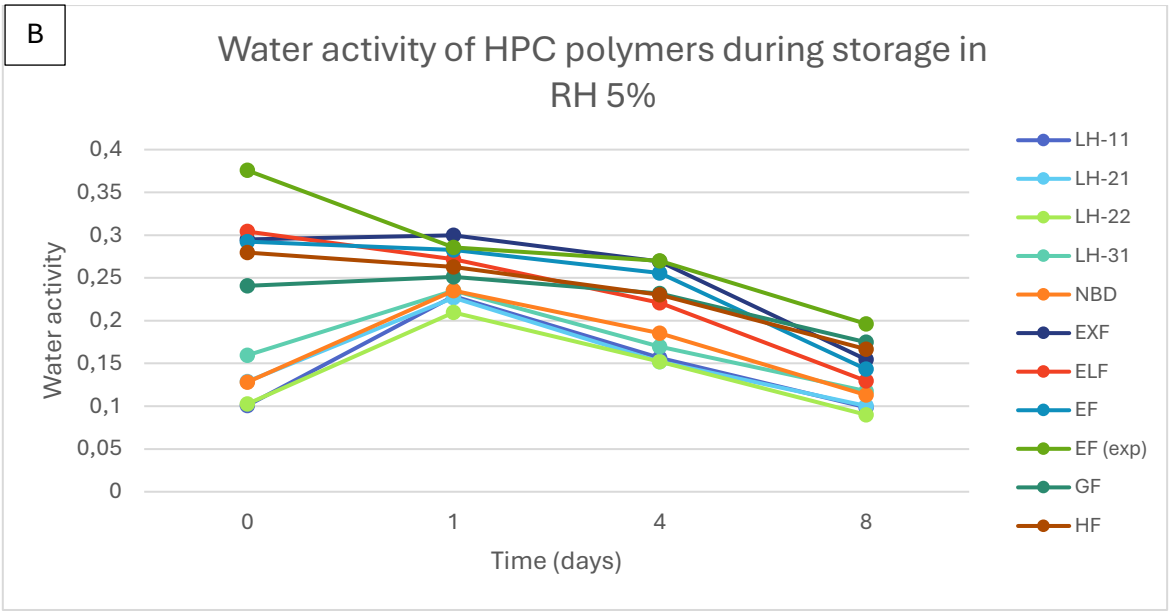

Figure 22. Water activity of HPMC (A) and HPC (B) polymers during storage in a desiccator of RH 5% (~21.5 °C).

3.3.2. Binary mixtures

3.3.2.1. Water activity results

At the starting point and after equilibrium, the water activity of binary mixtures is basically the same regardless of the polymer, including between HPMC and HPC. As in the preliminary tests, the A_w results of HPMC polymers which had been preconditioned in RH 75% were slightly higher than those of HPC polymers, which was also observed in the preparation of the binary mixtures. Excluding E4M and XR, the A_w results of HPMC were usually over 0.7 and for HPC polymers the results were slightly under 0.7. None of the properties of E4M and XR appeared to explain the reason, as they did not differ significantly from other HPMC polymers in any of their properties.

The difference of A_w results of RH 75% preconditioned polymers may be due to the generally more hydrophilic nature of HPMC polymers compared to HPC polymers.[74] Essentially, methoxy groups reduce hydrophilicity and hydroxypropyl groups increase hydrophilicity because the latter can form hydrogen bonds with water. However, in the case of cellulose polymers, the degree of substitution of methoxy and hydroxypropyl groups can have a notable effect, and therefore, their hydrophilic behavior is complex. HPMC polymers contain both groups, which in the right proportion may actually improve hydrophilicity because methoxy groups can prevent too strong intra-polymer interactions, allowing water to

penetrate between the polymer chains. Therefore, due to molecular structure and particle level of HPMC polymer, it is able to retain water better than HPC, making it more hydrophilic.

Depending on the RH of the desiccator, the water activity of the mixtures at equilibrium was either approx. 0.35-0.38 in RH 34% or approx. 0.02-0.05 in RH 5%, which can be observed from Figure 23 (A and B). These are just examples, one binary mixture made from HPMC polymer and the other made from HPC polymer in both conditions. The remaining water activity graphs of the binary mixtures are provided in Appendices 1 (A_w of HPMC) and 2 (A_w of HPC). Figure 23 (on the right side) shows that the mixtures in desiccator of RH 34% stabilized after a day and remained the same. In turn, the A_w results of the mixtures in the desiccator of RH 5% decreased over the days. This may have been due to the desiccator's silica being unable to reduce the humidity to 5% in a day. In contrast, the desiccator of RH 34% reached the desired humidity within a day.

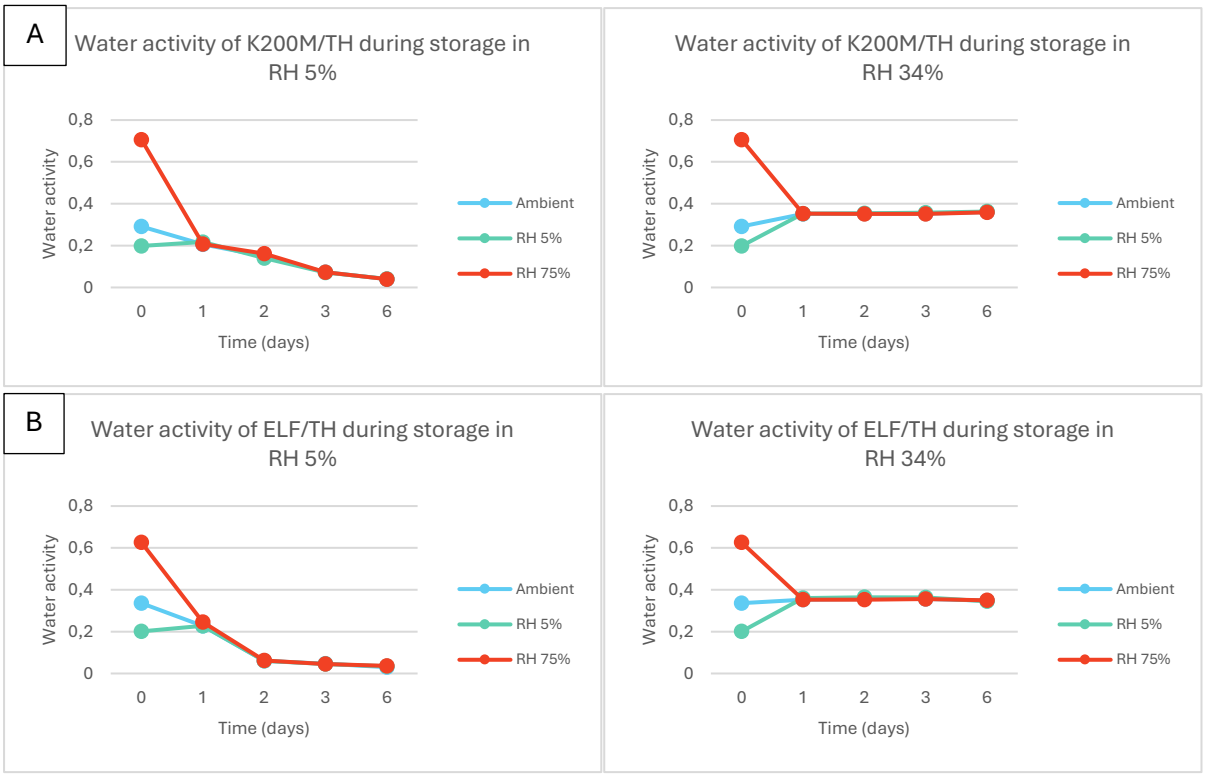

Figure 23. Water activity of binary mixtures made from HPMC polymer K200M (A) and HPC polymer ELF (B) during storage in RH 5% (left) and RH 34% (right). The pretreatment conditions are with different colors.

HPC/TH mixtures made of polymers from the same supplier behave similarly in terms of A_w results. However, there's a difference between the results of RH 5% and ambient conditions at the first measurement point when observing the different suppliers, Ashland and Shin-Etsu. This can be observed Figure 24 (A and B), which are A_w results of Shin-Etsu and Ashland polymer binary mixtures in a desiccators of RH 34%. The A_w results of different suppliers in a desiccator of RH 5% are available in Appendix 3.

Water activity measures the free water in a material. An A_w indicates how easily a compound releases or absorbs water its surroundings. Shin-Etsu polymers at ambient or preconditioned in RH 5% have a lower water activity than Ashland polymers, which indicates they are having less free water at the first measurement point. However, this does not correlate with what can be visually interpreted from NIR spectra later in the NIR results section, but it could be due to the degree of substitution of the hydroxypropyl groups. The relationship between water activity and free water in binary mixtures could potentially be further investigated later.

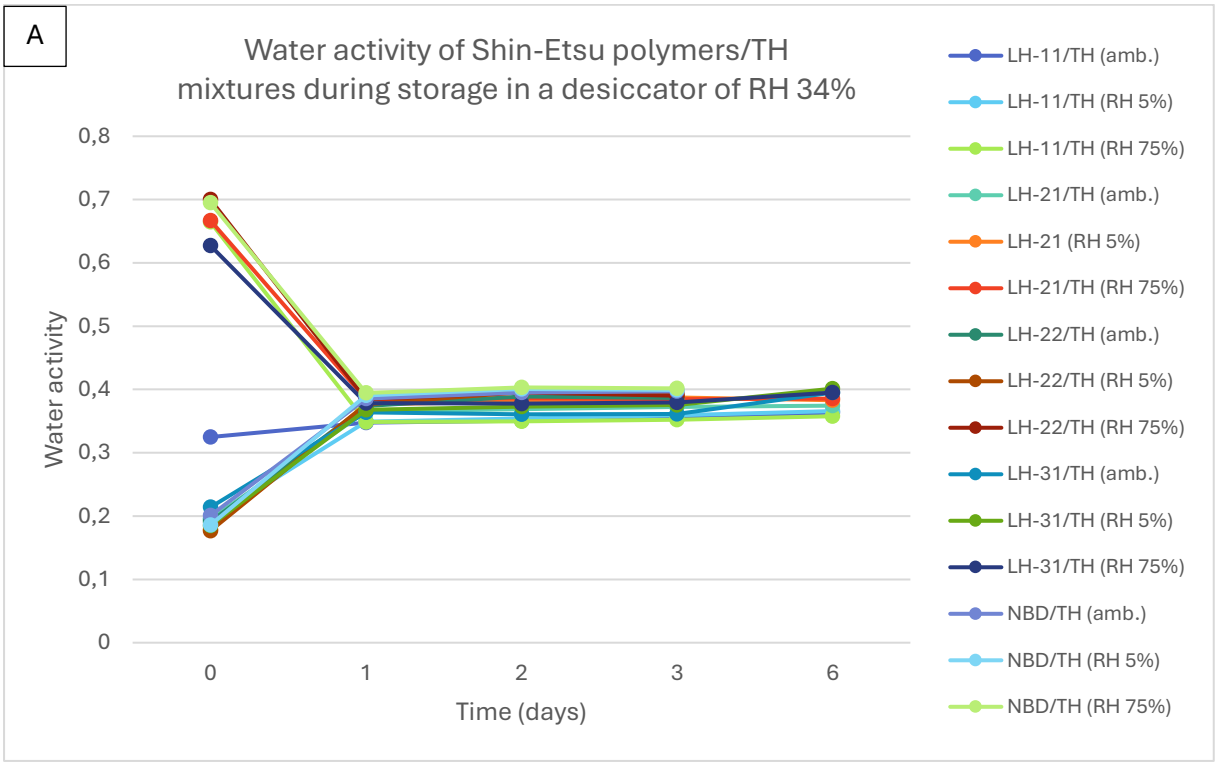

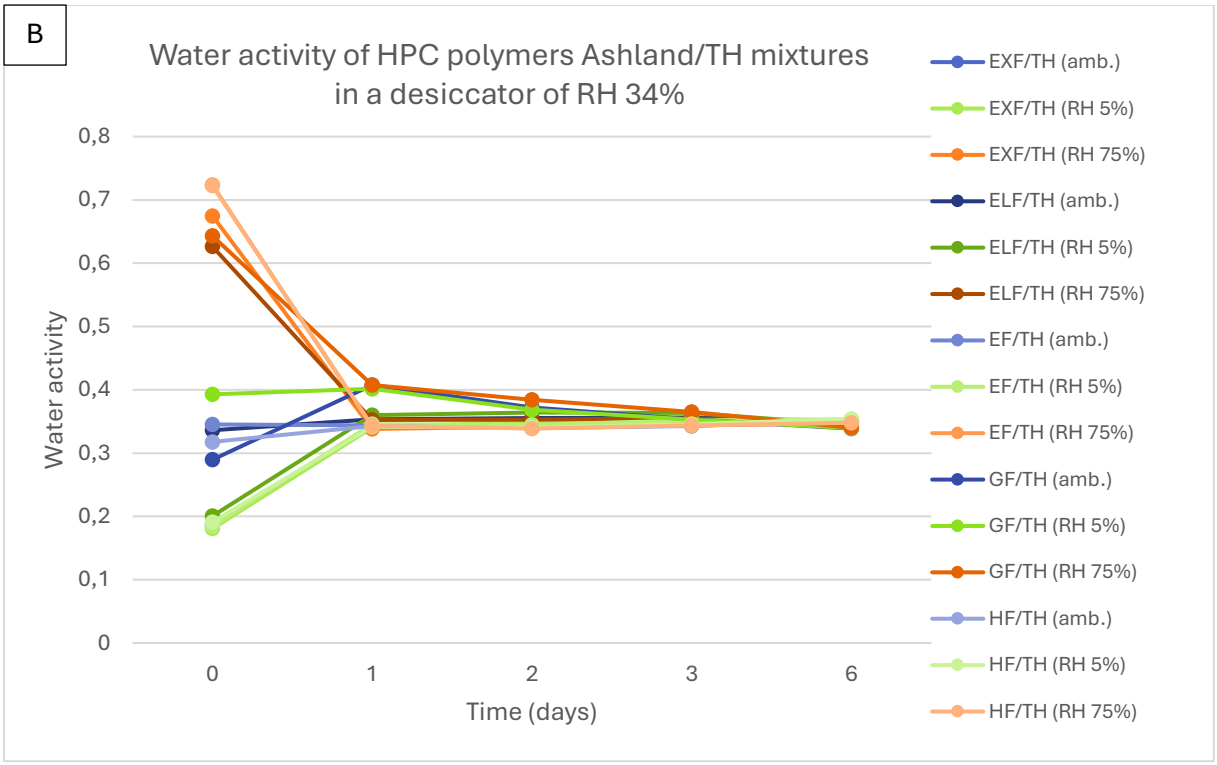

Figure 24. Water activity of binary mixtures made from HPC polymer of Shin-Etsu (A) and Ashland (B) supplier during storage in RH 34%.

Based on preliminary experiments of polymers in this study, it was observed that water activity of polymers remains the same after 7 days (Figures 20-22). The water activity measurements were continued for four binary mixtures until the eighth day and indeed the water activity of binary mixtures did not change any further after 6 days regardless of the polymer (Figure 25 A and B & Appendix 4). The rest of the water activity of the binary mixtures was measured only up to 6 days (Appendices 1 and 2).

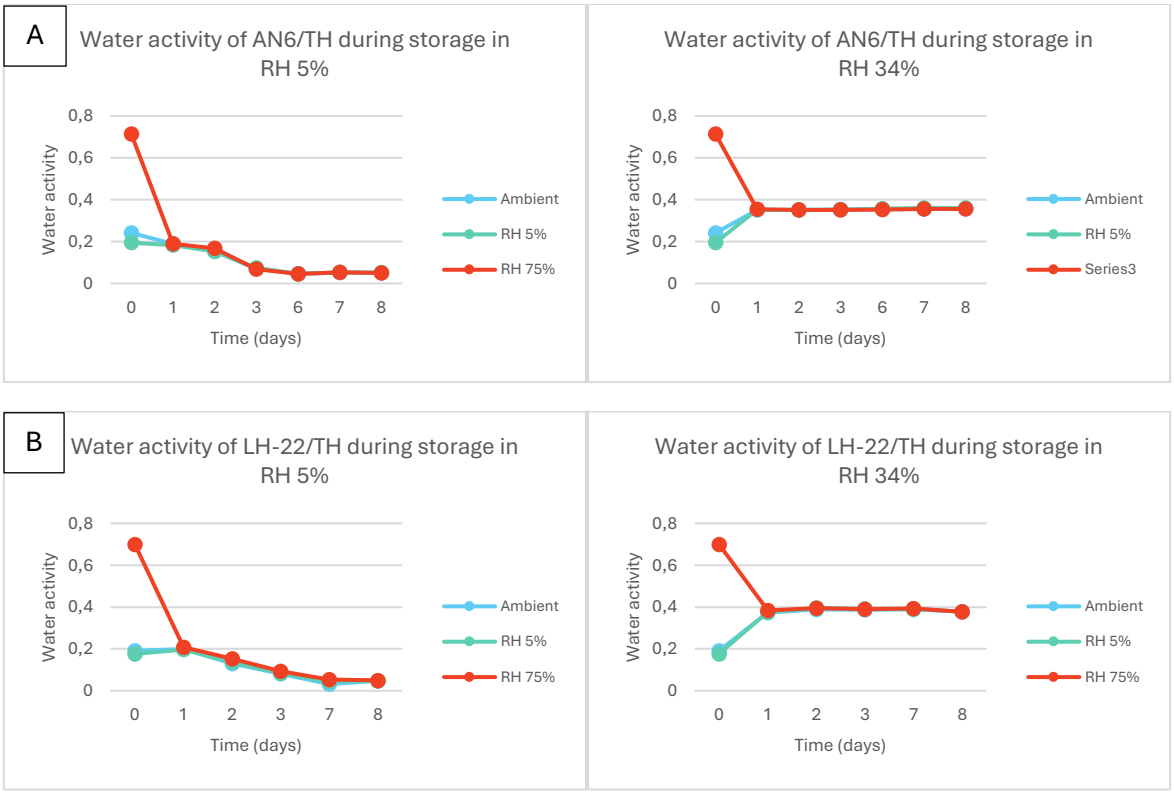

Figure 25. Water activity of binary mixtures made from HPMC polymer AN6 (A) and HPC polymer LH-22 (B) during storage in RH 5% and RH 34%.

3.3.2.2. Raman results

The Raman spectra of the anhydrate and monohydrate appear quite similar, but there are a few points in the entire spectral range where the conversion forms can be distinguished. The hydrate conversion of theophylline is observed in the spectrum at 1650-1750 cm^{-1} from C=O, which was used in this study to monitor the hydrate conversion.[75–77] Other regions are 1540-1585 cm^{-1} and 1585-1630 cm^{-1} from C=N and C=C stretching, where two peaks of anhydrate exhibit a small shift to the left, and 1160-1203 cm^{-1} from C-C and C-N bending vibrations, where the anhydrate has one peak, and the monohydrate has two peaks at this point in the spectrum.[76,77] These differences can be distinguished in Spectrum 1. The raw data of theophylline monohydrate, which was pretreated in RH 75% for over a week, and the anhydrate form of theophylline are on Appendices 5 and 6. Moreover, other differences are visible in the spectra, such as a large peak at 550 cm^{-1} in the monohydrate and a clearly smaller peak in the anhydrate, or a single peak in the anhydrate compared to a branched peak of the monohydrate below 200 cm^{-1}. However, these are already in such small wavelength ranges that they are not reliable for quantification with the equipment used in this study.

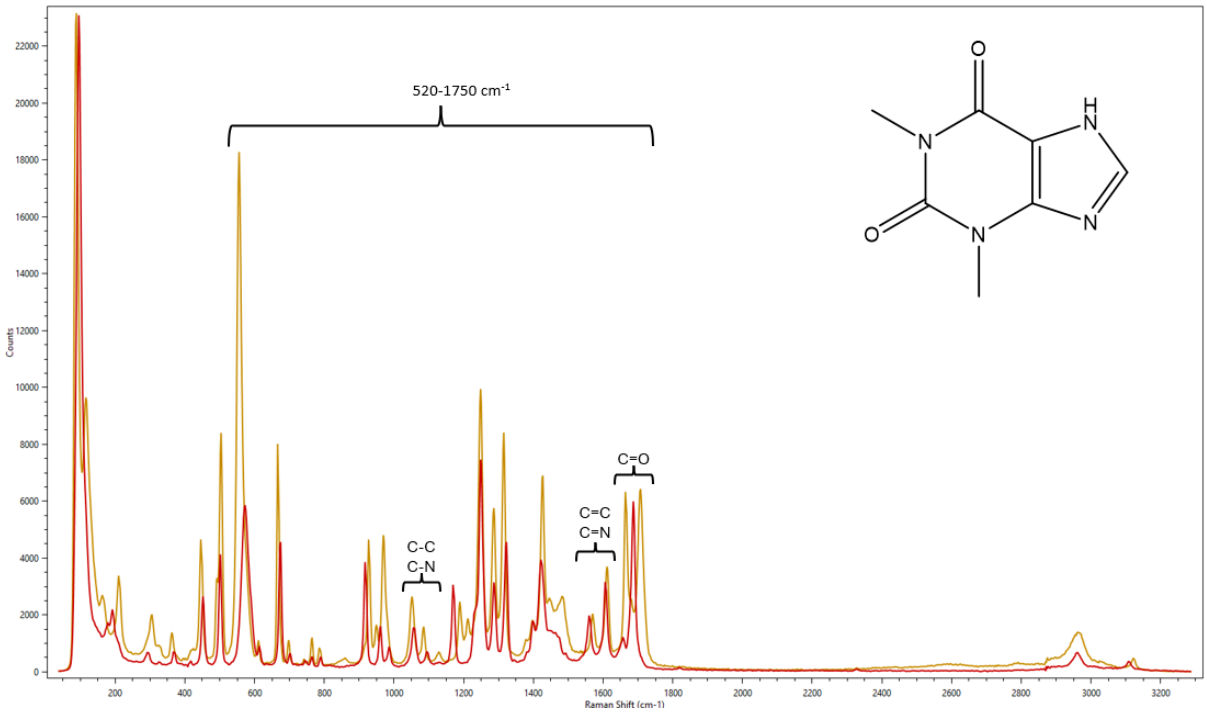

Spectrum 1. The Raman spectra of the anhydrate (red) and monohydrate (yellow) with the marked spectral range used for quantification.

The calibration model for the Raman results were made of using 73 training samples of physical mixtures of THA and THM with 0, 10, 30, 50, 70, 90 or 100% THA and 46 test samples of physical mixtures with 20, 40, 60 or 80% THA. The coefficient of determination (R^2) value, RMSEC, RMSECV and RMSEP were used to evaluate the model with a spectral range of 520-1750 cm^{-1}. SNV was used for all Raman spectra to normalize the spectral data and correct baseline shifts. The values of the calibration model for quantitative results are visible in Table 4.

Table 4. Quantitative model parameters of theophylline anhydrate on Raman.

Spectral range (cm^{-1})	R^2	RMSEC	RMSECV	RMSEP
520-1750	0.996048	2.20602	2.27025	2.62431

The quantitative model is not ideal since the predicted change in binary mixtures from monohydrate to anhydrate was not 100% even when the change was believed to be completed. Based on visual inspection of the spectra, it can be assumed that the change is completed when the prediction was over 85% and the model was good enough to evaluate the quantitative results of binary mixtures.

The binary mixtures were stored in two different conditions, in a desiccator of RH 5% and RH 34%. The change rate was slower for the samples in the desiccator of RH 34% than in RH 5%, which was expected. Based on a previous experiment arranged at Orion (data not shown), hydrate conversion occurred quickly in samples stored in a desiccator RH 5%, so it is easier to evaluate which factors possibly affect the conversion kinetics for samples stored in a desiccator of RH 34%. After mixing with Turbula all binary mixtures were further mixed with a spoon three times clockwise and counterclockwise before dispensing into Aqualab cups. The results for LH-31 are uncertain as it was one of the first polymer binary mixtures to be made and was not mixed before dispensing. This may have contributed to the model substance and polymer not having contact and surface area as much as the other binary mixtures.

In this study, the effect of the molecular weight, particle size, as well as the degree of substitution rate of the hydroxypropyl and/or methoxy groups of the polymers on the conversion of theophylline hydrate in binary mixtures was investigated. First, the effect of the difference in the molecular weight was examined with HPMC polymers 615 and 606, since their other properties are practically the same (Table 2). Theophylline monohydrate in binary mixtures made of RH 5% and RH 75% preconditioned polymers are converted to theophylline anhydrate at approximately the same rate with both polymers, but at ambient preconditioned, the conversion was slightly faster with 606 despite storage conditions. Figure 26 displays the hydrate conversion in a desiccator RH 34% and the conversion in RH 5% is Appendix 7. The MW of 606 is lighter, but nothing can be concluded about this yet.

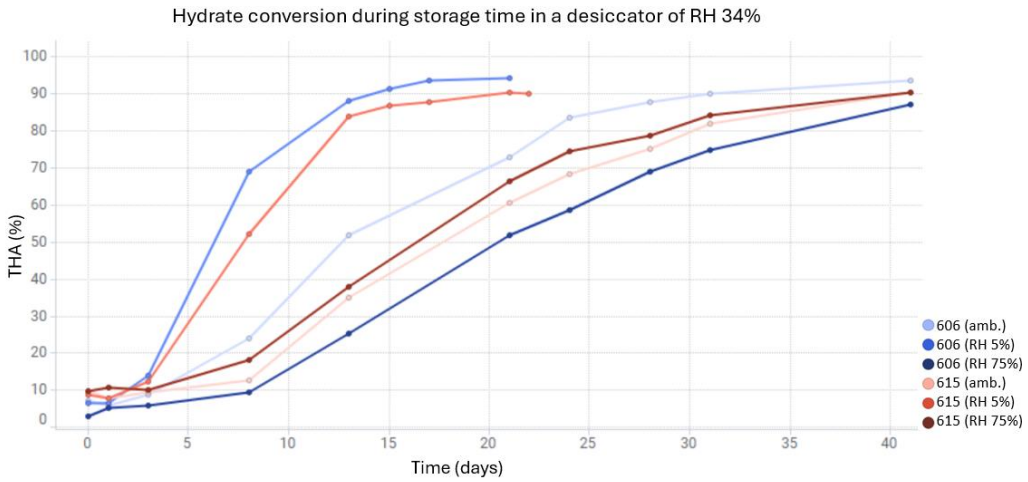

Figure 26. 615/TH and 606/TH binary mixtures in a desiccator of RH 34% with polymers preconditioned in RH 5%, ambient and RH 75%.

Secondly, binary mixtures made from K200M and DC polymers are compared. In addition to MW, they differ in particle size (149 µm & 67 µm, respectively). Opposite to earlier, THM in the binary mixture made from the heavier polymer (K200M) is converted faster if preconditioned only in RH 75% in both storage conditions (Figure 27 & Appendix 8). Other conversion rates are approximately the same. However, with this pair it is worth noting that the binary mixture made of a preconditioned in RH 75% polymer with a smaller particle (DC) size converts more slowly. Smaller particle size means more surface area, which might protect better against drying and therefore, the conversion. Thus, THM in a binary mixture made from a smaller particle size converts slightly slower compared to a larger particle size polymer as it did with 615 (approx. 87 µm) and 606 (approx. 89 µm).

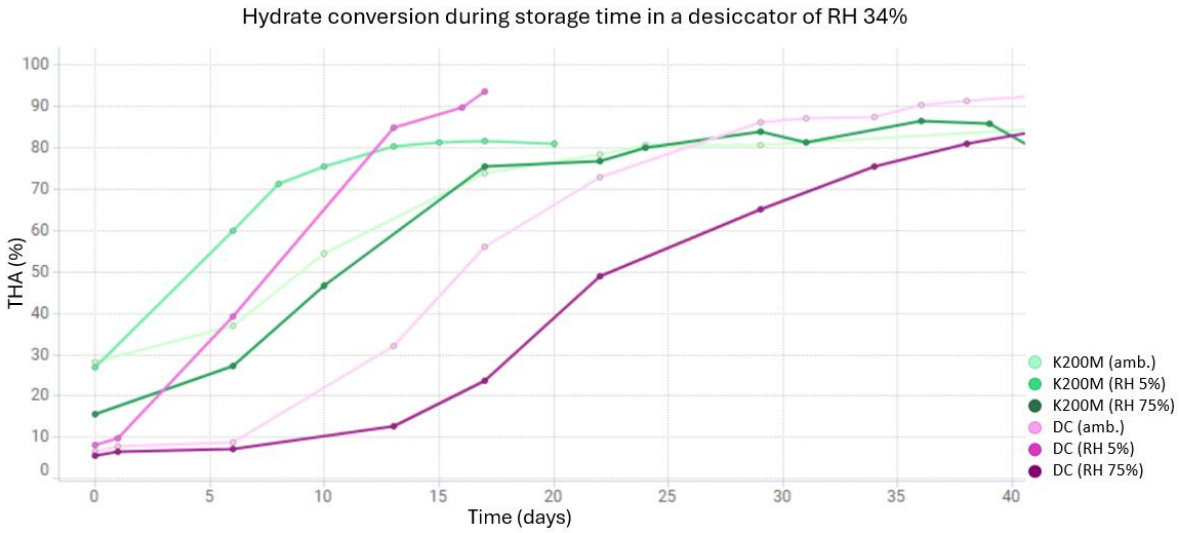

Figure 27. K200M/TH and DC/TH binary mixtures in a desiccator of RH 34% with polymers preconditioned in RH 5%, ambient and RH 75%.

Finally, when comparing binary mixtures made from K100LV and DC polymers, THM converts faster in binary mixtures of K100LV than DC at each preconditions regardless of the storage conditions (Figure 28 & Appendix 9). The MW of K100LV is lighter, and it has a 6 µm smaller particle size. Moreover, its hydroxypropyl content is 1 percentage point higher. Higher HDP content may increase the hydrophilicity of the molecule, which improves the water solubility in general. More hydrogen bonds are possibly formed between water molecules and the HDP groups, which could be expected to accelerate the conversion from TMH to THA. Hence, this interaction could be an explanatory factor, since the water molecule of TMH is exposed to the formation of hydrogen bonds with HDP groups of polymer. However, it is not distinct yet if the 1 percentage point higher HDP content accelerated the conversion.

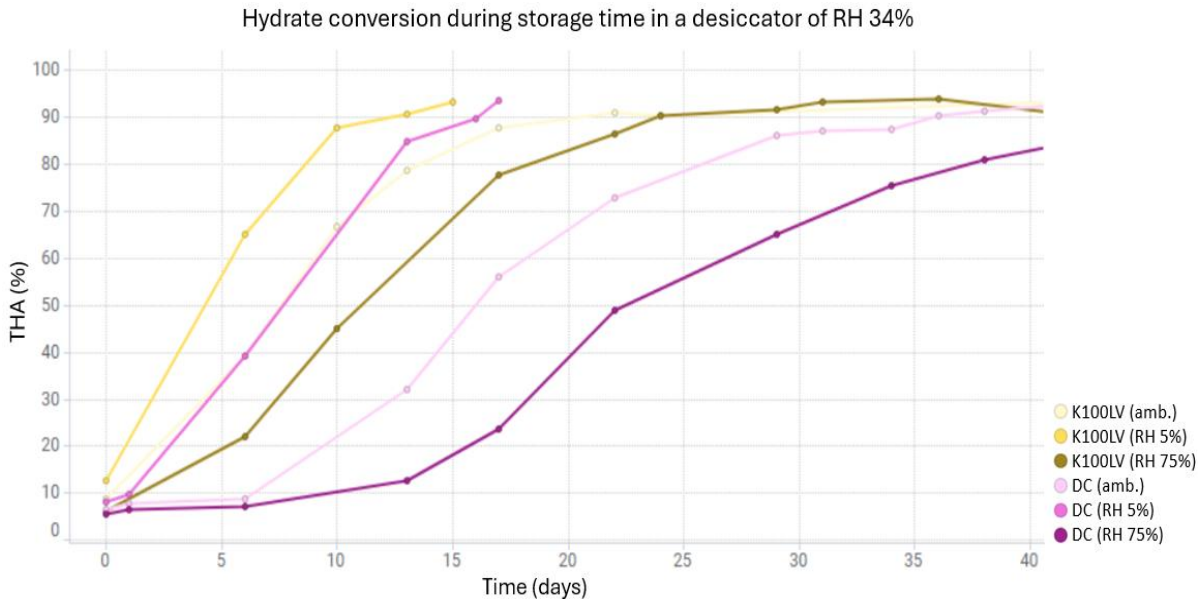

Figure 28. K100LV/TH and DC/TH binary mixtures in a desiccator of RH 34% with polymers preconditioned in RH 5%, ambient and RH 75%.

In the case of HPC polymers, higher molecular weight seems to accelerate hydrate conversion. GF and ELF have different MWs (370000 g/mol & 40000 g/mol, respectively) and particle sizes (461 µm & 339 µm, respectively). At the same time, GF and EF (80000 g/mol) can be compared, which differ in addition to the properties mentioned above from HDP content. EF has approximately a 1 percentage point higher HDP content. In both cases, GF is significantly heavier and has a larger particle size, and the conversion of TMH to THA in binary mixture is faster than ELF or EF (Figure 29 & Appendix 10). As mentioned before, a smaller particle size indicates a larger surface area that could protect against the conversion. Hence, the conversion rate is slower with ELF and EF. However, according to Zografi et al. water uptake does not depend on the specific surface area if the material can absorb water into its solid structure.[78] Thus, the surface area may not have a definitive impact and further investigation is required before any conclusions can be drawn.

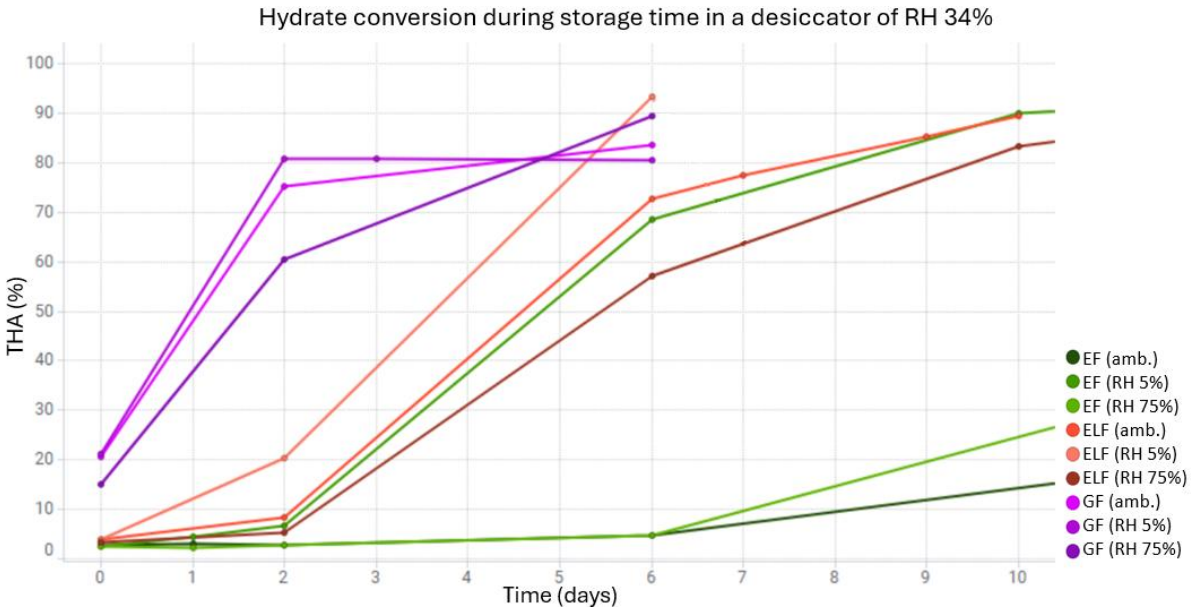

Figure 29. GF/TH and ELF/TH and EF/TH binary mixtures in a desiccator of RH 34% with polymers preconditioned in RH 5%, ambient and RH 75%.

It should also be noted that on the day of preparation (day 0), the binary mixtures made from K200M and GF had already been converted by about 15-30%, depending on the preconditioning. In turn, the conversion of mixtures made from other polymers is less than 15% and most of them are less than 10%. K200M and GF are clearly heavier in MW compared to those polymers, whose MW were precisely known. Therefore, a considerably heavier MW could accelerate the hydrate conversion.

In addition to MW and HDP content, HPMC polymers also have methoxy content, which may have a role in the rate of hydrate conversion. Let us explore this MT content further by comparing binary mixtures made of E4M and XR, which have the same MW, but XR has a 5 percentage point lower MT content. In addition, the particle size of E4M (90 µm) differs only slightly from XR (94 µm). Their rates of conversion do not appear to differ from each other (Figure30) regardless of preconditioning or storage conditions. In this case, the MT content does not appear to affect the conversion rate.

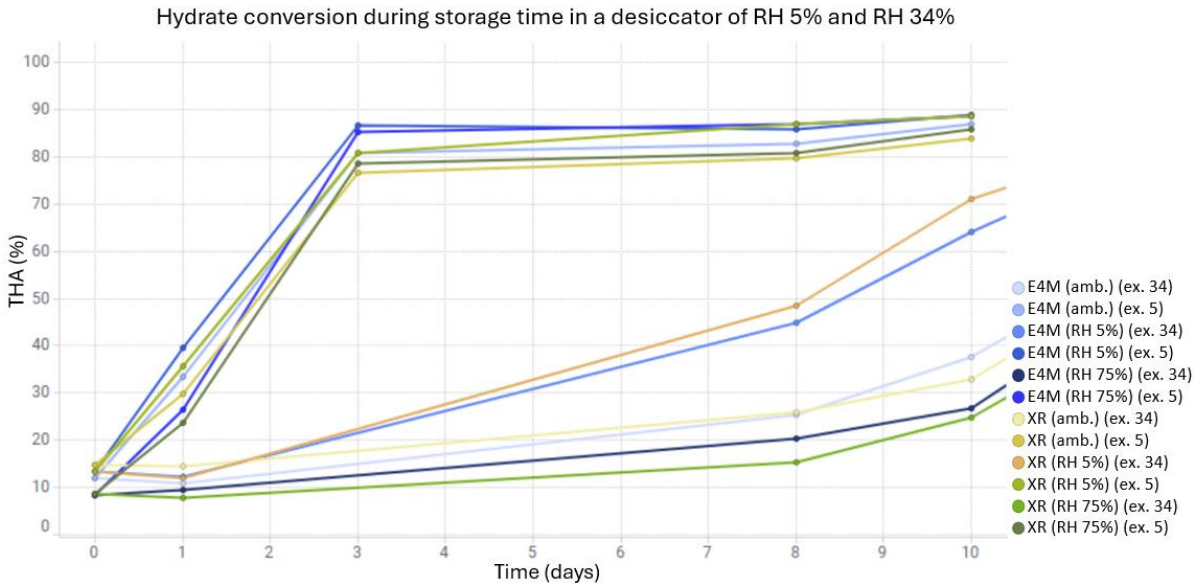

Figure 30. E4M/TH and XR/TH binary mixtures in a desiccator (= ex.) of RH 5% and RH 34% with polymers preconditioned in RH 5%, ambient and RH 75%.

However, when comparing E4M to DC (67 µm), their particle size differs more than between E4M and XR. Even in this case, the larger particle size E4M (90 µm) as a component of binary mixture drives the THM to convert faster (Figure 31 & Appendix 11). Further, a 6 percentage point lower MT content of DC may have a role to play by reducing the hydrophobicity of the polymer, but instead of increasing the rate of the conversion, it actually decreases it compared to a higher MT content of E4M.

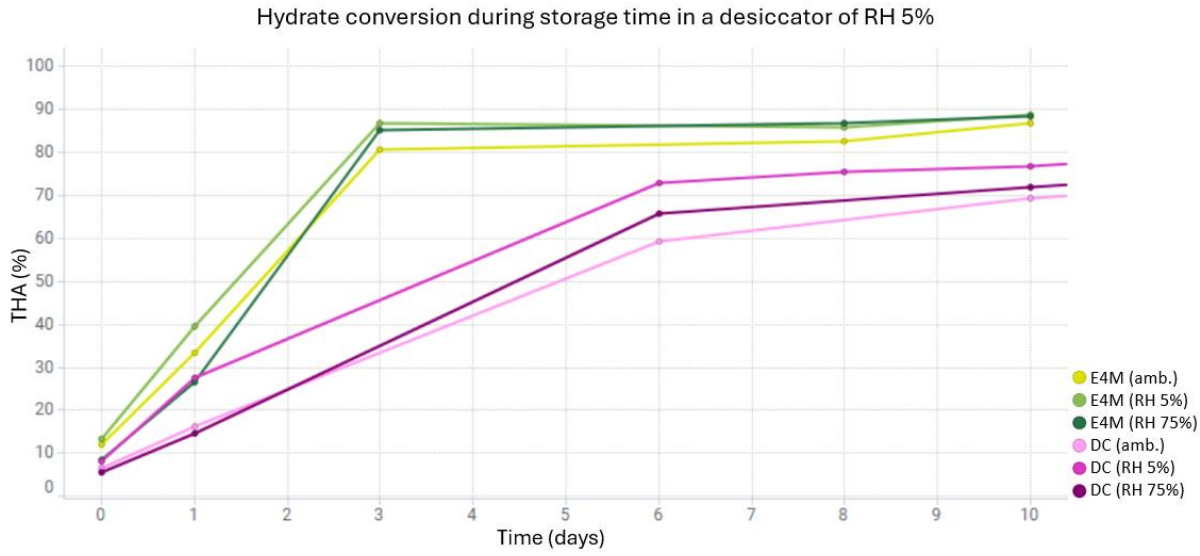

Figure 31. E4M/TH and DC/TH binary mixtures in a desiccator of RH 5% with polymers preconditioned in RH 5%, ambient and RH 75%.

When comparing AN6 and K4M, AN6 is converted faster only in a desiccator of RH 5% when polymers are preconditioned at ambient conditions (Figure 32 & Appendix 12). However,

when polymers preconditioned in RH 5% and storage condition of RH 34% K4M converts faster (Figure 32 & Appendix 13). Other rates of conversion are practically the same (Figure 32). AN6 also has a 6 percentage point higher MT content, which correlates with the previous polymer pair that one with a higher MT content has a faster hydrate conversion rate. This is just an assumption, since the exact value of the molecular weights was not known, so it was not considered. AN6 and K4M also differ slightly in HDP content, only a 0.5 percentage point. However, this may be relevant when considering other pairs that have a difference between HDP contents.

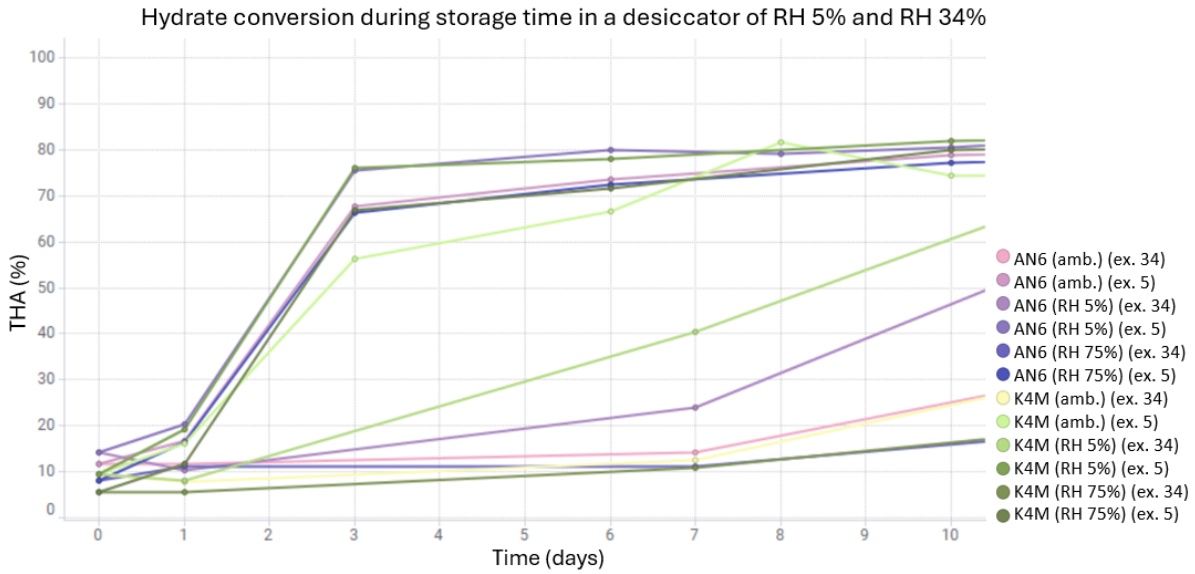

Figure 32. AN6/TH and K4M/TH binary mixtures in a desiccator (= ex.) of RH 5% and RH 34% with polymers preconditioned in RH 5%, ambient and RH 75%.

HPC polymers do not have MT content, so only comparing the effect of HDP content can be studied. NBD (40 µm) has a 5 percentage point higher HDP content, but a smaller particle size compared to LH-22 (44 µm). According to previous polymer pairs, those with a larger particle size convert faster, as does with this pair (Figure34). However, an assumption must be made that these polymers have the same MW or that it does not affect, since the MW of Shin-Etsu polymers has not been reported. When comparing LH-22 with LH-21 (50 µm), the former converts faster (Figure 33). More detailed figures are displayed in Appendices 14-18. In turn, LH-21 has a larger particle size, but not markedly. Therefore, it may be possible that a higher HDP content slows down the conversion, because LH-22 has a lower HDP content compared to both polymers: 5 percentage point to NBD and 3 percentage point to LH-21.

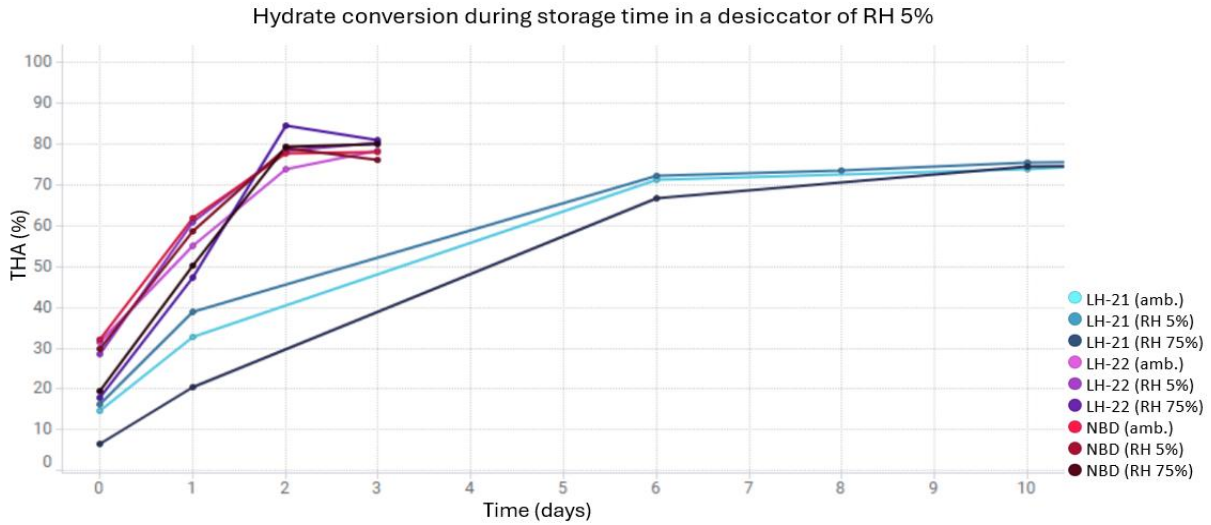

Figure 33. LH-22/TH and NBD/TH binary mixtures in a desiccator of RH 5% with polymers preconditioned in RH 5%, ambient and RH 75%.

The MW of the Shin-Etsu polymers was not known, but we compared Ashland polymers with the same molecular weight: EXF and EF. Their particle sizes differ significantly, with EXF being 53 µm and EF being 421 µm. The HDP content of EXF is reported to be between 50-80% and EF's is 74%, so the effect of HDP content cannot be considered. The binary mixture made from EF converts more quickly from TMH to TAH, which follows the same pattern as previous results, that larger particle sizes convert more quickly (Figure 34). Appendices 19-22 display more detailed figures. However, when comparing EXF to HF, the former converts faster (Figure 34). The particle size of HF (508 µm) is significantly larger than the size of EXF (53 µm), so the result does not correlate with the generally observed results.

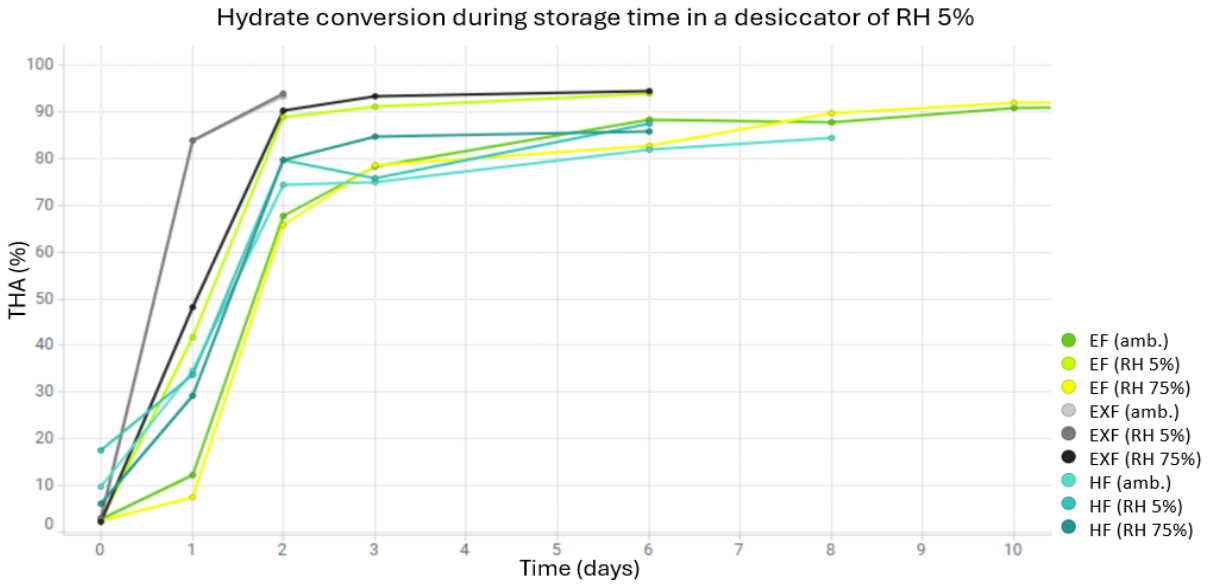

Figure 34. EF/TH and EXF/TH and HF/TH binary mixtures in a desiccator of RH 5% and RH 34% with polymers preconditioned in RH 5%, ambient and RH 75%.

Further, it is noteworthy and can be discovered in Figure 35 that K200M has changed 26% by the mixing day (day 0), when it was preconditioned in RH 5% or ambient (~21.5 °C & RH ~45%). When utilizing other polymers and K200M preconditioned in RH 75%, the binary mixtures were converted only 3-15%. K200M has a much larger particle size than other HPMC polymers, which could have an influence. However, the K200M particle size changed drastically when it was preconditioned in RH 75%, which was seen in the preliminary experiments (Figure 18). This may be the reason why its behavior became similar to other polymers after pretreatment in RH 75%.

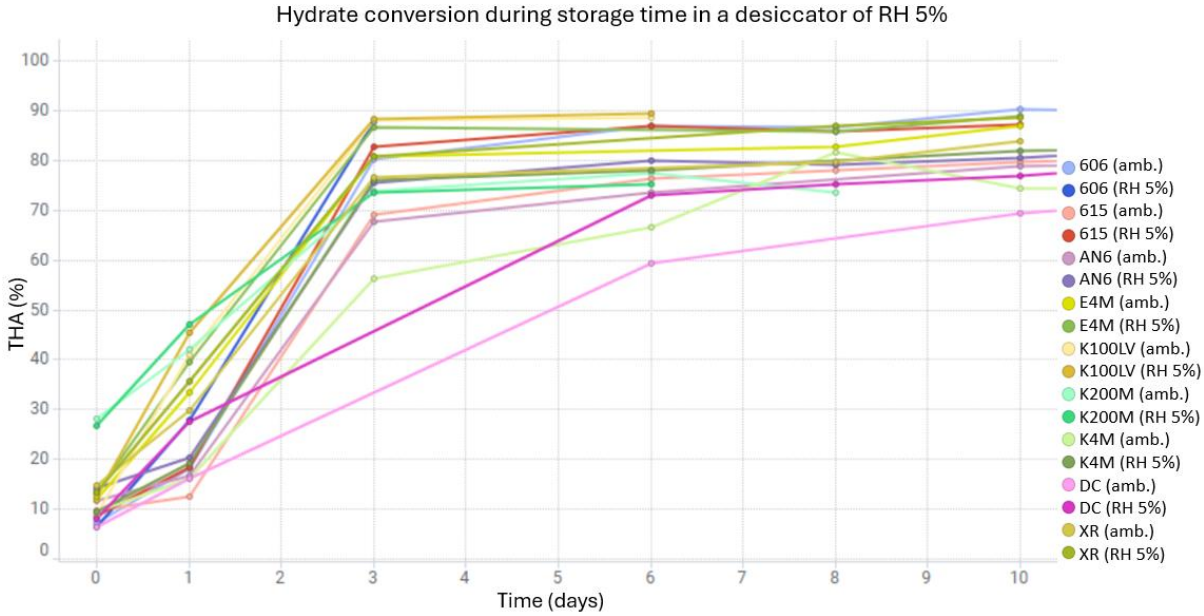

Figure 35. HPMC/TH binary mixtures in a desiccator of RH 5% with polymers preconditioned in RH 5%, ambient and RH 75%.

Generally, when polymer was preconditioned in RH 5%, the rate of hydrate conversion was the fastest and in RH 75% preconditioned it was the slowest. It is also worth noting that at ambient conditions (~21.5 °C & RH ~45%) only EF was slower to change than preconditioned in RH 75%. However, according to the study conducted by Ibrahim et al. HPC from Shin-Etsu swelled significantly when the relative humidity was 75% and the room temperature (25 °C), but at low humidity no significant swelling was observed.[79] If swelling causes a change in the three-dimensional structure of the particle and the effect of the surface area of the hydroxypropyl groups reduces. This could partly explain why polymers preconditioned at higher humidity change more slowly.

3.3.2.3. Near-infrared spectroscopy results

In general, free water is visible in the region of about 1400-1500 nm in the NIR spectrum and crystalline water in the region of 1900-2500 nm, especially in the region of 2200 nm.[50,80,81] According to Räsänen et al. the water absorption of THM appeared around 1475 nm and 1970 nm in the NIR region.[68] Crystalline water is often less visible than free water and its peaks are weaker and narrower because its motion is more restricted as it is bound to a compound as a part of the crystal lattice.

In Spectrum 2, the purple line is the silicon wafer alone, which has been used as a background for the Aqualab cup. The blue curve is the Aqualab cup, which has a small peak at around 1400 nm. Typically, free water is absorbed at that point, but it is unfortunate that the cup spectrum may cover it or part of it. The red and green curves are the spectra of theophylline without the cup. THA is a red curve, in which free water could feasibly be described by a small peak at just below 1450 nm. Hence, there is no visible peak in the spectrum at 1900-2100 nm which would be crystal water. This was reasonable to assume since there should be no crystal water in the anhydrate. THM is a green curve and in its spectrum a medium-sized peak is observed at just below 1500 nm, which could be caused by free water. However, the most important difference from the anhydrate is a clear and large peak between 1900-2000 nm with 1970 nm of maxima. It is definitely a spike from water of crystallization because the monohydrate has crystal water, and the anhydrate does not.

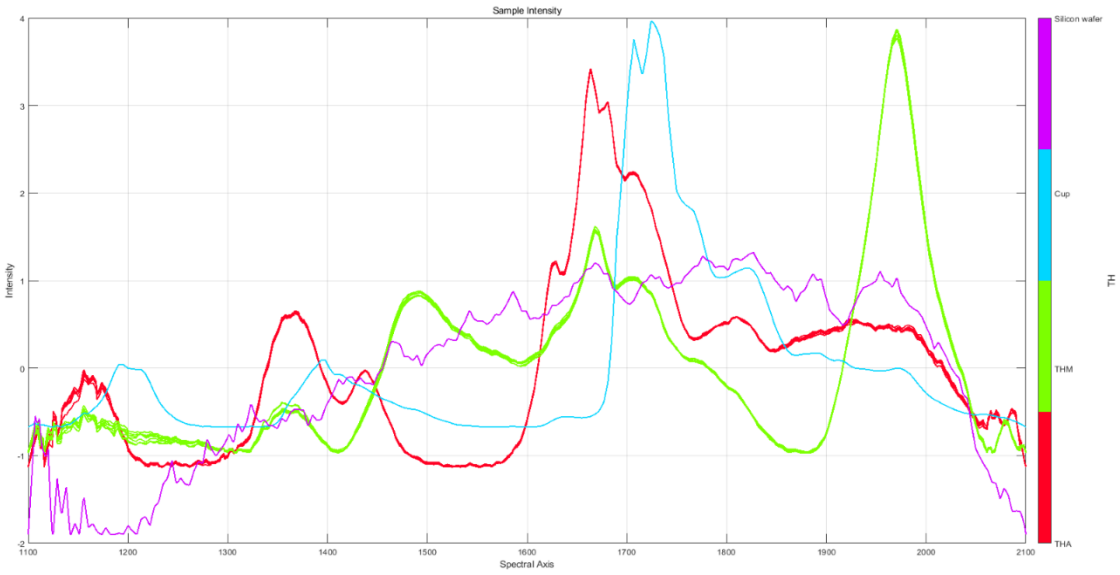

Spectrum 2. NIR spectra of silicon wafer as the background for Aqualab cup (purple), Aqualab cup (blue), theophylline anhydrate (THA) (red) and theophylline monohydrate (THM) (green).

The calibration model was built to determine and quantify free water in binary mixtures. Calibration must be used for processing NIR spectra to receive quantitative results, and another analytical method (e.g. KF for determination of water) must be used for correct results for reference materials.[2] In this study, the used analytical method for quantification of water in reference material was LOD. HPC polymer LH-21 was used as a reference material, and it was equilibrated at different humidities (5, 11, 34, 43, 65 and 75 %) over a week. Afterward, the LOD results and NIR spectra of these samples were measured (Table 5 & Spectrum 3).

Table 5. Loss on drying results of HPC polymer LH-21.

RH	**5 %**	**11 %**	**34 %**	**43 %**	**65 %**	**75 %**
LOD	1.89	3.63	6.48	8.13	11.79	14.56

Generally, the calibration model is validated either by using samples of the same material that have not been used for calibration or by taking, e.g. 2 samples from each point.[2] In this study, the test samples were from the same RH condition group as the training samples and there was a total of 18 training samples and 6 test samples. The RMSEC, RMSECV and RMSEP were used to evaluate the model, and their values were around 2, which indicates good predictability (Table 6). However, the coefficient factor (R^2) was 0.7962, which was worse than desired.

Table 6. Calibration model parameters of NIR.

Spectral range (cm^{-1})	**R^2**	**RMSEC**	**RMSECV**	**RMSEP**
1870-2015	0.796211	1.94534	2.27227	1.97352

Below (Spectrum 3) are the spectra of the polymer (LH-21) used as the reference material of calibration model (red, orange, yellow, green and bright blue curves). From these it can be concluded that at 1400-1500 nm in binary mixtures the polymer covers the water in THA and THM, whether free or crystal water. It can also be noted that the water in the polymer does not give the spectrum at the same point as the crystal water in THM. However, the calibration model made from the polymer certainly gives an indication of what the quantitative results of THM might be approximately.

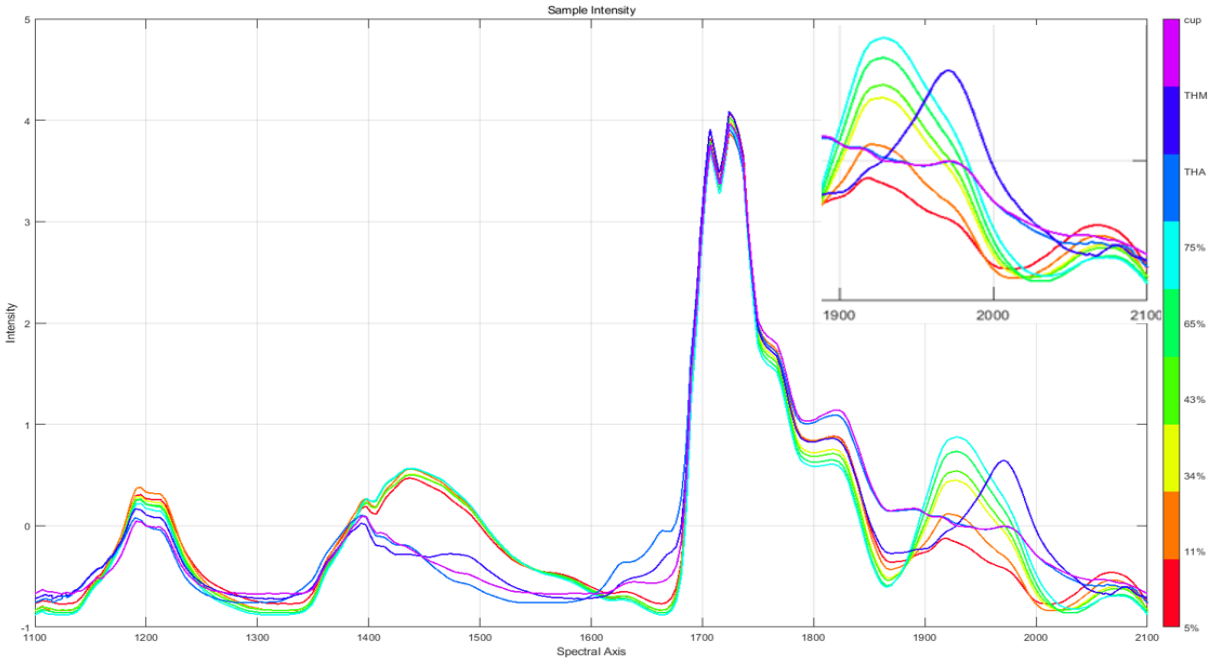

Spectrum 3. NIR spectra of THA (light blue), THM (dark blue) and Aqualab cup (purple) as well as NIR spectra of reference material polymer LH-21 (red, orange, yellow, green and bright blue) equilibrated in defined conditions.

The spectra of the binary mixtures were measured through the Aqualab cup. There are the spectra of the THA (lighter blue) and the THM (dark blue) through the Aqualab cup, as well as the spectrum of the Aqualab cup (purple) in Spectrum 3. It can be noticed from the spectrum that the Aqualab cup does interfere with the spectrum of free water, but for the THM there is a small peak slightly before 1500 nm that is visible. In addition, between 1900-2000 nm the THM provides a clear peak compared to the THA, whose spectrum mimics the spectrum of the Aqualab cup. Therefore, the spectral range for calibration model was chosen only for the monohydrate peak range 1870-2015 nm.

The example binary mixtures were those made from ELF and LH-21 polymers, because the kinetics of their Raman and NIR spectra differed the most from each other in the storage conditions of RH 5% (Figures 33 and 34). On the other hand, these polymers also differ considerably in particle size and hydroxypropyl content. The effect of molecular weight cannot be compared, as it was not reported for Shin-Etsu polymers.

Spectrum 4 shows the binary mixtures made of polymers (ELF & LH-21) preconditioned in RH 5% and stored in a desiccator of RH 5%. At the first measurement point (Day 0), the spectra of both binary mixtures (red and greenish yellow) provide a more intense peak at

1400-1500 nm, where the absorption of THM is observed. The spectrum is higher at the beginning than at the final points (End), when the theophylline of binary mixtures had undergone the hydrate conversion (orange and bright green). However, the difference in the spectra at the beginning and the end points is not very significant, but the trend is the same for both binary mixtures. Further, there is a significant difference between 1900-2000 nm where crystal water presumably absorbs. At the initial point (Day 0), the peak of ELF binary mixture (red) is higher than that of LH-21 (greenish yellow) mixture. Besides, the peak maximum of ELF mixture is at 1970 nm, indicating the water of crystallization. In turn, the LH-21 peak is distributed between 1900-2000 nm, which indicates that both free and crystalline water absorbs in the LH-21 binary mixture at that point. However, the binary mixtures made of other polymers showed the same distributed peak between 1900-2000 nm than LH-21.

Additionally, Spectrum 4 displays that on day 0 the RH 75% preconditioned polymers (dark blue and turquoise) have a clearly higher water content than the RH 5% pretreated (red and greenish yellow), which is sensible. It is worth noting that at the end point, the binary mixtures made from LH-21 have the same amount of water regardless of the precondition humidity. The spectra of the ELF binary mixtures are not at the same level at the end, but the RH 5% preconditioned is clearly lower than the RH 75% preconditioned, which could be later studied further.

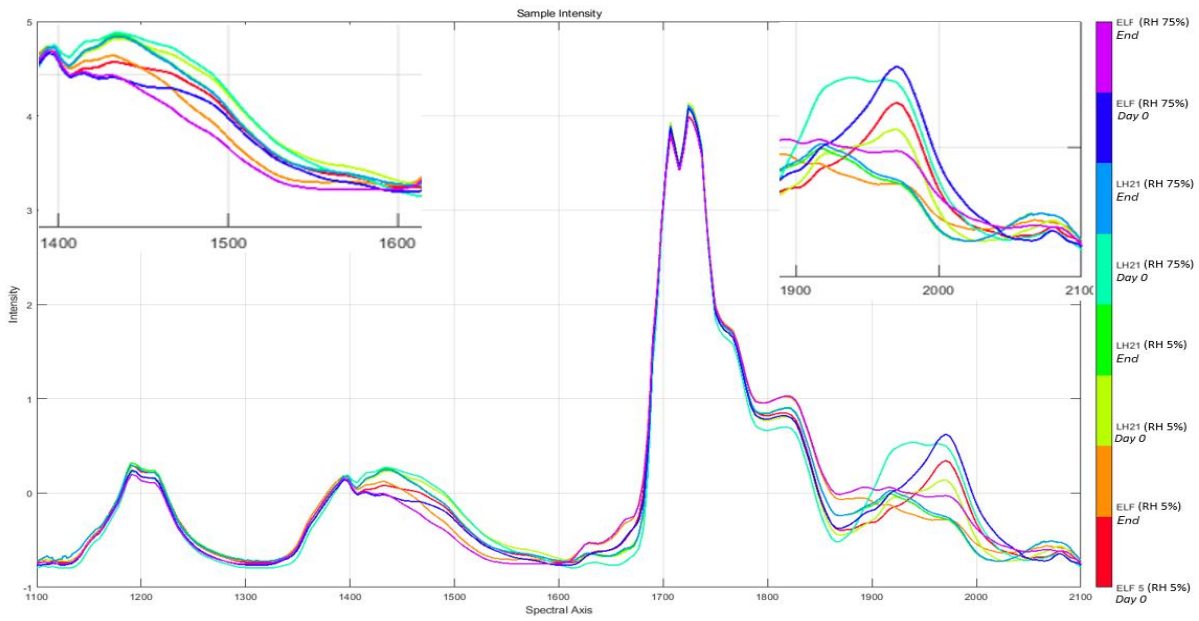

Spectrum 4. NIR spectra of binary mixtures in desiccator of RH 5% and polymers preconditioned in RH 5% and RH 75%.

The particle size of these polymers is different, with ELF (339 µm) being almost 7 times larger than LH-21 (53 µm), and the hydroxypropyl content of ELF is also greater (63 percentage point). Considering the circumstances, the larger particle size and the higher hydroxypropyl content could correlate with the greater amount of crystalline water. On the other hand, the binary mixture made of LH-21 polymer had already converted 15% from MH to AH according to Raman on the first day (Figure 37), when the polymer was at ambient or preconditioned in RH 5%. At the final point (purple and light blue), the spectra are visually less distinct than at the beginning. However, it is noteworthy that the amount of water decreases more in ELF than in LH-21 mixture, whose free water at 1400-1500 nm stays higher too (Spectrum 4). The hydrate conversion of LH-21 mixture took considerably longer (31 days) than in ELF binary mixture, which had it for 6 days. In this respect, it is evident that if there's more free water in the polymer at the beginning, it decreases the rate of hydrate conversion.

Raman does not measure free water, but only the water in the monohydrate, i.e. crystal water. NIR, on the other hand, measures both waters. Therefore, Figures 36 and 37 do not quite correlate with each other, although they are approximately related to each other. The ELF figure provides negative values because the model was made with LH-21. As stated earlier, a separate calibration model should be created for each polymer if a perfectly working model was desired.

SEM images showed that ELF and LH-21 are structurally different. ELF is sharp and flaky, which may mean that water could remain on the surface more easily. The NIR spectrum (Spectrum 4) of ELF addresses that there is no free water, which means that water could only remain on the surface of the polymer and not get inside the structure. In RH 75% preconditioned ELF clumped, which could indicate that water would not go inside the substance. LH-21 is fibrous-like and therefore would absorb water more easily. On the other hand, the NIR spectrum of LH-21 shows that there is already water in the polymer on the first day.

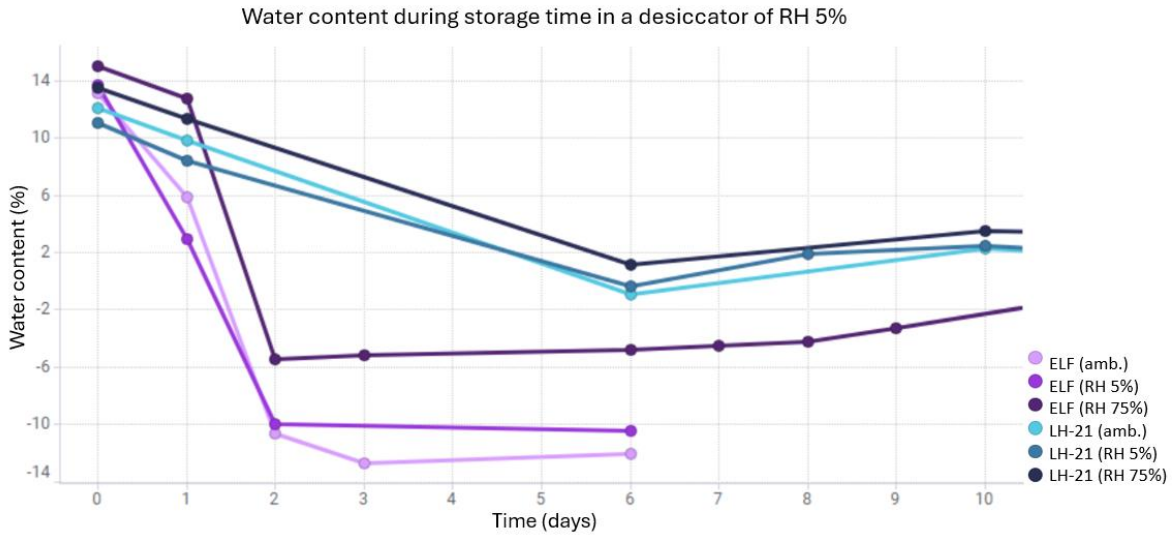

Figure 36. Quantitative results of water content (%) from NIR data for ELF and LH-21 binary mixtures.

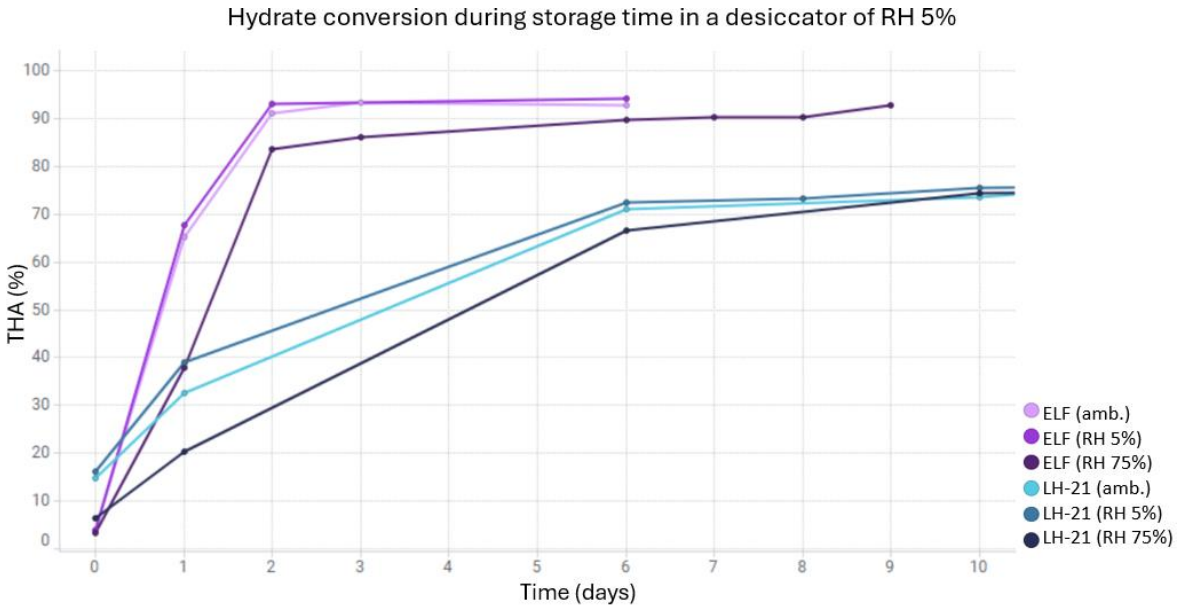

Figure 37. Quantitative results of hydrate conversion from THM into THA of ELF and LH-21 binary mixtures in a desiccator of RH 5% with polymers preconditioned in RH 5% and RH 75%.

In Spectrum 5, red curves were measured on the day of the binary mixture preparation and show that at 1900-2000 nm, where water of crystallization usually absorbs, the spectrum of the RH 5% preconditioned polymer is lower than that of the RH 75% preconditioned polymer. In turn, free water usually absorbs at 1450-1550 nm, where differences between the preconditioned polymers are also visible. It is noteworthy that the preconditioned spectra for crystallization of water are different from those for free water.

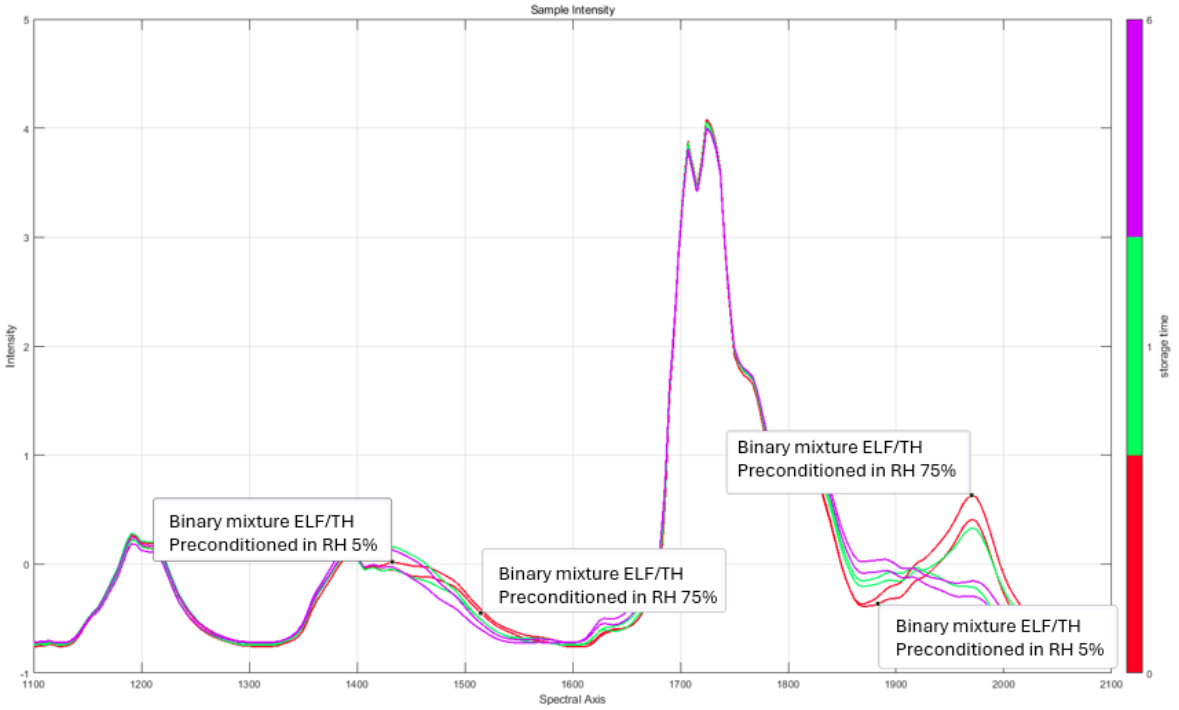

Spectrum 5. NIR spectra of ELF/THM binary mixtures in desiccator of RH 5% and polymers preconditioned at RH 5% and RH 75% on day 0, 1 and 6.

The spectrum 6 clearly shows the difference between the different polymer suppliers. The spectrum 6 A is from Shin-Etsu polymers (such as LH-21) and the spectrum 6 B is form Ashland polymers (such as ELF), both of which have spectra under storage conditions RH 5% (red) and RH 34% (purple).

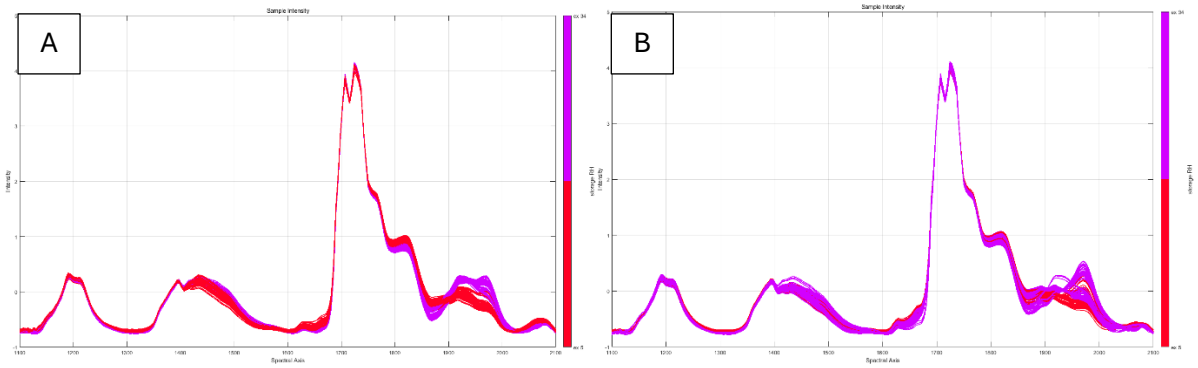

Spectrum 6. NIR spectra of HPC binary mixtures made of Shin-Etsu (A) or Ashland (B) polymers. Binary mixtures stored in a desiccator RH 5% (red) and RH 34% (purple).

Below (Spectrum 7) is a closer look at one of Ashland's polymers, which produces a peak just after 1900 nm unlike the other polymers. This is NIR spectra of EF/TH from storage days 15 and 17. The spectra from the other measurement days are shown gray in the background.

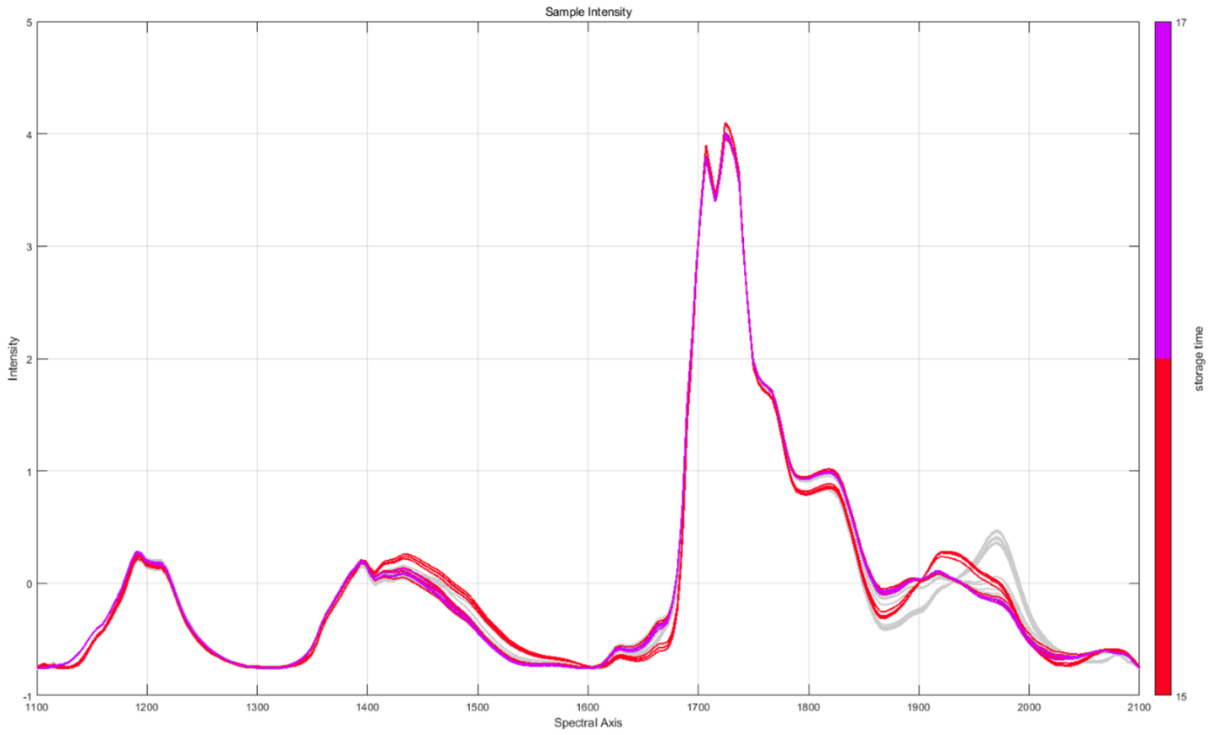

Spectrum 7. NIR spectra of EF/TH binary mixtures on days 15 (red) and 17 (purple) as well as other measurement days (gray).

Figure 38 A demonstrates quantitative water results for a binary mixture of the same polymer. There's a small bump in the spectrum, which is an increase in water content. However, it is not reflected in the hydrate conversion in any way (Figure 38 B) and may just be a measurement error. Therefore, no conclusions can be drawn from this.

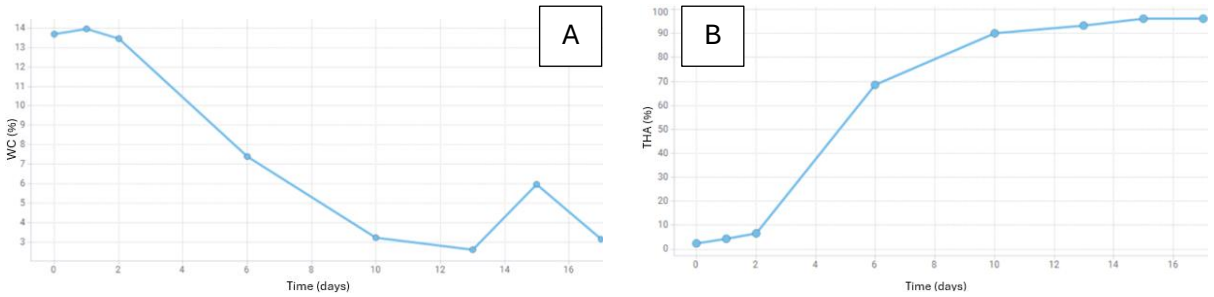

Figure 38. Quantitative results of water content (%) from NIR data (A) and Raman (B) for EF/TH binary mixtures.

The original goal was to quantify free water in binary mixtures, which is demanding with these materials because there are two types of water involved. The calibration model was simplified by using only one polymer to create it. However, the challenge is that polymers do not contain crystal water, and the spectrum of the polymer covers the spectral range of TH water at

1400-1500 nm. In addition, the spectrum of theophylline monohydrate and free water of polymer overlap at 1900-2000 nm. Therefore, the determination of free water was not possible with the measurement method used and hence, the model does not fulfill its task of separating free and crystal water but rather reveals total water in binary mixtures. The quantitative result given by the model is a combination of free and crystallization water, and its values are indicative, but there are better water determination methods. However, the measurements can still be assessed visually, and differences can be seen in the NIR spectra, as was noted earlier for binary mixtures made by ELF and LH-21.

4. Concluding remarks

NIR is a reliable and rapidly developing analytical method, which is a useful technique for determining water. Water can have an impact on the stability and polymorphism of pharmaceuticals and hence will likely affect them and their manufacturing in the future, at least due to the humidity in the air. NIR offers a fast, non-destructive and cost-effective method to analyze the composition of pharmaceuticals from different matrices and even through packaging. In the future, NIR can be used more in real-time process control, allowing the manufacturing process to be better optimized and monitored. This can speed up the time to market of drugs and reduce production costs. As the use of artificial intelligence increases, NIR could be integrated into production systems, making it part of automated quality control. NIR could be a key part of the future development of the pharmaceutical industry with its wider and increasing use.

According to the data from experimental study, there was no correlation between hydrate conversion and water activity. The water activities of all binary mixtures followed the same pattern. They reached desiccator humidity within a couple of days regardless of whether they were stored in a desiccator of RH 5% or RH 34%. Further, the water activity and the movement of crystal water between the monohydrate and the anhydrate did not correlate either. However, the movement of crystal water in binary mixtures appeared to be related to hydrate conversion. For example, the polymer did not capture crystal water at first and then the model substance changed to anhydrate, but these occurred simultaneously. The Raman calibration model worked well in tracking the hydrate conversion. In turn, the NIR calibration

model requires improvement. For these binary mixture compounds, it was not possible to create a calibration model that would only show free water. It did not give reliable quantitative results for free water, but for the total amount of water. However, it is moderately suitable for this.

In general, the experimental setup could have been improved because opening the desiccators affected the samples. The laboratory humidity increased the humidity of the desiccator of RH 5% each time it was opened, so possibly using an isolator could be a better option. However, the effect was partially blocked by using lids on the Aqualab cups, which were placed on the samples when the desiccator was opened for the first time on the measurement days. Furthermore, a better experimental setup would have been to measure the spectrum without the Aqualab cup, as it overlapped with the water spectrum. Of course, the crystal water was visible in the spectrum, but a better spectrum without interference would be obtained by measuring directly from the compound.

Certain polymer properties appeared to influence the kinetics of theophylline hydrate conversion. Typically, higher molecular weight and larger particle size of the polymer had an accelerating effect on the conversion from MH to AH. The former is sensible as large compounds are unable to fit into tight structures because they have difficulty organizing due to steric hindrance. Additionally, the smaller particle size has a larger surface area which could allow closer contact with theophylline resulting in better protection from drying and therefore, the hydrate conversion. Furthermore, in most cases the hydroxypropyl content had a retarding effect perhaps due to the help of retaining water in the powder mixtures and thus, the higher humidity slows down the conversion. While a higher content of methoxy groups appeared to accelerate the hydrate conversion. Nonetheless, the other properties of the compound or grade could also have an impact on kinetics. The effect and the degree of substitution of hydroxypropyl and methoxy groups on the actual surface area of the molecule and its consequences could be studied in more detail. In the future, other model substances that are susceptible to hydrate conversion could also be investigated.

References

1 M. W. J. Derksen, P. J. M. Van De Oetelaar and F. A. Maris, *J. Pharm. Biomed. Anal.*, 1998, **17**, 473–480.

2 S. Bobba, N. Zinfollino and D. Fissore, *J. Pharm. Sci.*, 2022, **111**, 1437–1450.

3 A. Patel, C. Jin, B. Handzo and R. Kalyanaraman, *J. Pharm. Biomed. Anal.*, 2023, **229**, 115381.

4 G. Fevotte, *Int. J. Pharm.*, 2004, **273**, 159–169.

5 S. Airaksinen, P. Luukkonen, A. Jørgensen, M. Karjalainen, J. Rantanen and J. Yliruusi, *J. Pharm. Sci.*, 2003, **92**, 516–528.

6 A. Porfire, C. Filip and I. Tomuta, *J. Pharm. Biomed. Anal.*, 2017, **138**, 1–13.

7 S. Li, Y. Zhao, L. Wang, H. Wu, Y. Gao, L. Zhang, Z. Wang and J. Han, *Microchem. J.*, 2021, **169**, 106497.

8 M. A. Lakeh, S. K. Karimvand, M. R. Khoshayand and H. Abdollahi, *Microchem. J.*, 2020, **154**, 104516.

9 D. L. Galata, A. Farkas, Z. Könyves, L. A. Mészáros, E. Szabó, I. Csontos, A. Pálos, G. Marosi, Z. K. Nagy and B. Nagy, *Pharmaceutics*, 2019, **11**, 400.

10 V. Bhavana, R. B. Chavan, M. K. C. Mannava, A. Nangia and N. R. Shastri, *Talanta*, 2019, **199**, 679–688.

11 D. Mainali, J. Li, P. Yehl and N. Chetwyn, *J. Pharm. Biomed. Anal.*, 2014, **95**, 169–175.

12 J. Mantanus, E. Ziémons, P. Lebrun, E. Rozet, R. Klinkenberg, B. Streel, B. Evrard and Ph. Hubert, *Anal. Chim. Acta*, 2009, **642**, 186–192.

13 J. Mantanus, E. Ziémons, P. Lebrun, E. Rozet, R. Klinkenberg, B. Streel, B. Evrard and Ph. Hubert, *Talanta*, 2010, **80**, 1750–1757.

14 P. Li, G. Du, W. Cai and X. Shao, *J. Pharm. Biomed. Anal.*, 2012, **70**, 288–294.

15 J. U. Porep, D. R. Kammerer and R. Carle, *Trends Food Sci. Technol.*, 2015, **46**, 211–230.

16 M. S. Kamat, R. A. Lodder and P. P. DeLuca, *Pharm. Res.*, 1989, **06**, 961–965.

17 G. Clua-Palau, E. Jo, S. Nikolic, J. Coello and S. Maspoch, *J. Pharm. Biomed. Anal.*, 2020, **183**, 113163.

18 K. Phetpan, V. Udompetaikul and P. Sirisomboon, *Powder Technol.*, 2019, **345**, 608–615.

19 P. H. Ciza, P.-Y. Sacre, C. Waffo, L. Coïc, H. Avohou, J. K. Mbinze, R. Ngono, R. D. Marini, P. Hubert and E. Ziemons, *Talanta*, 2019, **202**, 469–478.

20 M. Saeed, L. Probst and G. Betz, *J. Pharm. Sci.*, 2011, **100**, 1130–1141.

21 M. Saeed, S. Saner, J. Oelichmann, H. Keller and G. Betz, *J. Pharm. Sci.*, 2009, **98**, 4877–4886.

22 O. Berntsson, G. Zackrisson and G. Östling, *J. Pharm. Biomed. Anal.*, 1997, **15**, 895–900.

23 J. D. Rodriguez, B. J. Westenberger, L. F. Buhse and J. F. Kauffman, *Anal. Chem.*, 2011, **83**, 4061–4067.

24 M. L. F. Simeone, M. A. G. Pimentel, V. A. V. Queiroz, F. Santos, A. Brito, L. F. M. Aquino, J. C. E. Da C. Filho, C. B. De Menezes, M. C. D. Paes, C. S. Tibola, P. E. De O. Guimarães and R. D. S. Trindade, *J. Food Compos. Anal.*, 2024, **134**, 106502.

25 K. Kamada, S. Yoshimura, M. Murata, H. Murata, H. Nagai, H. Ushio and K. Terada, *Int. J. Pharm.*, 2009, **368**, 103–108.

26 J. Rantanen, H. Wikström, F. E. Rhea and L. S. Taylor, *Appl. Spectrosc.*, 2005, **59**, 942–951.

27 X. Zhou, P. Hines and M. W. Borer, *J. Pharm. Biomed. Anal.*, 1998, **17**, 219–225.

28 K. Wang, Z. Wang, H. Xu, Z. Lan, X. Lin, J. Ren and S. Kong, *J. Drug Deliv. Sci. Technol.*, 2025, **104**, 106528.

29 L. Martínez, A. Peinado and L. Liesum, *Int. J. Pharm.*, 2013, **451**, 67–75.

30 M. Blanco, R. Cueva-Mestanza and A. Peguero, *Talanta*, 2011, **85**, 2218–2225.

31 P. H. Ciza, P.-Y. Sacre, C. Waffo, L. Coïc, H. Avohou, J. K. Mbinze, R. Ngono, R. D. Marini, P. Hubert and E. Ziemons, *Talanta*, 2019, **202**, 469–478.

32 S. Bobba, N. Zinfollino and D. Fissore, *J. Pharm. Sci.*, 2022, **111**, 1437–1450.

33 Q. Zhang, Q. Li and G. Zhang, *Spectrosc. Int. J.*, 2012, **27**, 93–105.

34 H. Pataki, I. Csontos, Z. K. Nagy, B. Vajna, M. Molnar, L. Katona and G. Marosi, *Org. Process Res. Dev.*, 2013, **17**, 493–499.

35 L. Sun, C. Hsiung, C. G. Pederson, P. Zou, V. Smith, M. Von Gunten and N. A. O'Brien, *Appl. Spectrosc.*, 2016, **70**, 816–825.

36 J. Gabel, G. Gnegel, W. Kessler, P.-Y. Sacré and L. Heide, *Talanta Open*, 2023, **8**, 100270.

37 M. Brülls, S. Folestad, A. Sparén, A. Rasmuson and J. Salomonsson, *J. Pharm. Biomed. Anal.*, 2007, **44**, 127–136.

38 K. Koyanagi, K. Shoji, A. Ueno, T. Sasaki and M. Otsuka, *J. Drug Deliv. Sci. Technol.*, 2024, **101**, 106240.

39 D. Brouckaert, F. Vandenbroucke, F. Chauchard, M. Dollinger, Y. Roggo, L. Pellegatti and M. Krumme, *J. Pharm. Biomed. Anal.*, 2022, **209**, 114491.

40 F. De Leersnyder, V. Vanhoorne, A. Kumar, C. Vervaet and T. De Beer, *Int. J. Pharm.*, 2019, **565**, 358–366.

41 C. R. Avila, J. Ferré, R. R. De Oliveira, A. De Juan, W. E. Sinclair, F. M. Mahdi, A. Hassanpour, T. N. Hunter, R. A. Bourne and F. L. Muller, *Pharm. Res.*, 2020, **37**, 84.

42 L. M. Kandpal, J. Tewari, N. Gopinathan, J. Stolee, R. Strong, P. Boulas and B.-K. Cho, *Infrared Phys. Technol.*, 2017, **85**, 300–306.

43 M. Otsuka, Y. Kanai and Y. Hattori, *J. Pharm. Sci.*, 2014, **103**, 2924–2936.

44 J. Rantanen, H. Wikström, R. Turner and L. S. Taylor, *Anal. Chem.*, 2005, **77**, 556–563.

45 P. R. Wahl, G. Fruhmann, S. Sacher, G. Straka, S. Sowinski and J. G. Khinast, *Eur. J. Pharm. Biopharm.*, 2014, **87**, 271–278.

46 J. G. Rosas, M. Blanco, J. M. González and M. Alcalà, *Talanta*, 2012, **97**, 163–170.

47 O. Scheibelhofer, N. Balak, P. R. Wahl, D. M. Koller, B. J. Glasser and Johannes. G. Khinast, *AAPS PharmSciTech*, 2013, **14**, 234–244.

48 L. Chablani, M. K. Taylor, A. Mehrotra, P. Rameas and W. C. Stagner, *AAPS PharmSciTech*, 2011, **12**, 1050–1055.

49 J. Märk, M. Karner, M. Andre, J. Rueland and C. W. Huck, *Anal. Chem.*, 2010, **82**, 4209–4215.

50 C. C. Corredor, D. Bu and D. Both, *Anal. Chim. Acta*, 2011, **696**, 84–93.

51 J. J. Moes, M. M. Ruijken, E. Gout, H. W. Frijlink and M. I. Ugwoke, *Int. J. Pharm.*, 2008, **357**, 108–118.

52 T. Nishii, K. Matsuzaki and S. Morita, *Int. J. Pharm.*, 2020, **590**, 119871.

53 Z. Shi, R. P. Cogdill, S. M. Short and C. A. Anderson, *J. Pharm. Biomed. Anal.*, 2008, **47**, 738–745.

54 H. Wikström, W. J. Carroll and L. S. Taylor, *Pharm. Res.*, 2008, **25**, 923–935.

55 L. Obregón, L. Quiñones and C. Velázquez, *Control Eng. Pract.*, 2013, **21**, 509–517.

56 J. D. Kirsch and J. K. Drennen, *Pharm. Res.*, 1996, **13**, 234–237.

57 G. Hudovornik, K. Korasa and F. Vrečer, *Eur. J. Pharm. Sci.*, 2015, **75**, 160–168.

58 B. Szabó-Szőcs, M. Ficzere, O. Péterfi and D. L. Galata, *Int. J. Pharm.*, 2025, **668**, 124957.

59 L. Pieszczek and M. Daszykowski, *J. Pharm. Biomed. Anal.*, 2025, **256**, 116697.

60 A. Massei, N. Falco and D. Fissore, *Processes*, 2025, **13**, 452.

61 A. M. Zubak, A. Horvat, D. Čavužić and I. Fabijanić, *Talanta*, 2020, **211**, 120659.

62 Y. Zheng, X. Lai, S. W. Bruun, H. Ipsen, J. N. Larsen, H. Løwenstein, I. Søndergaard and S. Jacobsen, *J. Pharm. Biomed. Anal.*, 2008, **46**, 592–596.

63 R. Bobrovs, L. Seton and N. Dempster, *CrystEngComm*, 2015, **17**, 5237–5251.

64 K. Kamada, S. Yoshimura, M. Murata, H. Murata, H. Nagai, H. Ushio and K. Terada, *Int. J. Pharm.*, 2009, **368**, 103–108.

65 H. Veith, E. Turan, C. Luebbert and G. Sadowski, *Fluid Phase Equilibria*, 2020, **521**, 112677.

66 M. Otsuka and Y. Matsuda, *Chem. Pharm. Bull. (Tokyo)*, 1994, **42**, 156–159.

67 M. Otsuka, H. Hasegawa and Y. Matsuda, *Chem. Pharm. Bull. (Tokyo)*, 1997, **45**, 894–898.

68 E. Räsänen, J. Rantanen, A. Jørgensen, M. Karjalainen, T. Paakkari and J. Yliruusi, *J. Pharm. Sci.*, 2001, **90**, 389–396.

69 A. C. Jørgensen, S. Airaksinen, M. Karjalainen, P. Luukkonen, J. Rantanen and J. Yliruusi, *Eur. J. Pharm. Sci.*, 2004, **23**, 99–104.

70 H. Zhu, *Int. J. Pharm.*, 1996, **135**, 151–160.

71 D. A. Gómez, J. Coello and S. Maspoch, *Vib. Spectrosc.*, 2019, **100**, 48–56.

72 A. Gabrič, Ž. Hodnik and S. Pajk, *Pharmaceutics*, 2022, **14**, 325.

73 N. G. Patel and A. T. M. Serajuddin, *Int. J. Pharm.*, 2022, **616**, 121532.

74 P. Talik, J. Piotrowska and U. Hubicka, *AAPS PharmSciTech*, 2019, **20**, 187.

75 A. Jørgensen, J. Rantanen, M. Karjalainen, L. Khriachtchev, E. Räsänen and J. Yliruusi, *Pharm. Res.*, 2002, **19**, 1285–1291.

76 M. M. Nolasco, A. M. Amado and P. J. A. Ribeiro-Claro, *ChemPhysChem*, 2006, **7**, 2150–2161.

77 A. M. Amado, M. M. Nolasco and P. J. A. Ribeiro-Claro, *J. Pharm. Sci.*, 2007, **96**, 1366–1379.

78 G. Zografi, *Drug Dev. Ind. Pharm.*, 1988, **14**, 1905–1926.

79 I. Ibrahim, M. Carroll, A. Almudahka, J. Mann, A. Abbott, F. Winge, A. Davis, B. Hens, I. Khadra and D. Markl, *RSC Pharm.*, 2025, **2**, 369–386.

80 B. Czarnik-Matusewicz and S. Pilorz, *Vib. Spectrosc.*, 2006, **40**, 235–245.

81 H. Grohganz, M. Fonteyne, E. Skibsted, T. Falck, B. Palmqvist and J. Rantanen, *J. Pharm. Biomed. Anal.*, 2009, **49**, 901–907.

Appendices

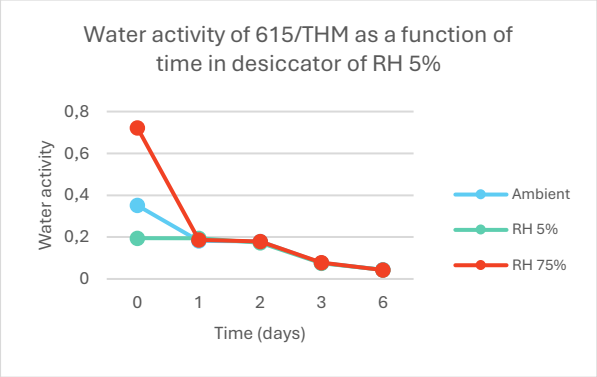
Water activity of 615/THM as a function of time in desiccator of RH 5%
Water activity
0,8
0,6
0,4
0,2
0
0
1
2
3
6
Time (days)
Ambient
RH 5%
RH 75%

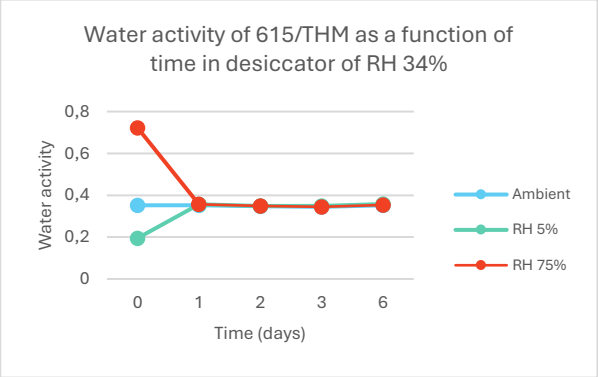
Water activity of 615/THM as a function of time in desiccator of RH 34%
Water activity
0,8
0,6
0,4
0,2
0
0
1
2
3
6
Time (days)
Ambient
RH 5%
RH 75%

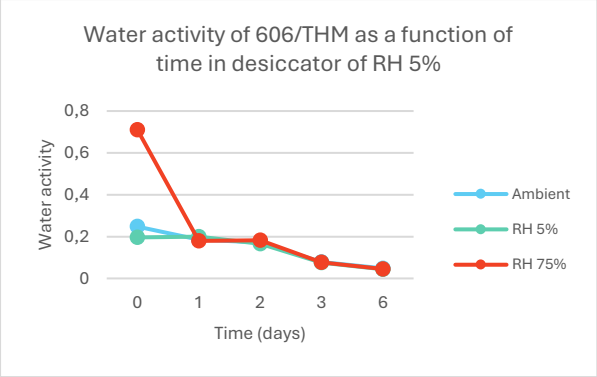
Water activity of 606/THM as a function of time in desiccator of RH 5%
Water activity
0,8
0,6
0,4
0,2
0
0
1
2
3
6
Time (days)
Ambient
RH 5%
RH 75%

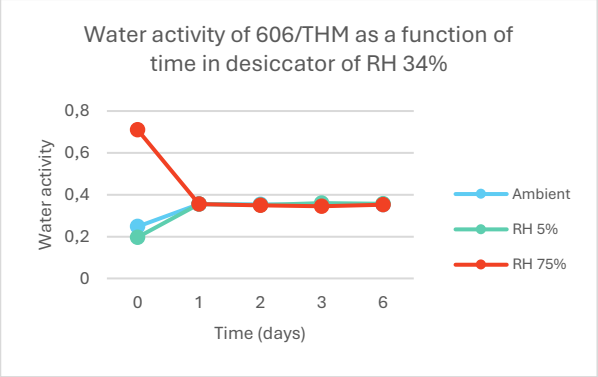
Water activity of 606/THM as a function of time in desiccator of RH 34%
Water activity
0,8
0,6
0,4
0,2
0
0
1
2
3
6
Time (days)
Ambient
RH 5%
RH 75%

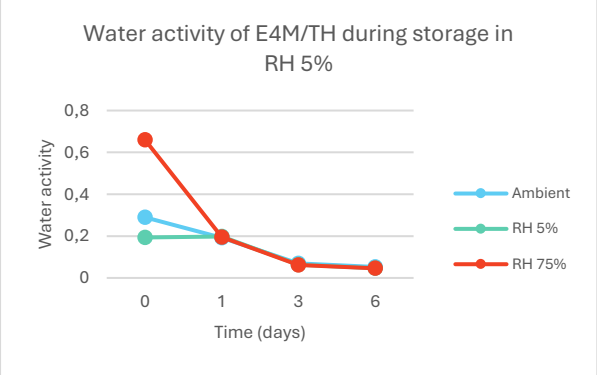
Water activity of E4M/TH during storage in RH 5%
Water activity
0,8
0,6
0,4
0,2
0
0
1
3
6
Time (days)
Ambient
RH 5%
RH 75%

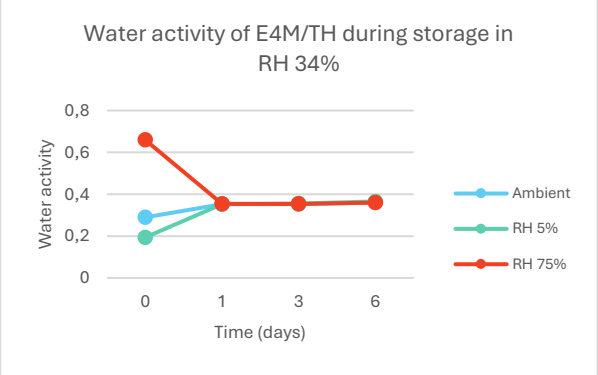
Water activity of E4M/TH during storage in RH 34%
Water activity
0,8
0,6
0,4
0,2
0
0
1
3
6
Time (days)
Ambient
RH 5%
RH 75%

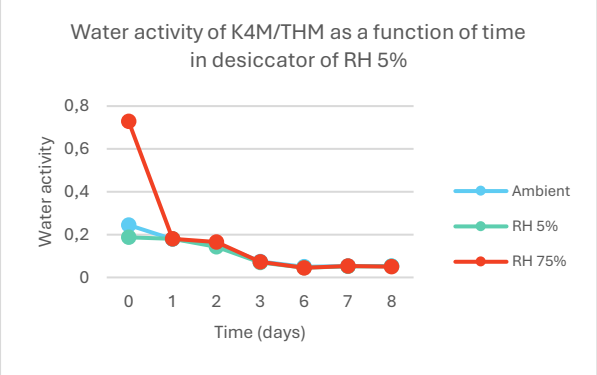
Water activity of K4M/THM as a function of time in desiccator of RH 5%
Water activity
0,8
0,6
0,4
0,2
0
0
1
2
3
6
7
8
Time (days)
Ambient
RH 5%
RH 75%

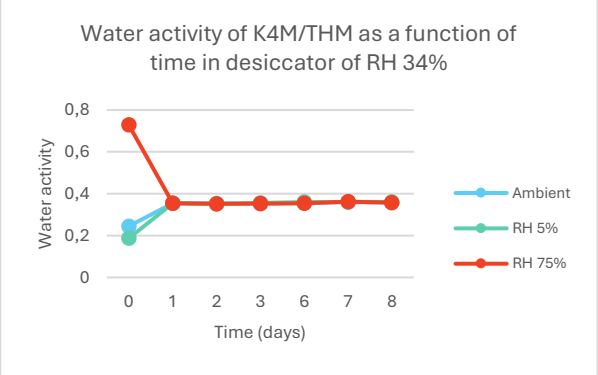
Water activity of K4M/THM as a function of time in desiccator of RH 34%
Water activity
0,8
0,6
0,4
0,2
0
0
1
2
3
6
7
8
Time (days)
Ambient
RH 5%
RH 75%

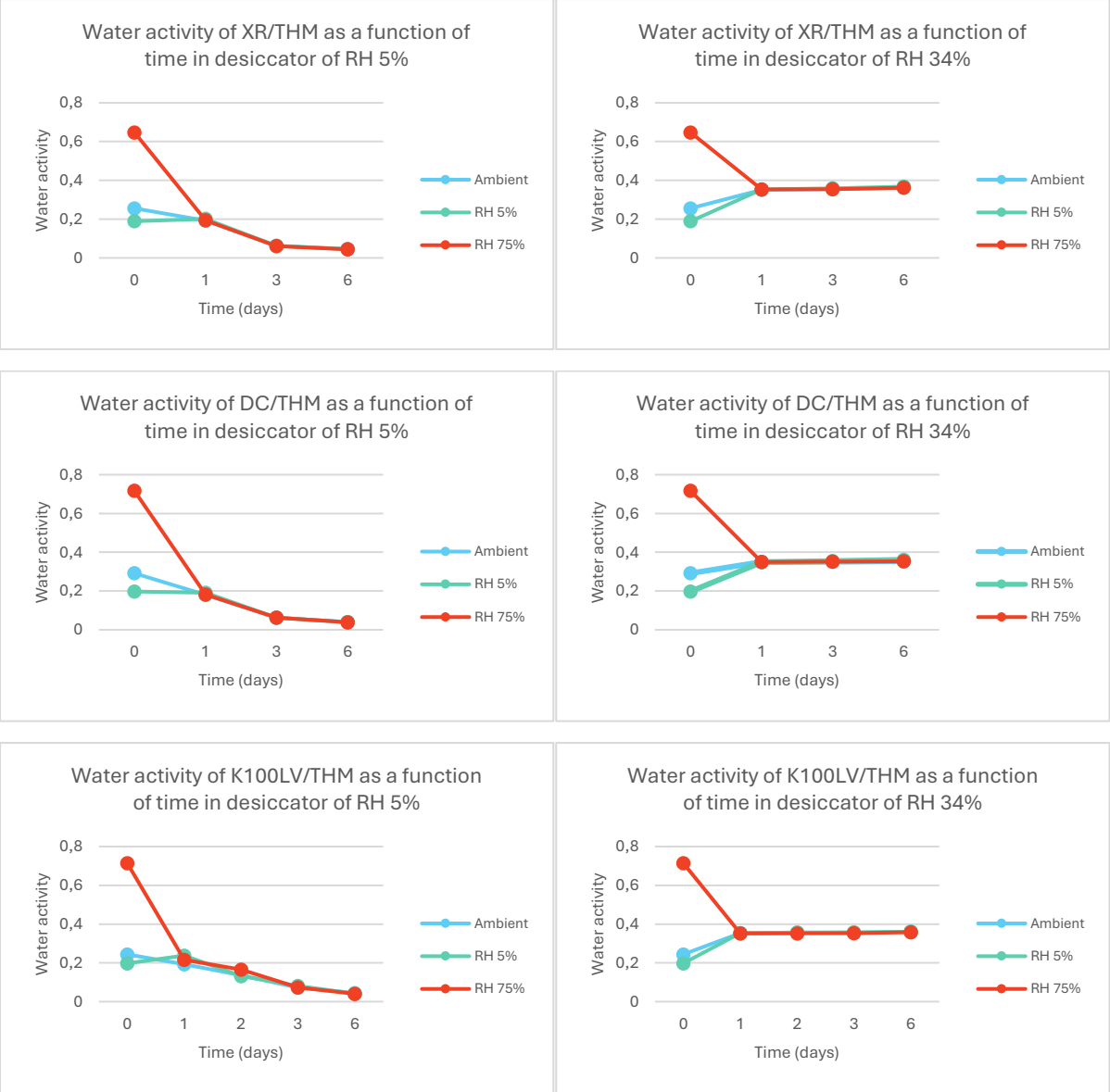

Appendix 1. Water activity of binary mixtures from HPMC polymers as a function of time in desiccator of RH 5% or RH 34%. The pretreatment conditions are with different colors.

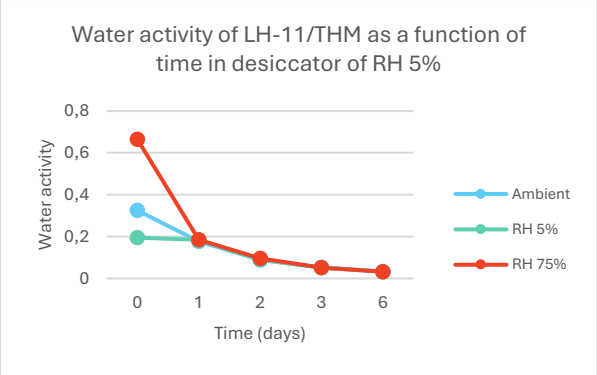
Water activity of LH-11/THM as a function of time in desiccator of RH 5%
Water activity
0,8
0,6
0,4
0,2
0
0
1
2
3
6
Time (days)
Ambient
RH 5%
RH 75%

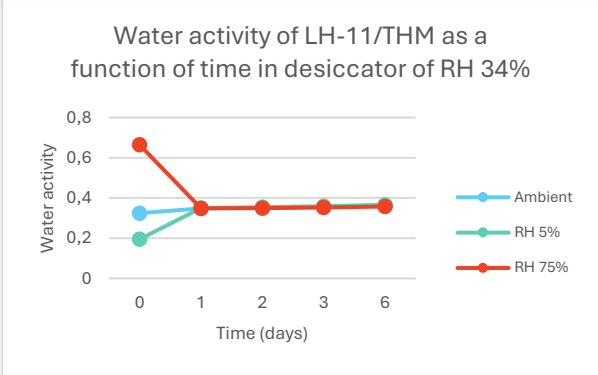
Water activity of LH-11/THM as a function of time in desiccator of RH 34%
Water activity
0,8
0,6
0,4
0,2
0
0
1
2
3
6
Time (days)
Ambient
RH 5%
RH 75%

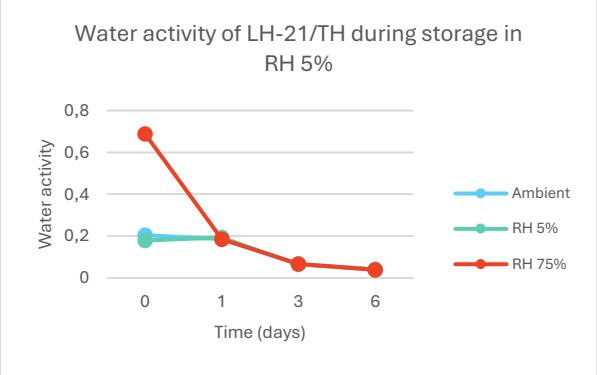
Water activity of LH-21/TH during storage in RH 5%
Water activity
0,8
0,6
0,4
0,2
0
0
1
3
6
Time (days)
Ambient
RH 5%
RH 75%

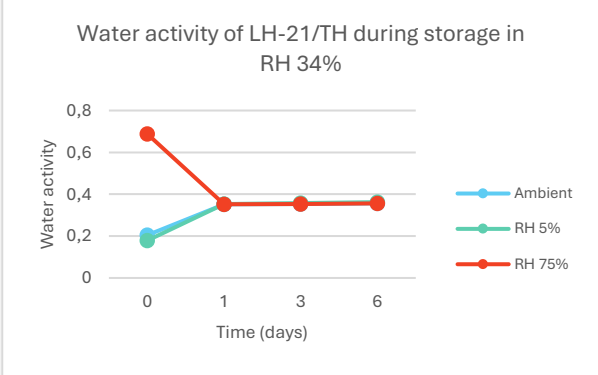
Water activity of LH-21/TH during storage in RH 34%
Water activity
0,8
0,6
0,4
0,2
0
0
1
3
6
Time (days)
Ambient
RH 5%
RH 75%

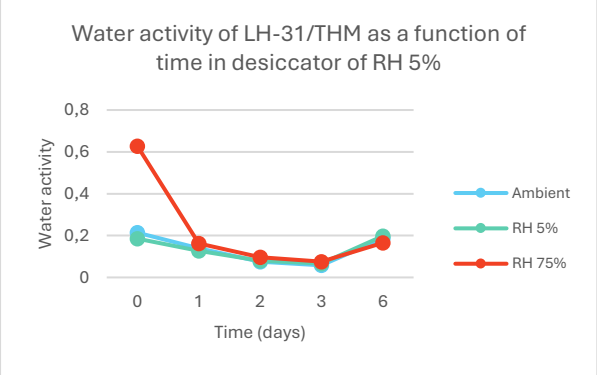
Water activity of LH-31/THM as a function of time in desiccator of RH 5%
Water activity
0,8
0,6
0,4
0,2
0
0
1
2
3
6
Time (days)
Ambient
RH 5%
RH 75%

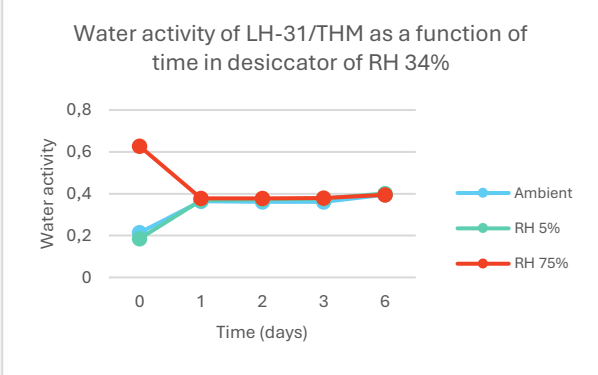
Water activity of LH-31/THM as a function of time in desiccator of RH 34%
Water activity
0,8
0,6
0,4
0,2
0
0
1
2
3
6
Time (days)
Ambient
RH 5%
RH 75%

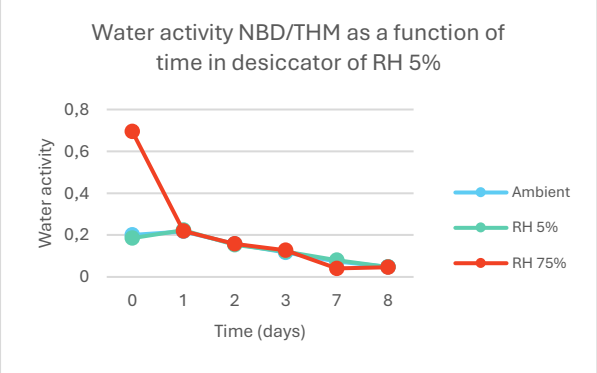
Water activity NBD/THM as a function of time in desiccator of RH 5%
Water activity
0,8
0,6
0,4
0,2
0
0
1
2
3
7
8
Time (days)
Ambient
RH 5%
RH 75%

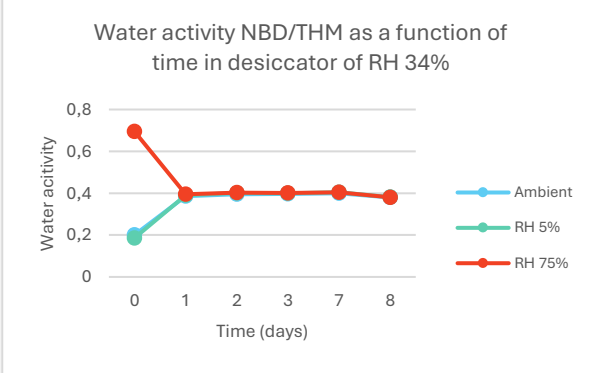
Water activity NBD/THM as a function of time in desiccator of RH 34%
Water acitivity
0,8
0,6
0,4
0,2
0
0
1
2
3
7
8
Time (days)
Ambient
RH 5%
RH 75%

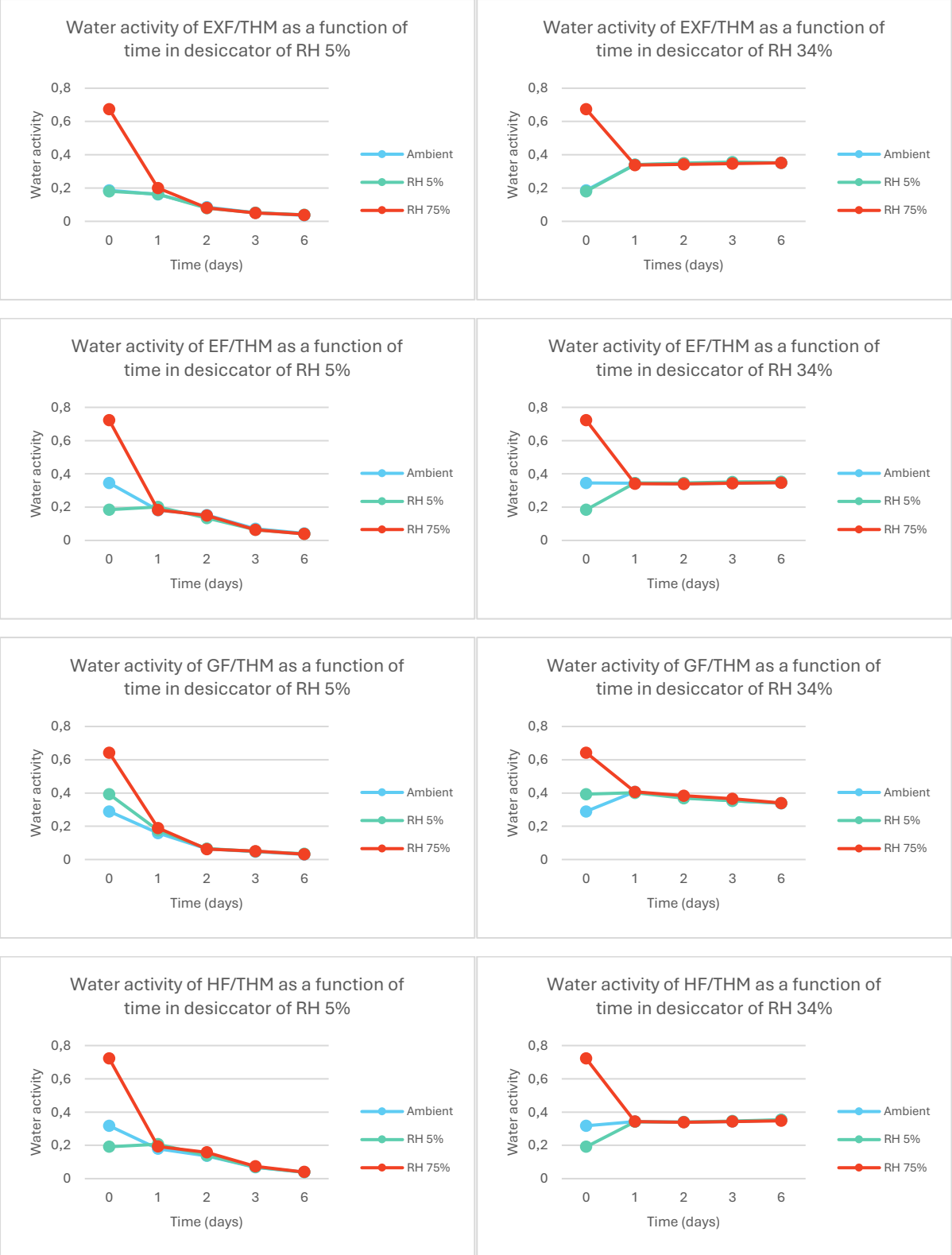

Appendix 2. Water activity of binary mixtures from HPC polymers as a function of time in desiccator of RH 5% or RH 34%. The pretreatment conditions are with different colors.

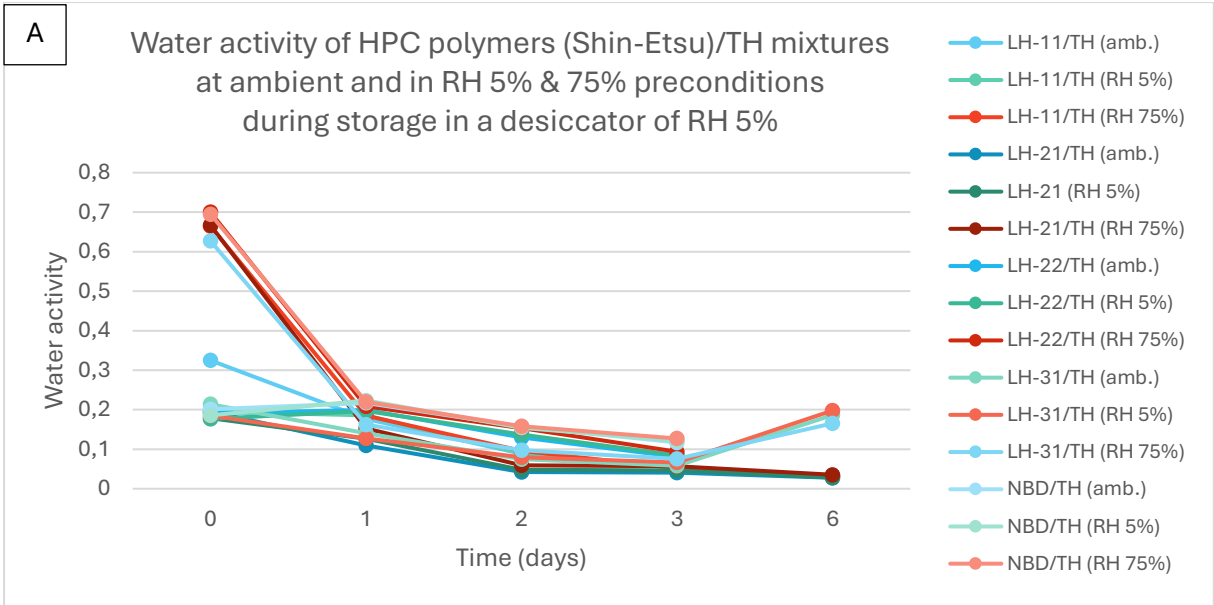

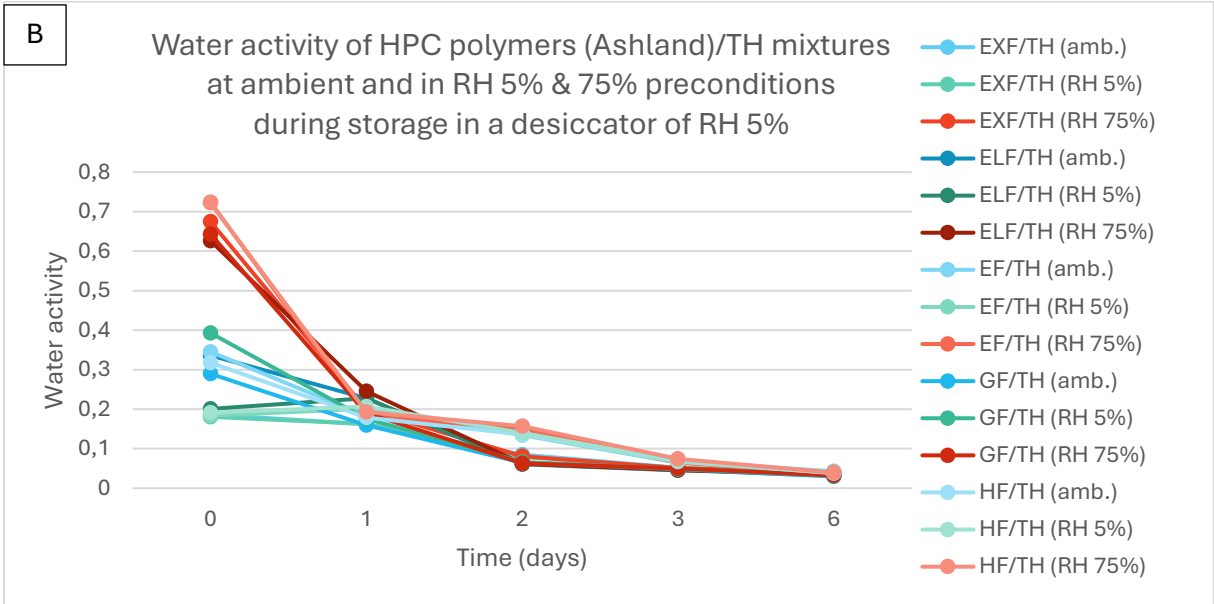

Appendix 3. Water activity of binary mixtures from HPC polymers of Shin-Etsu (A) and Ashland (B) during storage in desiccator of RH 5% or RH 34%.

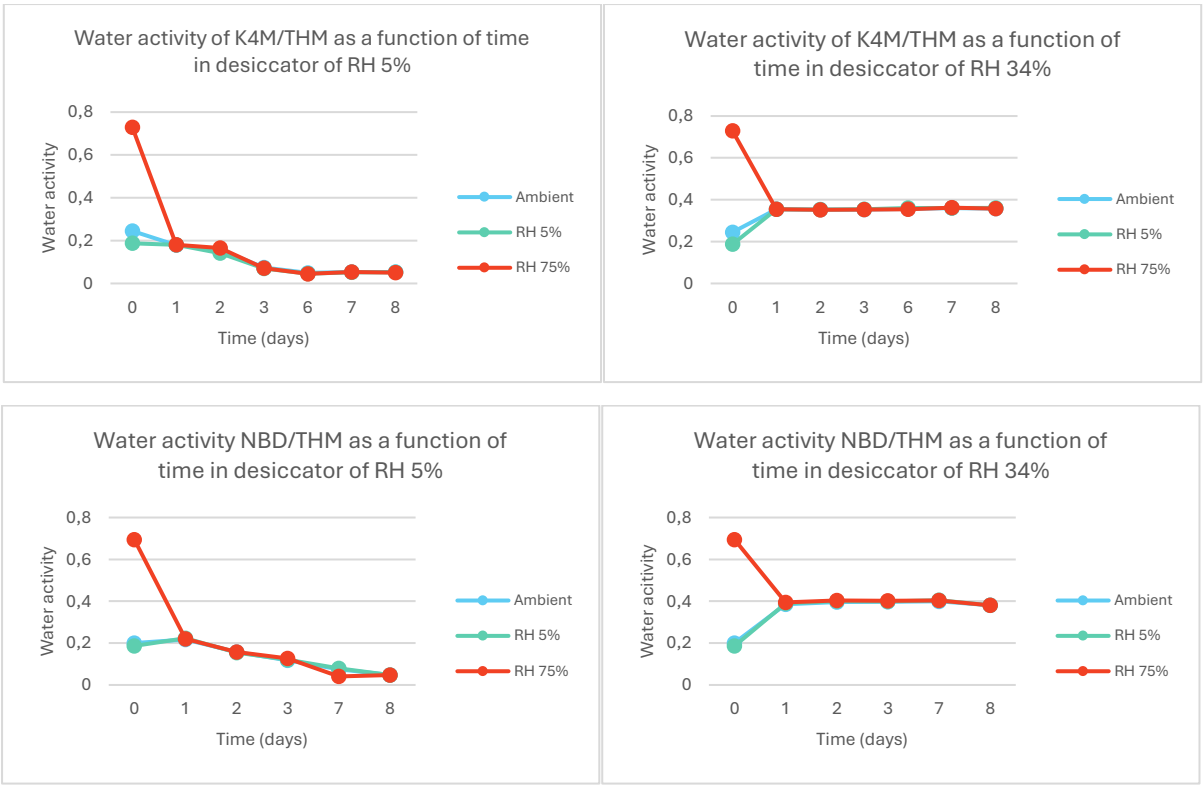

Appendix 4. Water activity of binary mixtures from HPMC polymer K4M (up) and HPC polymer NBD (down) during storage (up to 8 days) in desiccator of RH 5% or RH 34%. The pretreatment conditions are with different colors.

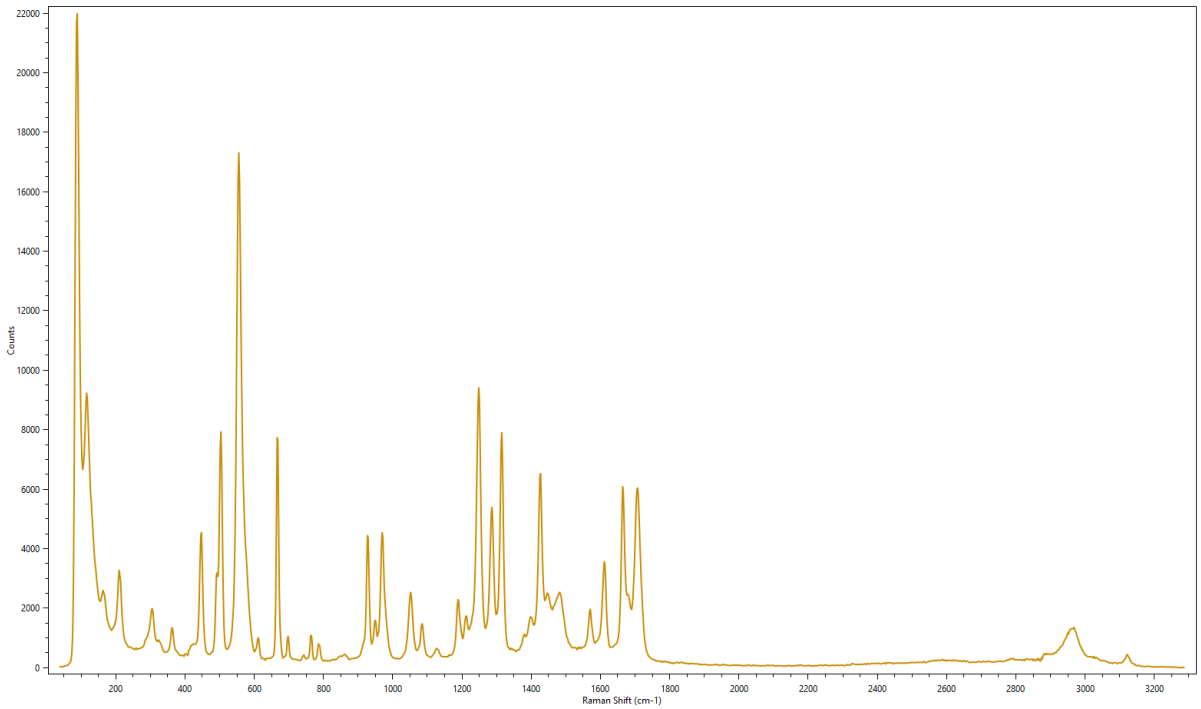

Appendix 5. Raman spectrum of theophylline anhydrate.

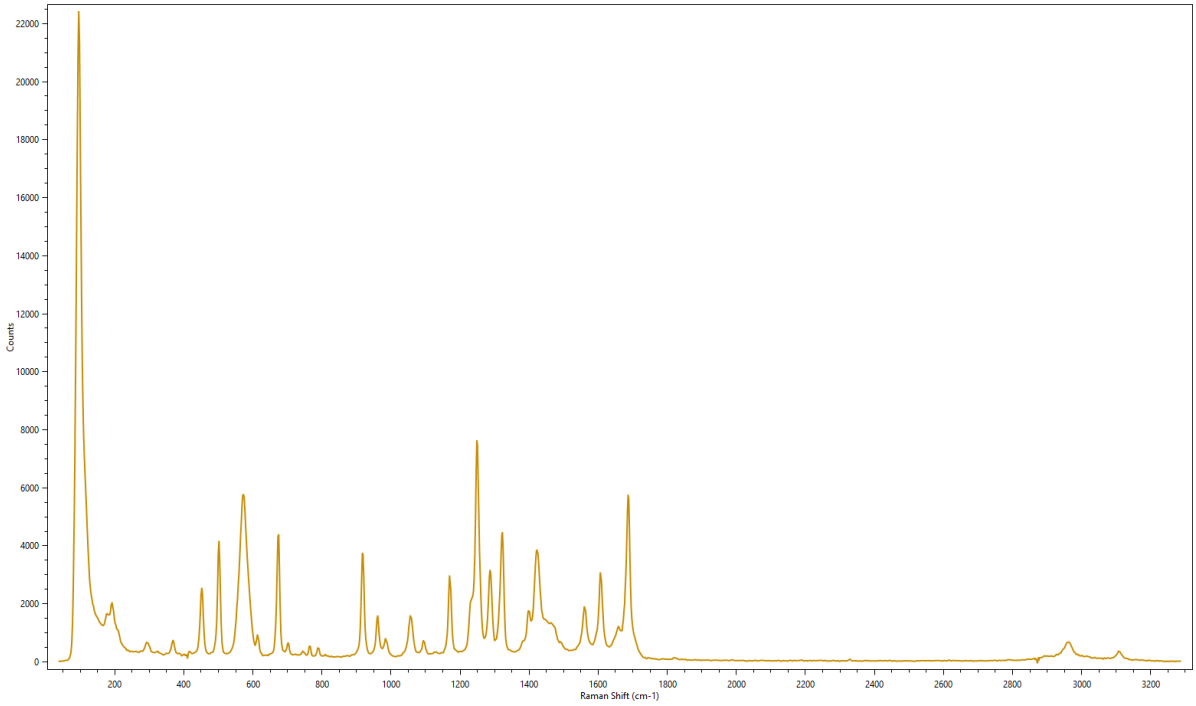

Appendix 6. Raman spectrum of theophylline monohydrate.

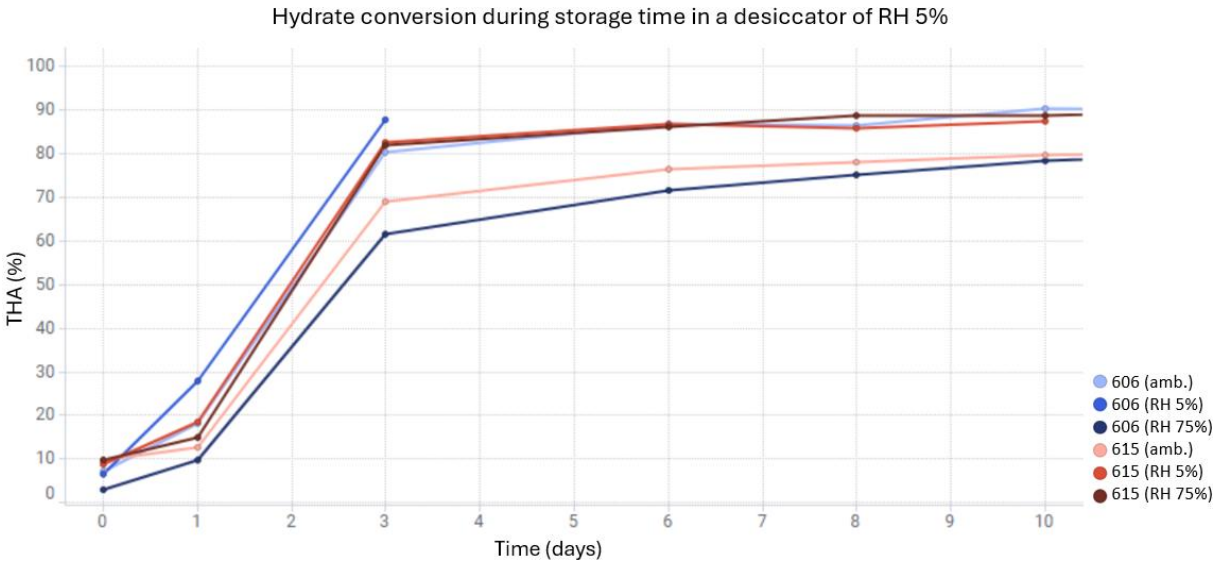

Appendix 7. 615/TH and 606/TH binary mixtures in a desiccator of RH 5% with polymers preconditioned in RH 5%, ambient and RH 75%.

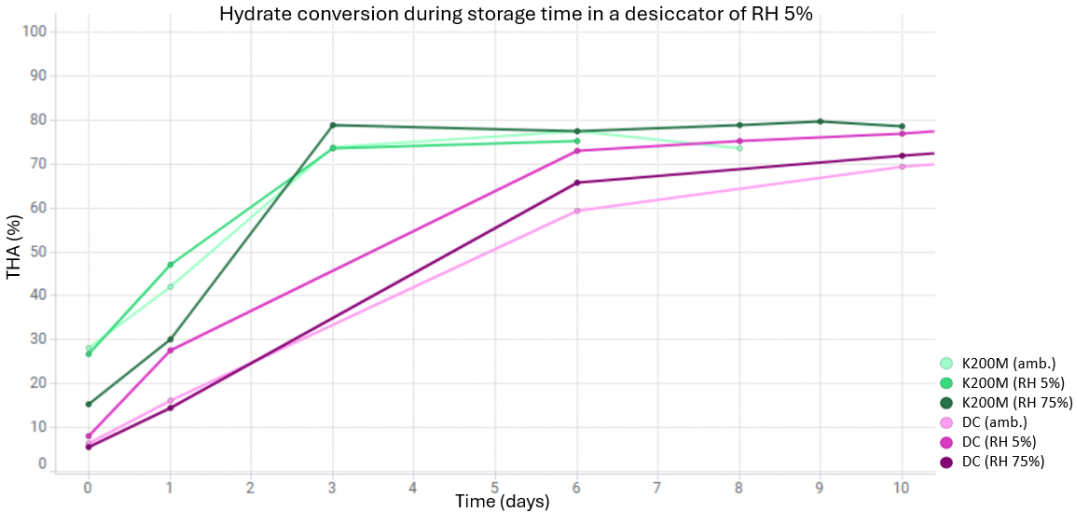

Appendix 8. K200M/TH and DC/TH binary mixtures in a desiccator of RH 5% with polymers preconditioned in RH 5%, ambient and RH 75%.

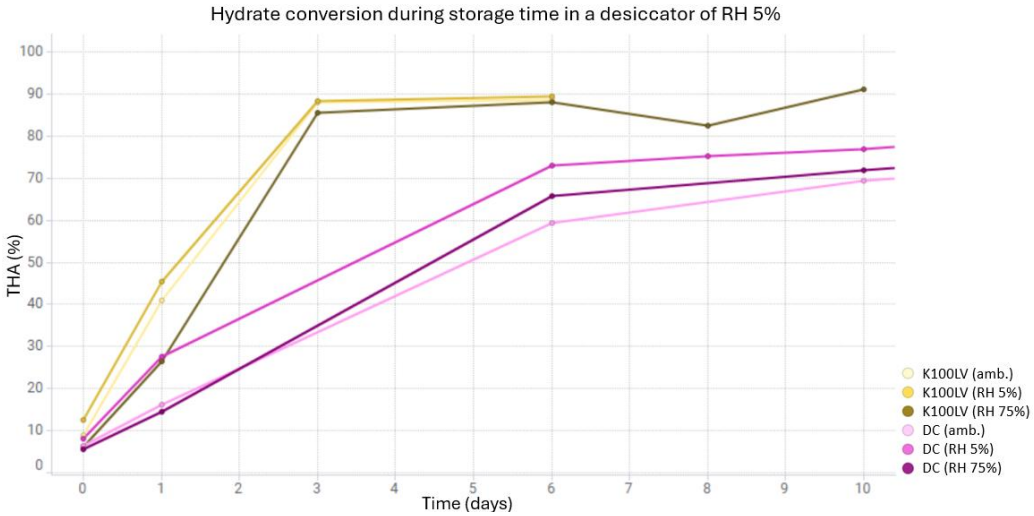

Appendix 9. K100LV/TH and DC/TH binary mixtures in a desiccator of RH 5% with polymers preconditioned in RH 5%, ambient and RH 75%.

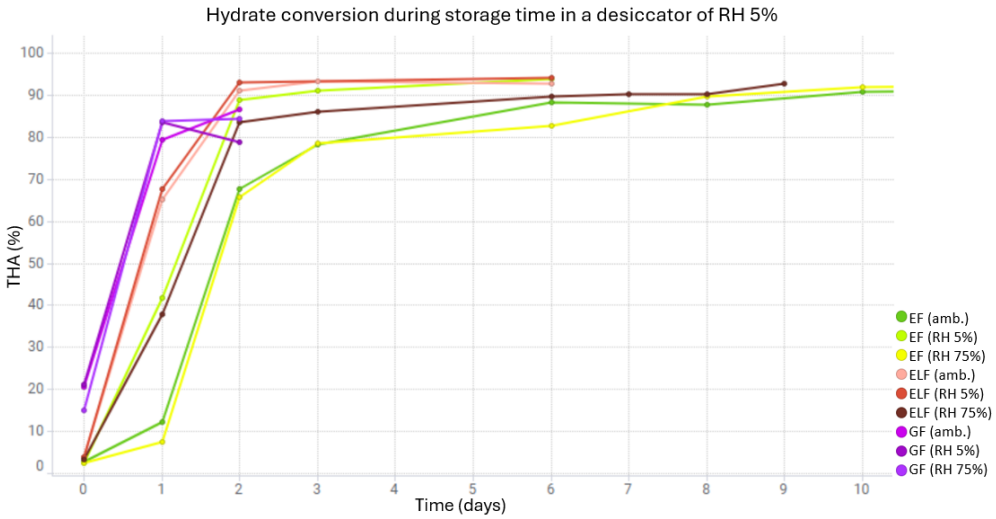

Appendix 10. EF/TH and ELF/TH and GF/TH binary mixtures in a desiccator of RH 5% with polymers preconditioned in RH 5%, ambient and RH 75%.

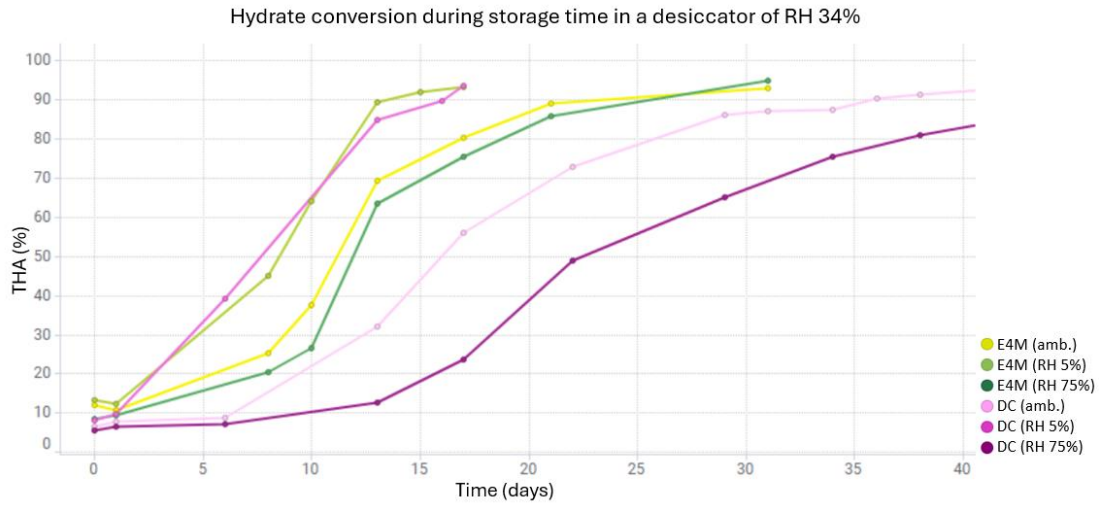

Appendix 11. E4M/TH and DC/TH binary mixtures in a desiccator of RH 34% with polymers preconditioned in RH 5%, ambient and RH 75%.

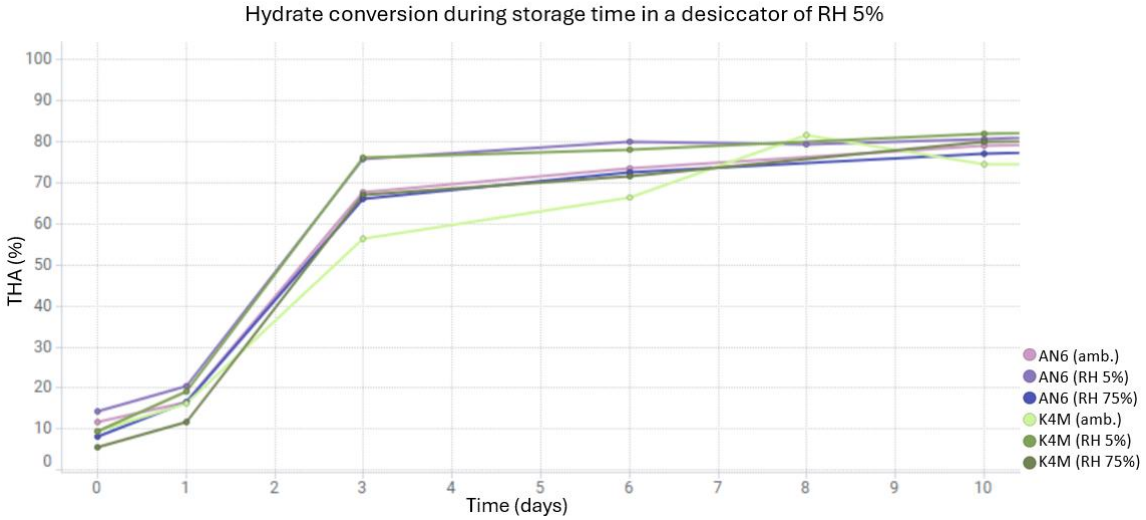

Appendix 12. AN6/TH and K4M/TH binary mixtures in a desiccator of RH 34% with polymers preconditioned in RH 5%, ambient and RH 75%.

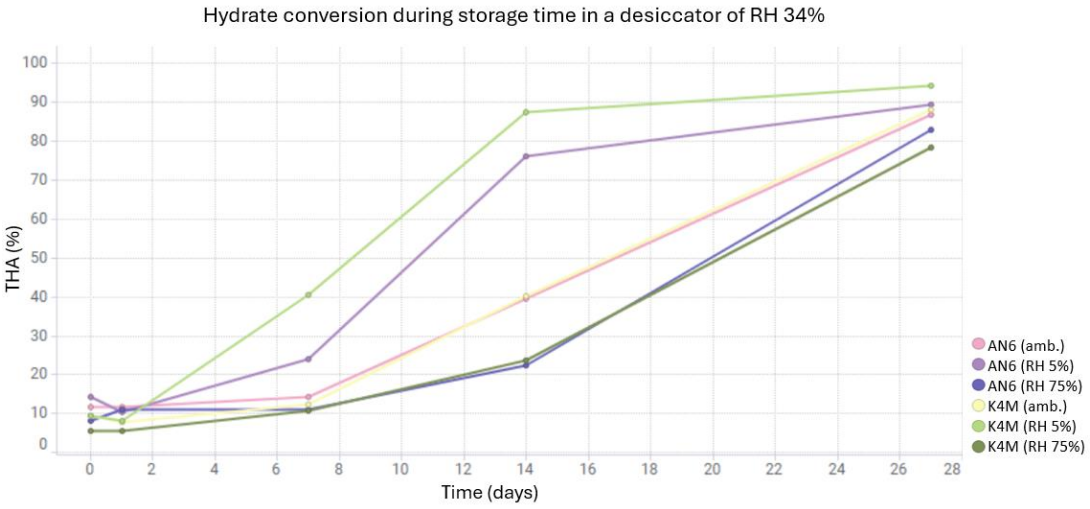

Appendix 13. AN6/TH and K4M/TH binary mixtures in a desiccator of RH 34% with polymers preconditioned in RH 5%, ambient and RH 75%.

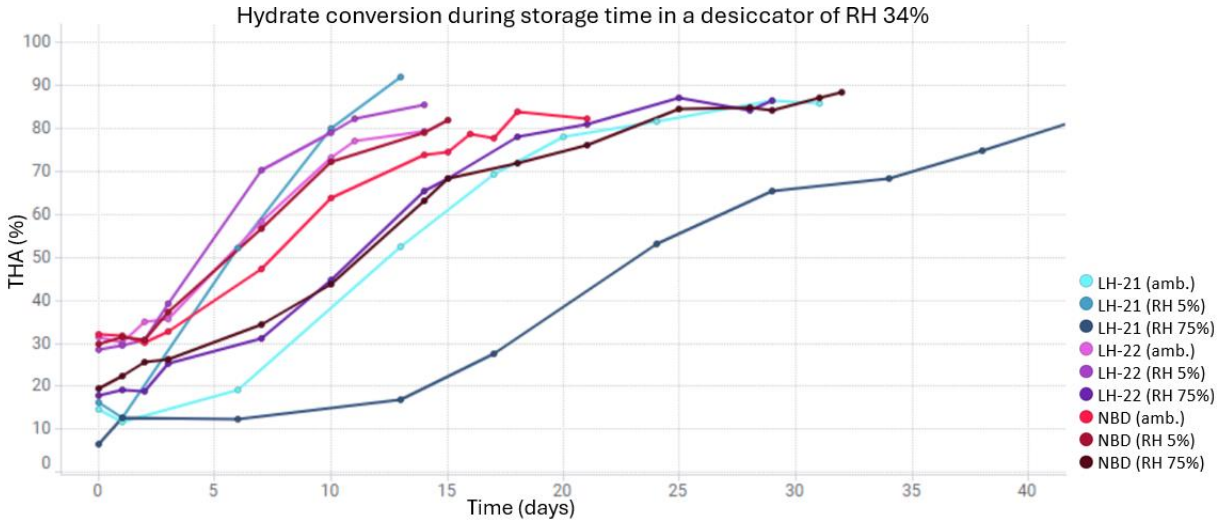

Appendix 14. LH-21/TH and LH-22/TH and NBD/TH binary mixtures in a desiccator of RH 34% with polymers preconditioned in RH 5%, ambient and RH 75%.

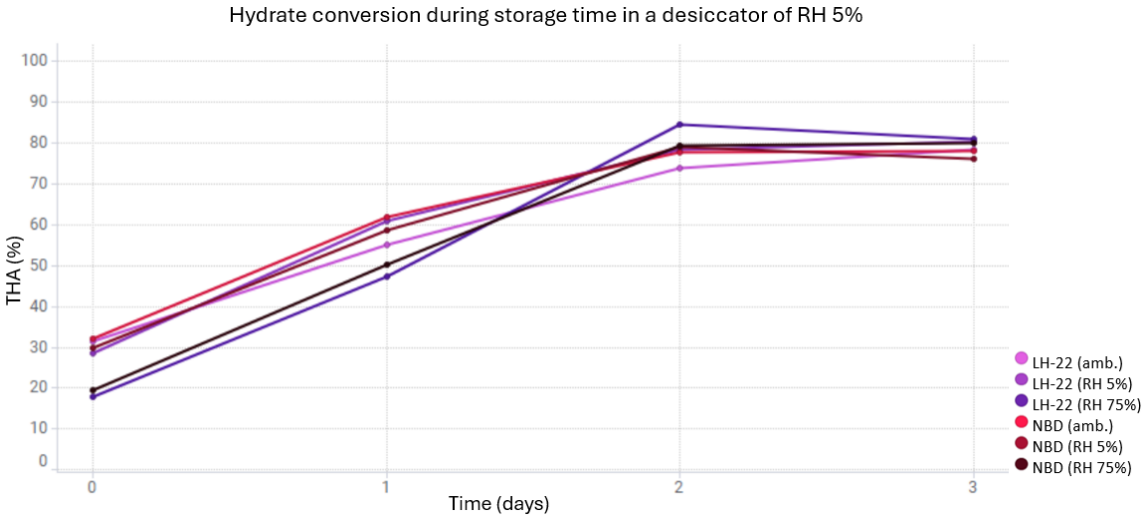

Appendix 15. LH-22/TH and NBD/TH binary mixtures in a desiccator of RH 5% with polymers preconditioned in RH 5%, ambient and RH 75%.

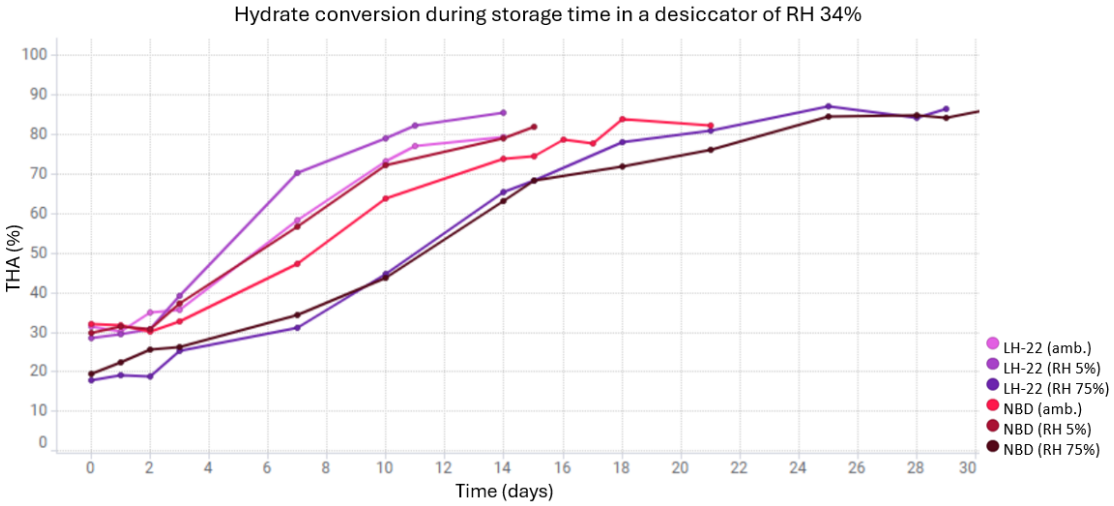

Appendix 16. LH-22/TH and NBD/TH binary mixtures in a desiccator of RH 34% with polymers preconditioned in RH 5%, ambient and RH 75%.

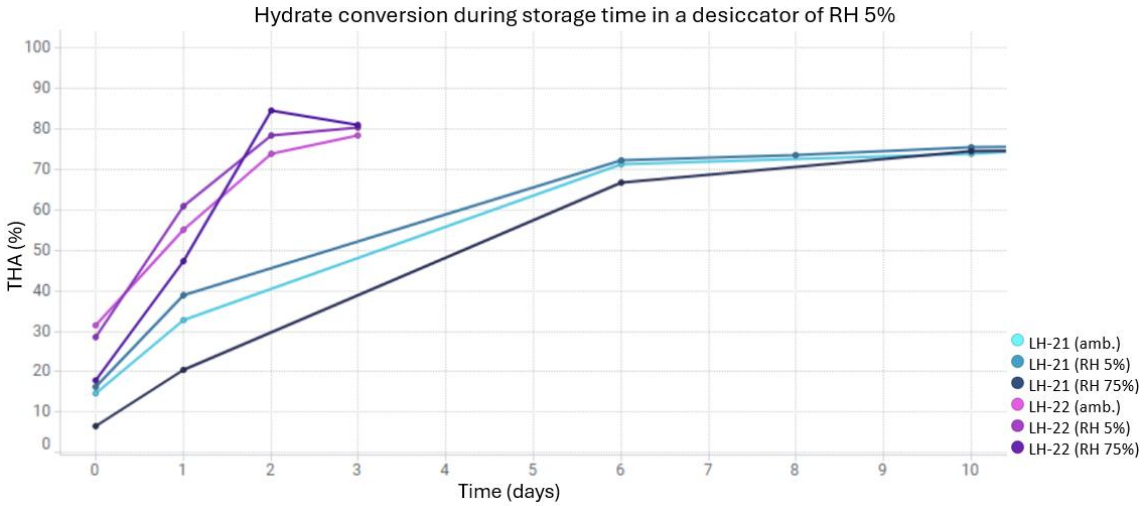

Appendix 17. LH-21/TH and LH-22/TH binary mixtures in a desiccator of RH 5% with polymers preconditioned in RH 5%, ambient and RH 75%.

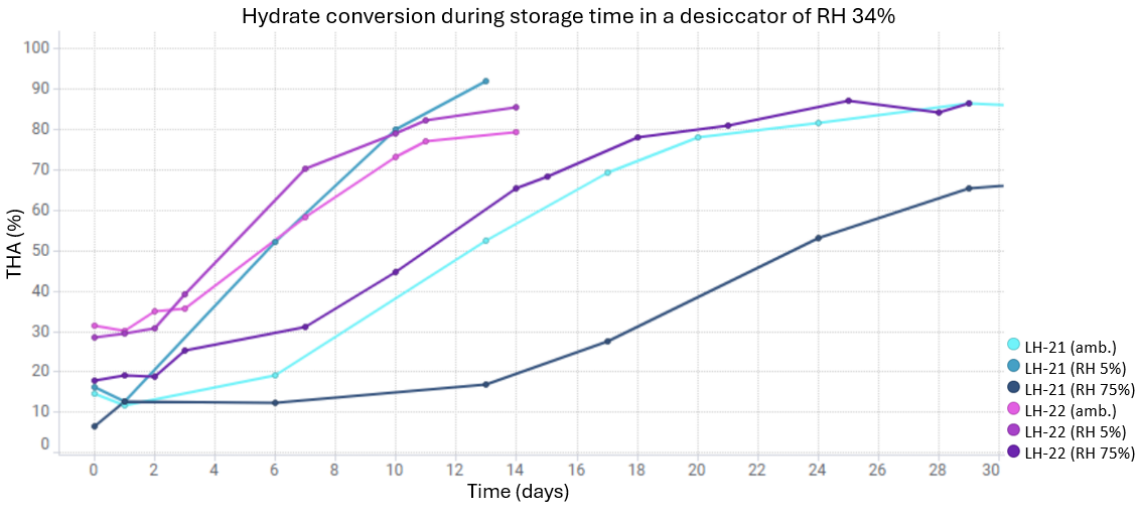

Appendix 18. LH-21/TH and LH-22/TH binary mixtures in a desiccator of RH 34% with polymers preconditioned in RH 5%, ambient and RH 75%.

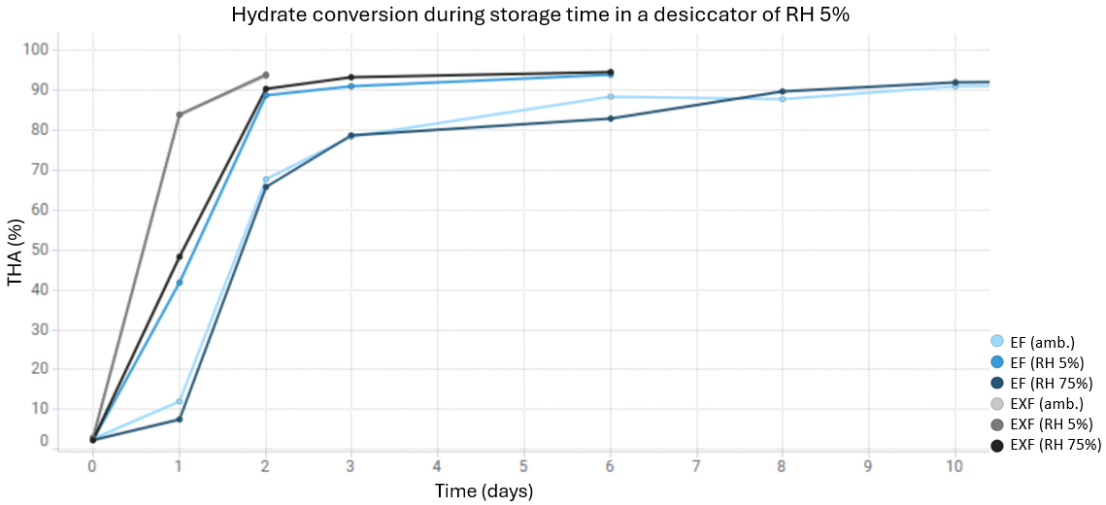

Appendix 19. EF/TH and EXF/TH binary mixtures in a desiccator of RH 5% with polymers preconditioned in RH 5%, ambient and RH 75%.

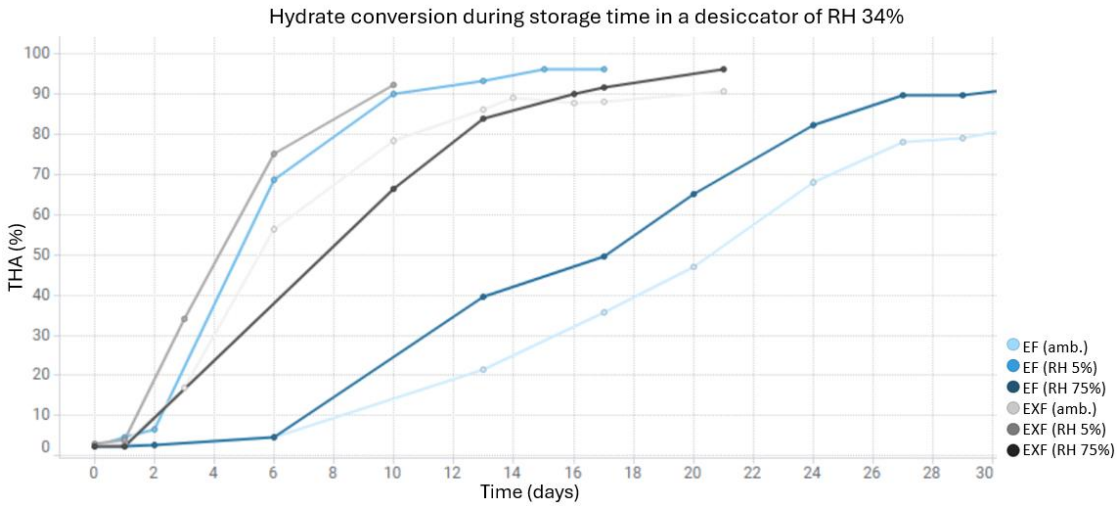

Appendix 20. EF/TH and EXF/TH binary mixtures in a desiccator of RH 34% with polymers preconditioned in RH 5%, ambient and RH 75%.

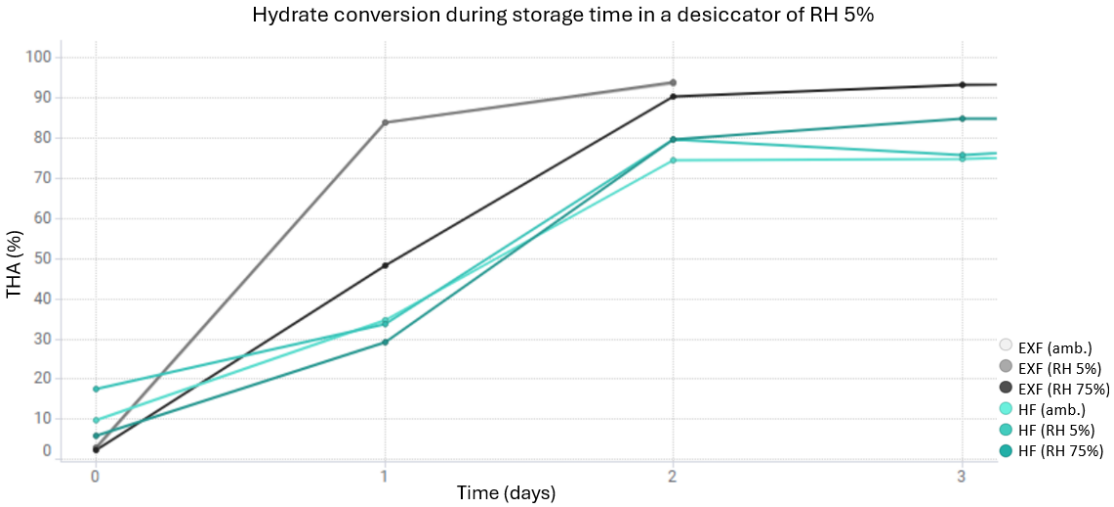

Appendix 21. EXF/TH and HF/TH binary mixtures in a desiccator of RH 5% with polymers preconditioned in RH 5%, ambient and RH 75%.

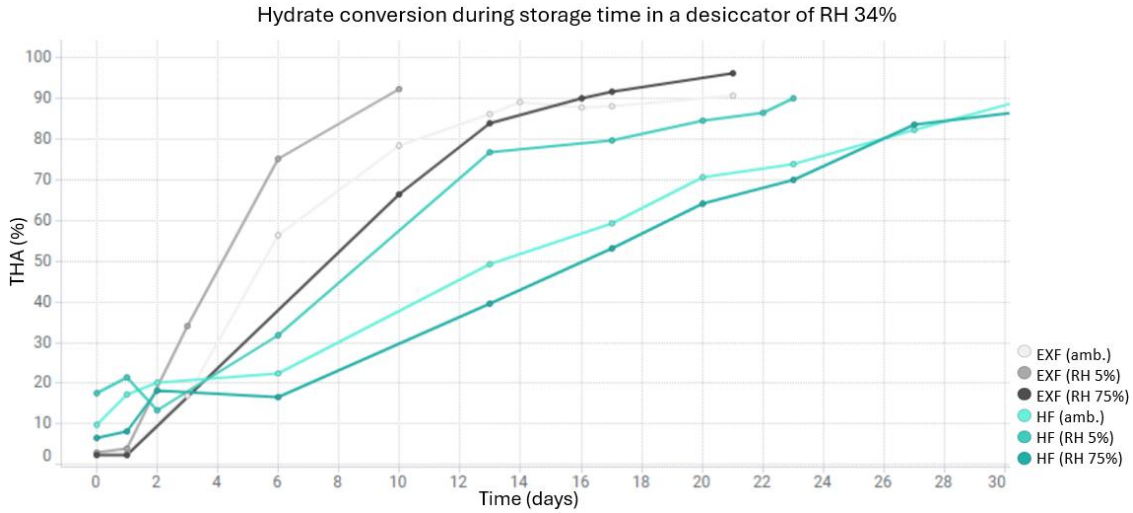

Appendix 22. EXF/TH and HF/TH binary mixtures in a desiccator of RH 34% with polymers preconditioned in RH 5%, ambient and RH 75%.

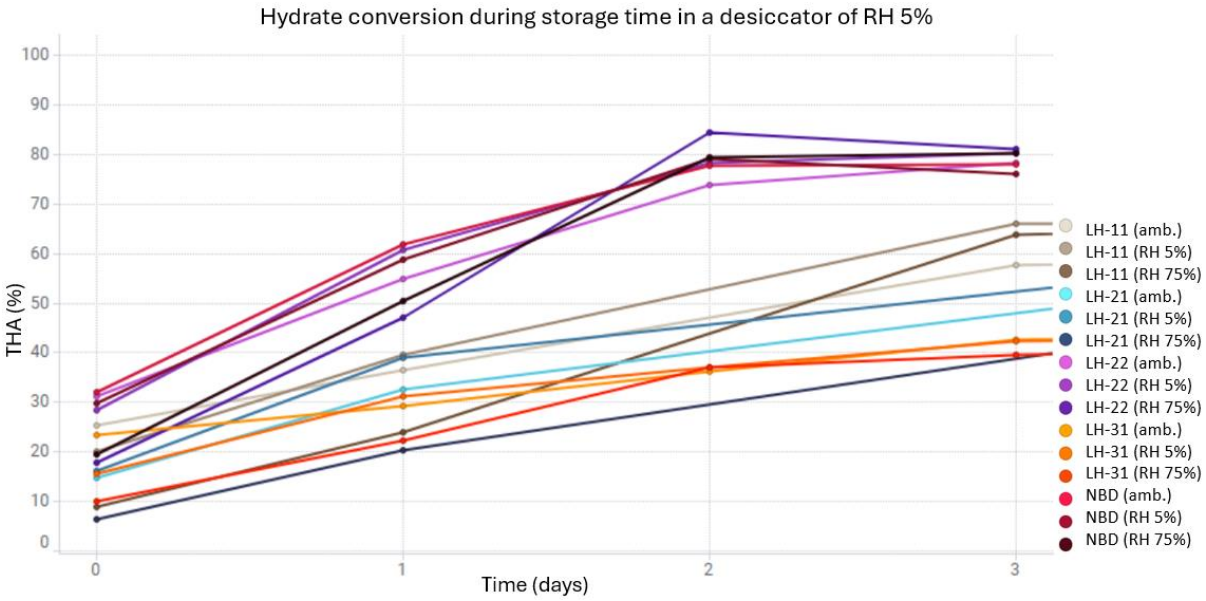

Appendix 23. Binary mixtures made from Shin-Etsu polymers and TH in a desiccator of RH 5% with polymers preconditioned in RH 5%, ambient and RH 75%.

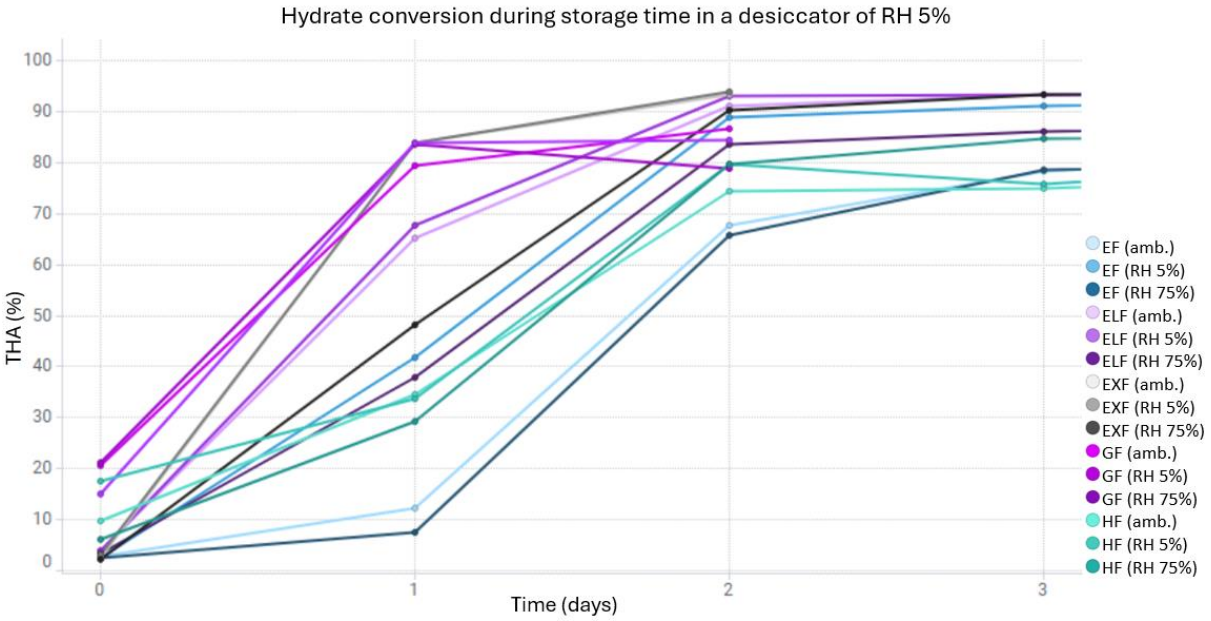

Appendix 24. Binary mixtures made from Ashland polymers and TH in a desiccator of RH 5% with polymers preconditioned in RH 5%, ambient and RH 75%.

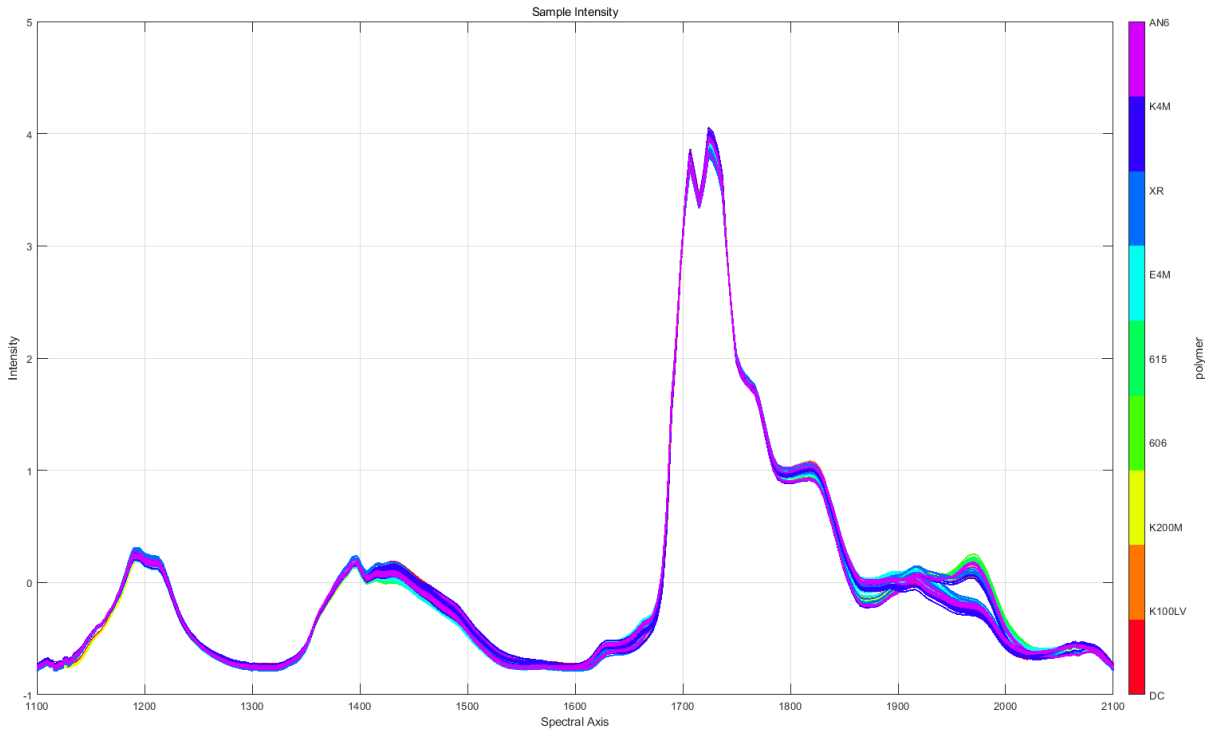

Appendix 25. NIR spectra of HPMC binary mixtures in a desiccator RH 5% with polymer preconditioned in RH 5%, ambient and RH 75%.

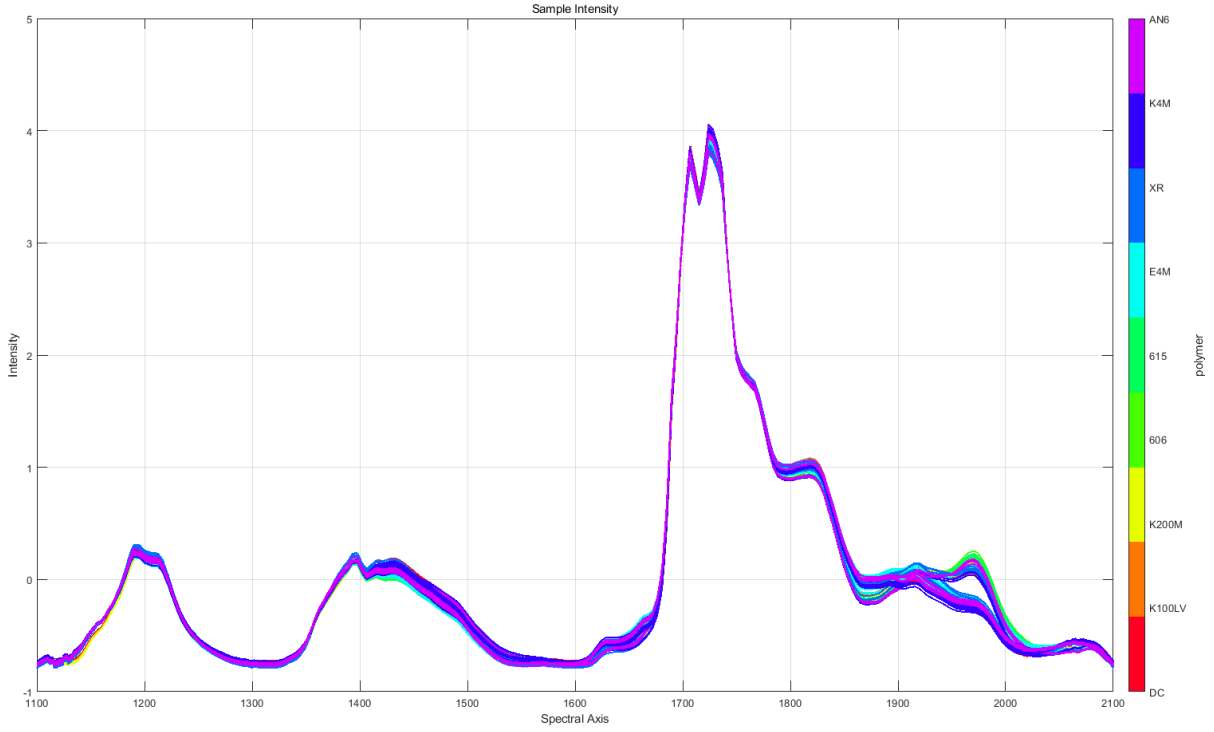

Appendix 26. NIR spectra of HPMC binary mixtures in a desiccator RH 34% with polymer preconditioned in RH 5%, ambient and RH 75%.